The role of SHR-SCR-SCL23-JKD regulatory network in shoot apical meristem development

Inaugural-Dissertation

Zur Erlangung des Doktorgrades

der Mathematisch-Naturwissenschaftlichen Fakultät der Heinrich-Heine-Universität Düsseldorf

vorgelegt von

Elmehdi Bahafid

aus Essaouira (Marokko)

Düsseldorf, November 2021

aus dem Institut für Entwicklungsgenetik der
Heinrich-Heine-Universität Düsseldorf

Gedruckt mit der Genehmigung der
Mathematisch-Naturwissenschaftlichen Fakultät der
Heinrich-Heine-Universität Düsseldorf

Referent: Professor Dr. Rüdiger Simon
Korreferent: Professor Dr. Ikram Blilou

Tag der mündlichen Prüfung: 31.01.2022

This study was funded by DFG through CEPLAS (EXC 2048) and ERC-2020-SyG-951292.

Eidesstattliche Erklärung

Eidesstattliche Versicherung zur Dissertation mit dem Titel:

The role of SHR-SCR-SCL23-JKD regulatory network in shoot apical meristem development

Ich versichere an Eides Statt, dass die Dissertation von mir selbständig und ohne unzulässige fremde Hilfe unter Beachtung der „Grundsätze zur Sicherung guter wissenschaftlicher Praxis an der Heinrich-Heine-Universität Düsseldorf“ erstellt worden ist.

Außerdem versichere ich, dass ich diese Dissertation nur in diesem und keinem anderen Promotionsverfahren eingereicht habe und dass diesem Promotionsverfahren kein gescheitertes Promotionsverfahren vorausgegangen ist.

Düsseldorf, 24/11/2021

_____ _____

Ort, Datum Unterschrift

Acknowledgements

I would like to take time to acknowledge all the people who have helped me through this journey. Whether it be advice, critical suggestions or support, everyone mentioned here have played their part in helping me shape myself and my thesis as they are today.

Firstly, Rüdiger, I owe you an enormous Thank You.

You offered me the opportunity to join your group and to pursue this PhD thesis. Thank you for all the fruitful discussions and for giving me the opportunity to be part of other projects, which allowed me to develop myself as a scientist. Thank you for all the useful advice and guidance, especially when I was passing through difficult time.

I would like to thank Ikram for the discussions at the early stages of this project and for sharing reporter lines to kickstart this project, which turned out to be quite interesting than I had initially imagined.

I would also like to thank Yvonne, for the discussions and feedbacks during my progress reports.

I must thank Patrick, who made me feel welcome from my first day in the lab and for being supportive even when I was experiencing some difficult situations. Thank you for all the help with both scientific as well as bureaucratic issues. Thanks for everything, man!

I wish to thank Karine for her great help in the lab especially at the beginning of my PhD. Thanks for all the nice weekend lunches and discussions. I appreciate it a lot!

I also would like to thank all the students who have been under my supervision: Hanna, Imke, Sophie, Angelina, Anne, Nicole, and Laura. Thanks for all the work you have done and for allowing me to practice and improve my teaching skills.

A huge Thank You! to Madhumitha, Vicky, Pavi and Meik for proof-reading and discussing my thesis. I appreciate it guys!

I need to thank all the AG Simon/Stahl members for all the good time and for their kindness - Karine, Madhumitha, Vicky, Maike, Rebecca, Vivien, Hajer, Svenja, Anika, Neda, Isaia, Jan, Meik, Edgar and Pavi. Thanks for everything!

I would like to thank our lovely technicians Cornelia, Silke, Carin, Nilgün and Mehmet for their patience and outstanding technical assistance.

I wish to thank all the people in the Center of Advanced Imaging (CAi), in particular Sebastian, for all the help with microscopy issues throughout my PhD.

I would also like to thank Susanne, for all the help with administrative work. and the people in JUNO for making it easy for me to settle down in Düsseldorf. I appreciate it a lot!.

I would like to thank all former lab colleagues Patrick, Cornelia, Nozomi, Jenia, Gwen, Greg Barbara and Monika, and a shoutout to my homies, Oumaima, Amine, Abdullah, and Jelle for the deep discussions and great company. Thank you for keeping me mentally healthy.

Last but not least, I would like to thank all members of my family that who have helped me along during my life and made this possible.

1. Abbreviations

Abbreviation	Definition
°C	Degree Celsius
2,4-D	2,4-Dichlorophenoxyacetic Acid
3D	3 Dimension
A. thaliana	*Arabidopsis Thaliana*
ACD	Asymmetric Cell Divisions
AIL6	Aintegumenta Like 6
ANT	Aintegumenta
ARF	Auxin Response Factors
AuxRE	Auxin Response Element
BAM	Barely Any Meristem
Bp	Base Pair
bp	Base Pair
cDNA	Complementary DNA
CEI	Cortex And Endodermis Initial
CEID	Cortex And Endodermis Initial Daughter
CLE	Clavata3/Embryo Surrounding Region
CLV1	Clavata1
CLV2	Clavata2
CLV3	Clavata3
Col-0	Ecotype Columbia
CRN	Coryne
CYCD6;1	Cyclind6;1
CZ	Central Zone
DAG	Days After Germination
DAPI	4′,6-Diamidino-2-Phenylindole
DBD	DNA-Binding Domain
DEX	Dexamethasone
DNA	Deoxyribonucleic Acid
DRM	Distal Root Meristem
DRN	Dornroschen
DZ	Division Zone
E. coli	*Escherichia Coli*
Fig	Figure

FLIM	Fluorescence Lifetime Imaging *Microscopy*
FRET	Fluorescence Resonance Energy Transfer
G1	Gap 1
G2	Gap 2
gDNA	Genomic DNA
GFP	Green Fluorescent Protein
GM	Growth Media
GRN	Gene Regulatory Network
GT	Ground Tissue
HAM	Hairy Meristem
IAA	Indole-3-Acetic Acid
IDD	Bird/Indeterminate Domain
JKD	Jackdaw
kb	Kilobase Pair
L	Litre
L1	Layer 1
L2	Layer 2
L3	Layer 3
LD	Long Day
L*er*	*Landsberg Erecta*
LFY	Leafy
LRC	Lateral Root Cap
M	Molar
MIP	Maximal Intensity Projection
ml	Milli litre
mM	Milli Molar
MP	Monopteros
MR	Middle Region
mRNA	Messenger RNA
MS	Murashige & Skoog
MW	Molecular Weight
N	Number
N. benthamiana	*Nicotiana Benthamiana*
NLS	Nuclear Localization Signal
NPA	*N*-1-Naphthylphthalamic Acid
OC	Organizing Center

OD	Optical Density
OP	Organ Primordia
P	Primordium
PCR	Polymerase Chain Reaction
pg	Picogram
PI	Propidium Iodide
PIN1	Pinformed1
PlaCCI	Plant Cell Cycle Indicator
PRM	Proximal Root Meristem
PZ	Peripheral Zone
QC	Quiescent Center
qRT-PCR	Quantitative Real Time-PCR
RAM	Root Apical Meristem
RFP	Red Fluorescent Protein
RNA	Ribonucleic Acid
RT	Reverse Transcriptase
RZ	Rib Zone
S	Synthesis
SAM	Shoot Apical Meristem
SCL23	Scarecrow-Like 23
SCN	Stem Cell Niche
SCR	Scarecrow
SD	Standard Deviation
SHR	Short-Root
TAIR	The Arabidopsis Information Resource
TF	Transcription Factor
TIR1/AFB	Transport Inhibitor Response1/ Auxin Signaling F-Box Proteins
TZ	Transition Zone
w/v	Weight Per Volume
WOX	Wuschel-Like Homeobox
WT	Wild Type
WUS	Wuschel
YFP	Yellow Fluorescent Protein

2. List of figures and tables

2.1. List of figures

General introduction

The SHR-SCR module coordinates shoot meristem development and auxin dependent organ initiation

2.2. List of Tables

The SHR-SCR module coordinates shoot meristem development and auxin dependent organ initiation

2.3. List of supplementary figures

The SHR-SCR module coordinates shoot meristem development and auxin dependent organ initiation

3. Summary

One of the central questions in plant developmental biology is how the plant body is established and how the tissue patterns are specified and maintained. Unlike animals, plants retain the capacity to continuously grow and develop new organs throughout their life cycles. The sources of cells for this continuous organogenesis are the apical meristems present at the growing tips of shoot and root. The shoot apical meristem (SAM) and root apical meristem (RAM) are established during embryogenesis and consist of a small pool of stem cells whose descendants provides cells to generate the aerial and the underground parts of a plant respectively.

The SAM is a complex structure divided into many functional domains. In the central zone (CZ), stem cells divide slowly and give rise to daughter cells that will be displaced towards the peripheral zone (PZ). In the PZ, cells undergo several rounds of cell divisions before getting incorporated into the lateral organ primordia (LOP). The acquisition of cell/tissue type identity in plants rely on positional information, determined by intercellular signalling.

Beside discovering gene regulatory networks controlling shoot stem cell homeostasis, and patterning different zones of the SAM, our current understanding of how cell fate specification within the different domains is modulated, what factors participate in this process and how the communication between these different domains is orchestrated are still elusive.
To that end, the present study investigates if the regulatory network comprising of the GRAS transcription factors SHORT ROOT (SHR) and SCERCROW (SCR) is involved in the tissue patterning and cell fate acquisition within the different functional zones in the SAM, besides its role in the RAM.

In the RAM, SHR is expressed in the stele and then moves outward into the endodermis and the quiescent center (QC), where it interacts with SCR, SCERCROW LIKE 23 (SCL23) and JACKDAW (JKD). The SHR-SCR-JKD complex directly activate the expression of *CYCLIN D6;1* (*CYCD6;1*) in the cortex endodermis initial (CEI) and promote formative divisions leading to the formation and specification of the ground tissue. While a lot is known about the function of the SHR regulatory network during RAM development its functions in SAM are not yet explored.

The results of this work reveal that the SHR-SCR-SCL23-JKD network plays an important role in the Arabidopsis SAM development by coordinating between lateral organ initiation at the periphery with the maintenance of stem cell activity in the central zone through synergistically working with the WUS-CLV3 pathway and in an auxin concentration-dependent manner. Thus,

a functional SHR-SCR-SCL23-JKD interaction network is required for the proper development and growth of the SAM.

To gain information about possible functions of these TFs in the SAM, the phenotypes of the *shr*, *scr*, *jkd* and *scl23* mutants were investigated by analysing: the plants morphology, plastochron, meristem size, cell area, cell size, rate of cell division, and expression of the auxin input and output reporters in the wild-type and in different mutant backgrounds. The analyses show that the mutant SAMs are smaller with low mitotic activity and long delay in lateral organ initiation compared to the wild-type SAMs. These results indicates that these TFs are functional in Arabidopsis SAM.

By studying the expression patterns of SHR, SCR, SCL23 and JKD in the SAM using transcriptional and functional translational reporter lines, it was found that all the four TFs were expressed in the SAM with a partial or complete overlap in the lateral organ primordia (LOP), and that SCR and SCL23 have a complementary expression pattern in the center of the SAM, with SCR expressing in the L1 and lowly in L2, and SCL23 in the L3.

Previous studies showed that SCR restricts the mobility of SHR and its directly regulated by SHR in the RAM. Using qRT-PCR and by analysing the expression of SCR in the *shr* mutant we found that SCR expression in the SAM is up-regulated by SHR in the LOP, and that SHR expression is concentrated in the nucleus in the presence of SCR compared to its absence.

Using *in vivo* FRET-FLIM, it was found that SHR, SCR and JKD physically interact in the SAM. Furthermore, expression analysis of the known targets of SHR-SCR-JKD complex, *CYCD6;1* demonstrates that *CYCD6;1* expression perfectly overlaps with that of SHR, SCR and JKD in the inner cells of the lateral primordia. Moreover, the expression of pCYCD6;1-GFP was strongly reduced in *shr* mutant LOP and very low in the sepal primordia. Together these findings suggest that the mechanism regulating expression of SCR, mobility of SHR and periclinal cell division in the RAM are also conserved in the SAM leading to cell proliferation in the SAM and providing cells for LOP formation.

Additionally, the genetic analysis also demonstrated that SHR expression is regulated by a MP-mediated auxin signalling pathway through a pair of AuxRE motifs present in the *SHR* promoter.

Interestingly, further genetic and molecular analyses revealed that SCL23 physically interacts with the homeodomain TF WUS in the organizing center (OC) to maintain shoot stem cell homeostasis, and that together SCL23 and WUS expression is subject to negative feedback regulation from stem cells by the CLV pathway.

Overall, the findings identify a novel uncharacterized function of SHR-SCR-SCL23-JKD gene regulatory network in which the convergence of SHR signaling pathway and WUS-CLV loop control the communication between the center and the periphery of the SAM in Arabidopsis.

4. General introduction

4.1. Plant meristems

Unlike most animals, plants continue to produce new organs and modify the existing organs post-embryonically throughout their lives. This is achieved by the activity of stem cell niches (SCNs) localized in their meristems. The model plant *Arabidopsis thaliana* (henceforth referred to as Arabidopsis) has two main meristems: shoot apical meristem (SAM) and root apical meristem (RAM), located at the tip of the shoot and the root, respectively (Fig. 1) (Gaillochet & Lohmann, 2015).

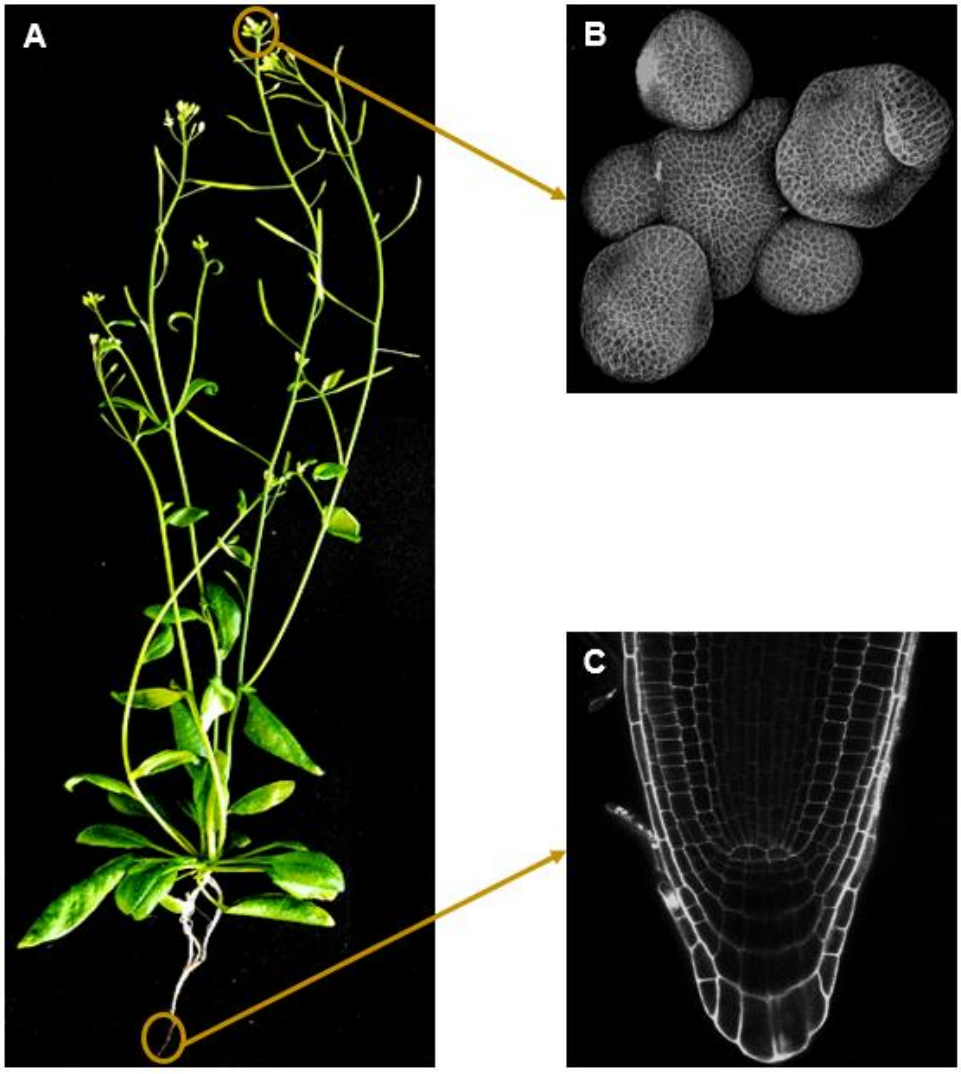

Fig. 1: Arabidopsis thaliana meristems.

(A) Arabidopsis thaliana plant at 42 days after germination (DAG). **(B)** 3D projection of confocal z-stack of shoot apical meristem (SAM). **(C)** Confocal image of root apical meristem (RAM).

4.2. Organization of the root apical meristem (RAM)

The Arabidopsis root is organized into three main zones (shootward from the root tip): the meristematic zone (MZ), the transition zone (TZ) and the differentiation zone (DZ) (Fig. 2A) (Dolan et al., 1993). The RAM is located in the meristematic zone of the primary root.

In a transversal section, the RAM is composed of concentrically arranged distinct cell files, consisting of (from the outside in): epidermis, cortex, endodermis, pericycle and vasculature (Fig. 2B) (Dolan et al., 1993). These different tissues are generated by divisions of four sets of stem cells, called initials, which are organized around the quiescent center (QC). The QC itself comprises four nearly mitotically inactive cells and is responsible for the maintenance of stem cell fate in the initials (Fig. 2B) (Terpstra & Heidstra, 2009, Drisch & Stahl, 2015).

Depending on their position within the RAM, stem cells form different tissue types by dividing asymmetrically to regenerate themselves and produce daughter cells. Columella cells derive from the distal initials, whereas endodermis and cortex cells come from the daughter cells of the cortex and endodermis initial (CEI), vasculature derive from proximal initials. The proximal lateral initials create the epidermis and lateral root cap (LRC) (Fig. 2B) (Dolan et al., 1993, Terpstra & Heidstra, 2009).

The molecular mechanisms regulating the timing and the position of the asymmetric divisions in the stem cells are key to the proper establishment and maintenance of correct tissue patterning during the root development.

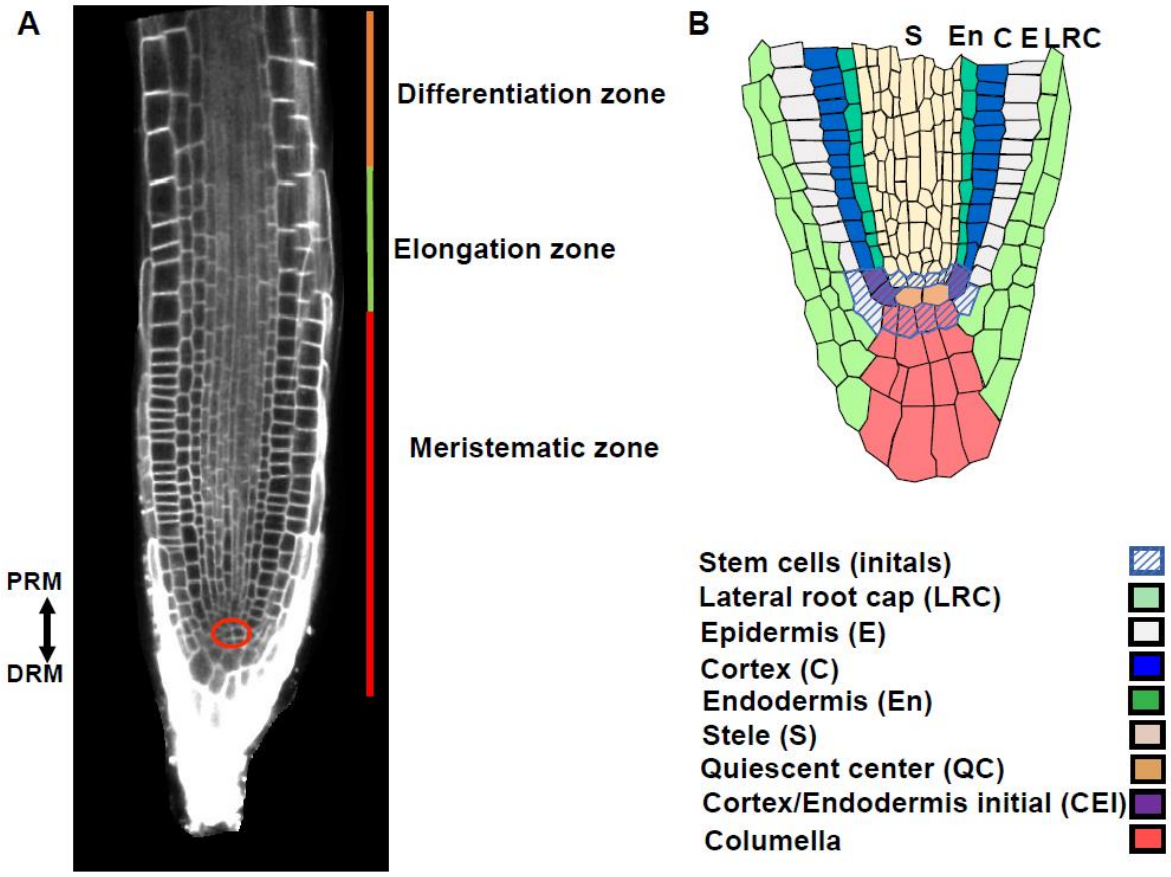

Fig. 2: Organization of the root apical meristem (RAM).

(A) Image of *Arabidopsis thaliana* root with developmental zones marked as colored lines (orange = differentiation zone, green = elongation zone, red = meristematic zone). The meristematic zone can be further divided into the proximal root meristem (PRM) containing all cells proximal to the quiescent center (QC) and the distal root meristem (DRM) containing all cells distal to the QC. QC is highlighted with a red circle. **(B)** Schematic representation of longitudinal, median section through RAM showing the arrangement of cells. Different cell types (represented by different colors) are arranged in cell files, forming concentric single-celled layers: lateral root cap (green), columella (pink), epidermis (white), cortex (blue), endodermis (dark green) and stele (off-white) (from outside to inside). Stem cells or initials (outlined in blue) are shown as hatched cells and are in direct contact to the quiescent center (QC) (orange).

4.2.1. Root stem cell maintenance

Maintenance stem cell identity in the root depends on the molecular circuitry in these cells and in the QC (Drisch & Stahl, 2015, Stahl et al., 2009). Central to this maintenance is the homeobox transcription factor WUSCHEL-RELATED HOMEOBOX 5 (WOX5) protein that is specifically expressed in the QC and acts as a key regulator for the root stem cell activity by controlling the balance between stem cell division and differentiation in a non-cell autonomous fashion (Berckmans et al., 2020, Drisch & Stahl, 2015, Sarkar et al., 2007).

The WOX5 protein moves from the QC into the neighboring CSCs to repress cell differentiation. The loss of function of *WOX5* causes differentiation of the CSCs, exemplified by the accumulation of starch granules (Sarkar et al., 2007). The plant phytohormone auxin is also essential for the maintenance of root stem cell identity (Moubayidin et al., 2013, Tian et al., 2014, Drisch & Stahl, 2015).

In the distal root meristem, the columella cell identity is maintained by the CLE40 peptide. CLE40 is a small peptide from the CLAVATA3/EMBRYO SURROUNDING REGION (CLE) polypeptide family. CLE40 signal negatively regulates the expression of WOX5 by restricting it to the QC via its receptor kinases CRINKLY4 (ACR4) and CLAVATA 1 (CLV1) (Berckmans et al., 2020, Drisch & Stahl, 2015, Stahl *et al.*, 2013, Stahl et al., 2009).

Furthermore, the plant-specific GRAS family transcription factors (TFs) SCARECROW (SCR) and SHORTROOT (SHR) are also required for the maintenance and specification of the QC, as *shr* and *scr* mutants show abnormal QC cells (Blilou et al., 2005, Petersson et al., 2009). Together, all these results show multiple pathways are in involved in the maintenance of stem cell identity in the RAM.

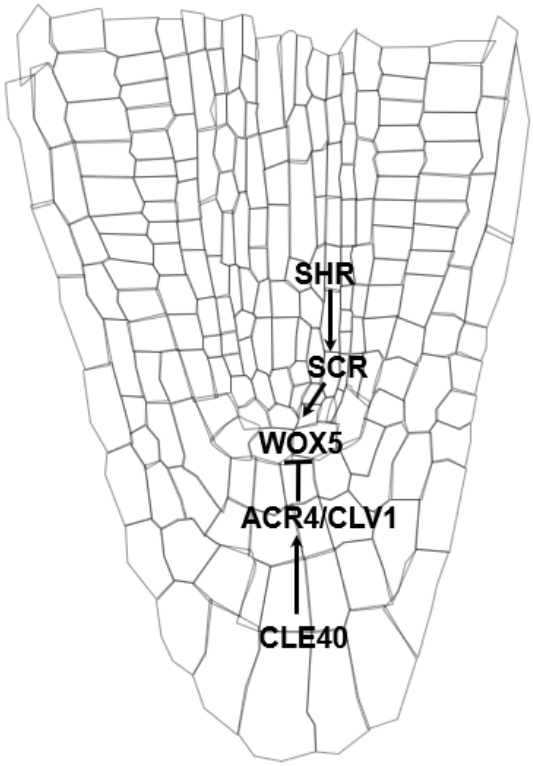

Fig. 3: Gene Regulatory networks controlling the maintenance of stem cells in the RAM

WOX5 is expressed in the QC. The peptide CLE40 is expressed in the columella cells and acts through the CLV1/ACR4 receptor complex to restricts WOX5 expression to the QC. SHR protein moves from the stele into the QC to activate the expression of SCR, and then a SHR-SCR protein complex is formed to regulate the expression of WOX5. Lines with arrows depict positive regulation and with bars depict negative regulation.

4.2.2. Genetic networks controlling endodermis and cortex patterning in the RAM

The establishment and the maintenance of a functional RAM depends on proper coordination of asymmetric cell divisions in the initials. In the RAM, the cortex and the endodermis, which are also called the ground tissue, originate from the cortex/endodermis initial (CEI) following a series of ACDs. First, an anticlinal division of CEI generates a self-renewed stem cell (CEI) and a daughter cell (CEID) (Fig. 4B). Then, the cortex/endodermis initial daughter cell (CEID) undergoes a periclinal division and the progeny generates cortex and endodermis tissues (Fig. 3B) (Cruz-Ramírez et al., 2012, Cui et al., 2007, Di Laurenzio et al., 1996, Helariutta et al., 2000, Scheres et al., 1994).

SHORT-ROOT (*SHR*) and *SCARECROW* (*SCR*) are required for the proper development of the cortex and endodermis layers, as they regulate ACD in the CEI. In fact, loss-of-function mutants *shr* and *scr* have a monolayered ground tissue, indicating that SHR and SCR are the

main fate determinant of the ground tissue (Scheres et al., 1995, Helariutta et al., 2000, Benfey et al., 1993). SHR is expressed in the stele and moves into the adjacent layer via plasmodesmata where it is recruited to the nucleus through a physical interaction with SCR. The resulting protein complex directly activates *SCR* transcription to maintains ground tissue identity (Cui et al., 2007, Long et al., 2017, Nakajima et al., 2001) (Fig. 4).

Previous studies have shown that the TF SCARECROW-LIKE 23 (SCL23), the closest homolog of SCR among GRAS TFs members, interacts with both SHR and SCR to specify the endodermis cell fate in the RAM (Long et al., 2015a). Here, SCL23 interacts with SHR and restricts its movement from the stele to the endodermis. Similar to SHR and SCR, the SHR-SCL23 heteromeric complexes directly activate the expression of SCL23 (Kim et al., 2017, Long et al., 2015a, Yoon et al., 2016). Furthermore, unlike SCR, SCL23 is a mobile TF with two mobility ranges: long-range mobility from differentiation zone to the meristematic zone and short-range movement from the ground tissue to the stele (Kim et al., 2017, Long et al., 2015a). Moreover, SCL23 and SCR function in a mutually antagonistic manner in the RAM and act redundantly to specify endodermal cell fate (Kim et al., 2017, Long et al., 2015a).

Other direct targets of SHR, known as BIRD/INDETERMINATE DOMAIN (IDD) TFs, such as JACKDAW (JKD), interact with SHR and SCR to restrict SHR movement to the endodermis and limit the range of SHR-SCR complex activity (Cui et al., 2014, Cui et al., 2007, Welch et al., 2007, Long et al., 2015b, Long et al., 2017) (Fig. 4A). In the CEID, a SHR-SCR-JKD heteromeric complex is formed and promotes asymmetric cell division by directly activating the expression of the cell cycle regulator *CYCLIND6;1* (*CYCD6;1*) (Di Laurenzio et al., 1996, Long et al., 2015b, Long et al., 2017, Sozzani et al., 2010, van den Berg et al., 1995). Auxin can also promote the transcription of CYCD6;1 in an SHR and SCR dependent manner(Cruz-Ramírez et al., 2012).

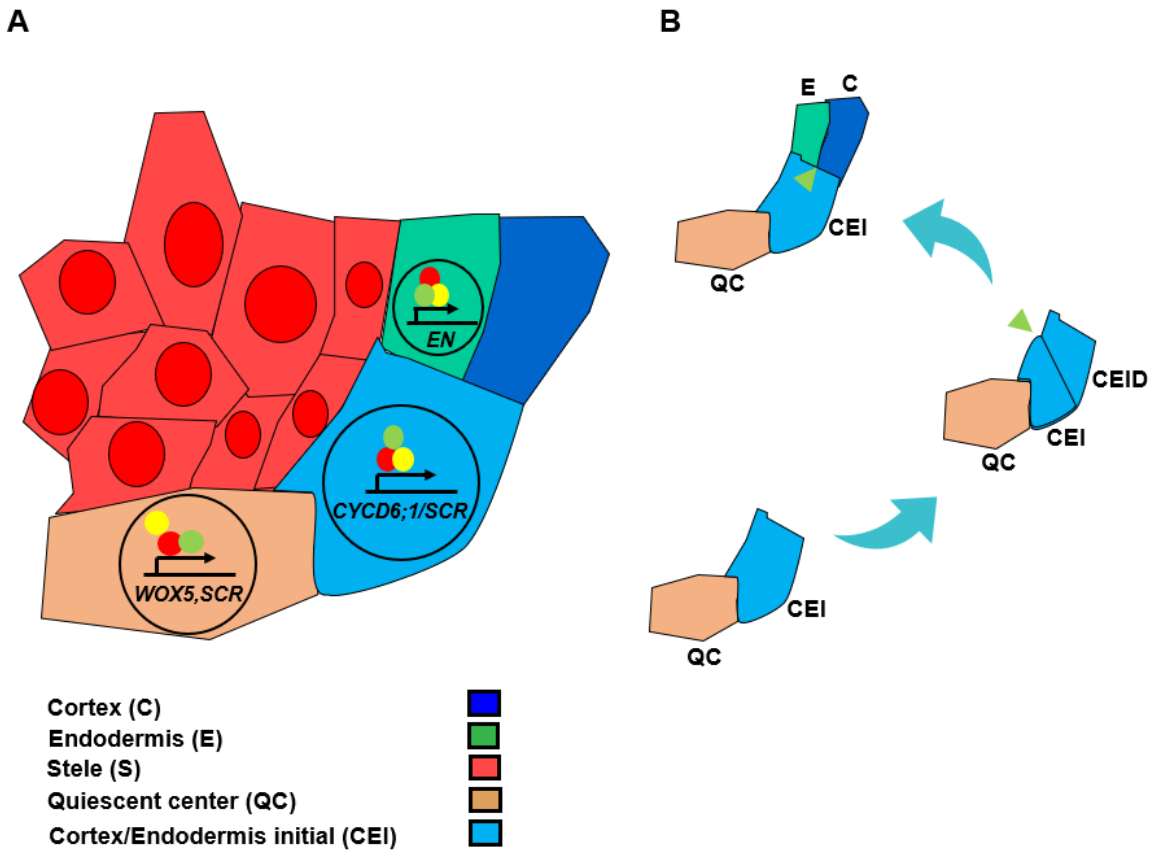

Fig. 4: Model of the main pathway contributing to radial patterning of the root ground tissue.

(A) Schematic representation depicting the spatial distribution of SHR-SCR-JKD protein complexes in the QC, cortex/endodermal initial cell (CEI) and endodermis. In the RAM, SHR moves from the stele, where it is expressed, to the directly adjacent cell layer. It interacts with SCR and JKD to positively regulate the expression of WOX5 in the QC, and to directly activate the expression of CYCD6,1 in the CEI. In the endodermis this complex is important for endodermal specification. **(B)** Asymmetric division of the CEI that generate the two cell layers of the ground tissue. The CEI divides anticlinally (axis perpendicular to the axis of growth) to self-renew and to generate a CEID. The CEID then divides periclinally (axis parallel to the elongating root axis) to generate cells of the endodermis (green) and the cortex (dark blue).

4.3. Organization of the shoot apical meristem (SAM)

The SAM is the progenitor of all above ground organs of a plant. This dome-like structure can be subdivided into different cell layers and different functional domains based on cell division orientation and rate (Gaillochet et al., 2015, Gaillochet & Lohmann, 2015, Steeves & Sussex, 1989) (Fig. 5).

Tissue organization is more complicated in the SAM compared that found in the root apex. In a longitudinal section, the SAM is subdivided in three clonally distinct cell layers termed as: Layer 1 (L1), Layer 2 (L2, L1 and L2 are collectively also referred to as “tunica”) and Layer 3 (L3, also called “corpus”) (Fig. 5). The L1 is the epidermal (out-most) layer, L2 is the sub-epidermal layer and L3 is the entire region located directly beneath the L2 layer (Fig. 5). Cells in the L1 and L2 divide exclusively in an anticlinal manner, in contrast, to the cells in the multilayer L3, which divide both anticlinally and periclinally (Jenik & Irish, 2000, Gaillochet et al., 2015, Steeves & Sussex, 1989).

At the top-center of the SAM is the central zone (CZ), which contains pluripotent stem cells that divide slowly. Their daughter cells from these divisions are displaced towards the peripheral zone (PZ). Cells in the PZ then exhibit a higher cell division rate and are pushed more outwards to the periphery and give rise to the lateral organ primordia (LOP) where cells start to differentiate. The organizing center (OC), a group of infrequently dividing cells located directly beneath the CZ, is required for the initiation and maintenance of stem cells during and after embryogenesis. Finally, the rib zone (RZ) is located beneath the OC and generates the plant’s stem (Bleckmann & Simon, 2009, Fletcher *et al.*, 1999, Stahl & Simon, 2005) (Fig. 5).

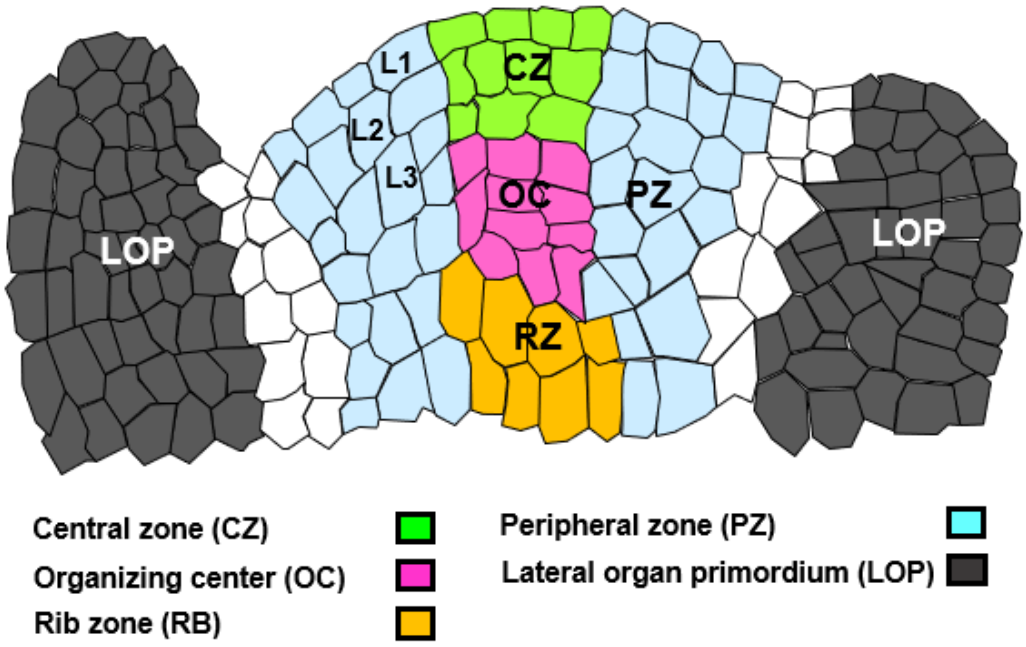

Fig. 5: Schematic representation of orthogonal view of an Arabidopsis SAM, showing the different functional domains.

The central zone (CZ), the peripheral zone (PZ), the organizing center (OC), the rib zone RZ and the lateral organ primordium (LOP). L1, L2 (Tunica) and L3 (Corpus) indicate the cell layers.

4.3.1. The WUSCHEL/CLAVATA shoot apical meristem maintenance pathway

In Arabidopsis the RAM and the SAM share relatively conserved factors for stem cell maintenance. In the SAM, the homeodomain TF WUSCHEL (WUS) which is a homologue of the WOX5 gene, is a key regulator of stem cell fate in the SAM (Mayer et al., 1998).

WUS is expressed in the OC (Mayer et al., 1998, Ohyama *et al.*, 2009). The WUS protein moves from the OC to the CZ through plasmodesmata to directly activates the expression of *CLAVATA3* (*CLV3*) the closest homologue of CLE40 gene (Fig. 6) (Daum et al., 2014, Yadav et al., 2011). Movement of WUS is necessary to maintain stem cell fate in the CZ, as a reduction in WUS mobility leads to an early termination of the SAM (Daum et al., 2014).

CLV3 peptide in it turn represses the expression of *WUS* and restricts it to the OC by binding to the plasma membrane-localized CLAVATA1 (CLV1) or CLAVATA2-CORYNE (CLV2-CRN) receptor protein complex (Fig. 6) (Schoof et al., 2000, Somssich et al., 2016). Plants lacking functional CLV3 have very large meristems as WUS expression is unrestricted resulting in expansion of the stem cell domain (Clark et al., 1997, Fletcher et al., 1999). These findings

demonstrate that WUS and CLV3 form a negative feedback loop that allows the CZ and the OC to regulate each other's sizes and maintain SAM homeostasis.

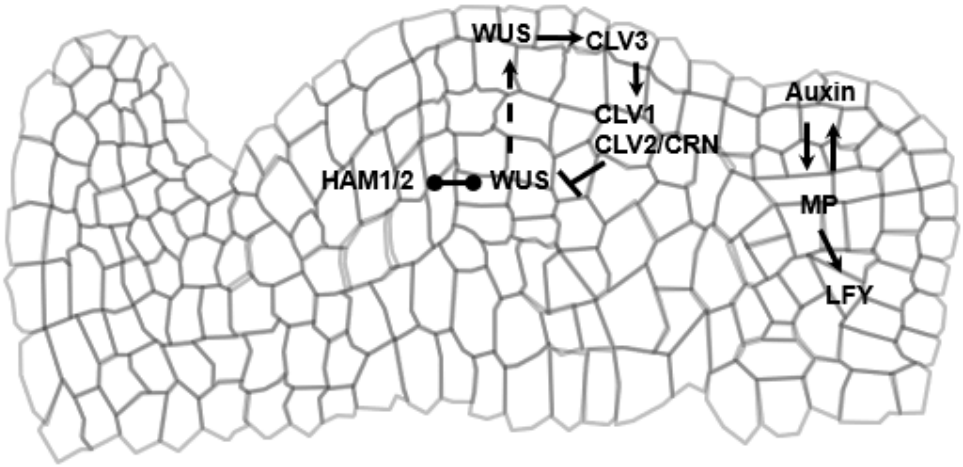

Fig. 6: Gene interaction network controlling SAM maintenance and organ primordia initiation.

WUS is expressed in the organizing center (OC), and WUS protein moves into the stem cell in the centrale zone (CZ) through plasmodesmata where it directly activates the transcription of *CLV3*. CLV3 is then secreted and acts through CLV1 and CLV2-CRN complex to repress *WUS* transcription. In the OC, HAM1/2 physically interact with WUS and act together to switch off CLV3 expression. At the flanks, PIN1 transports auxin to the periphery and creates an auxin maximum that determines the sites of lateral organ primordia. Auxin maxima activates MP, then MP in turn directly activates the expression of *LFY* to promote lateral organ initiation. Lines with arrows depict positive regulation, with bars depict negative regulation and with points depict protein-protein interaction.

4.3.2. The relation between *HAMs* and the WUS-CLV3 feedback circuit in the SAM

The *HAIRY MERISRTEM (HAM)* genes family encode GRAS domain TFs that are essential for maintaining shoot stem cells in an undifferentiated state (Stuurman et al., 2002, Engstrom et al., 2011). In the SAM, HAM1 and HAM2 are expressed in an overlapping domain with WUS and nearly complementary domain with CLV3 (Fig. 6) (Zhou et al., 2015).

Recent studies have demonstrated that HAM1 and HAM2 physically interact with WUS, and together control the production of shoot stem cells by shaping the apical-basal gradient of the CLV3 expression domain in the CZ (Schulze et al., 2010, Zhou et al., 2015). In the absence of *HAMs* expression in the SAM, *CLV3* is ectopically expressed in the rib meristem. These data

show that the *HAMs* are part of the CLV3-WUS feedback loop and act by limiting CLV3 transcription exclusively to the CZ (Zhou et al., 2015).

4.3.3. Auxin and lateral organ initiation in the SAM

At the periphery of the SAM, lateral organ primordia (LOP) are initiated at regular positions. The LOP are positioned in a regular arrangement, termed phyllotaxy where a divergent angle of 137.5° is established between successive organs that create the spiral phyllotaxy found in Arabidopsis (Reinhardt et al., 2003, Traas, 2013). This phyllotaxy is regulated by the growth regulator phytohormone auxin.

An auxin maximum is formed at the periphery of the meristem where a new primordium is initiated, and this maximum is established by the polar transport of auxin by PINFORMED1 (PIN1) protein, a member of auxin efflux carrier family (Fig. 6) (Gälweiler et al., 1998). PIN1 is required for production of the LOP and for normal shoot development. *pin1* mutant shows an altered distribution of auxin and develops a naked or pin-like inflorescence stem that lacks lateral organs (Gälweiler et al., 1998). These observations demonstrate that auxin signaling is a core regulator of lateral organ outgrowth.

4.3.4. Auxin perception and signal transduction

The plant specific phytohormone auxin has been shown to be fundamental to plant development and is involved in a host of processes including cell division and expansion (Perrot-Rechenmann, 2010), cell fate specification (Smit & Weijers, 2015), root and shoot growth (Overvoorde et al., 2010, Vernoux et al., 2010), phototropism and gravitropism (Band et al., 2012, Fankhauser & Christie, 2015), response to pathogens and leaf senescence (Ellis et al., 2005, Kazan & Manners, 2009). The most abundant auxin found in plants is the indole-3-acetic acid (IAA) which is synthesized from the cyclic organic compound indole, either through a tryptophan-dependent or a tryptophan-independent pathway (Korasick et al., 2013).

Auxin regulates gene expression by binding to the TRANSPORT INHIBITOR RESPONSE1/ AUXIN SIGNALING F-BOX PROTEINS (TIR1/AFB) family proteins. TIR1/AFB are F-Box proteins that act as a subunit of the SCF-type ubiquitin protein ligase complexes (Dharmasiri et al., 2005a, Dharmasiri et al., 2005b, Parry et al., 2009). When cellular auxin concentration is high, auxin binds to the binding pocket of TIR1/AFB and acts as a molecular glue that stabilizes its interaction with Aux/IAA transcriptional repressor family (Kepinski & Leyser, 2005, Dharmasiri et al., 2005b, Tan et al., 2007). Once bound to the $SCF^{TIR1/AFB}$ complexes, Aux/IAA proteins are ubiquitinated and subsequently degraded via the ubiquitin-proteasome pathway (Kepinski & Leyser, 2005, Dharmasiri et al., 2005b, Tan et al., 2007). Auxin-induced

degradation of Aux/IAAs releases the auxin response factor (ARF), which then either activate or repress expression of auxin responsive genes (Fig. 7A) (Tiwari et al., 2003, Ulmasov et al., 1997a).

4.3.5. ARF transcription factor family

In Arabidopsis, the ARF family comprises 23 members, with some acting as transcriptional activators while others act as transcriptional repressors (Remington et al., 2004).

Almost all the ARFs have a similar structure consisting of three domains: the N-terminal DNA-binding domain (DBD) that is required for interaction with the canonical TGTCTC auxin response element (AuxRE) within the promoters of their auxin-responsive target genes, a variable middle region (MR) that determines the activity of the ARF (Tiwari et al., 2003), and finally the C-terminal (PB1) domain that is involved in protein interaction with the Aux/IAA proteins (Fig. 7B) (Korasick et al., 2014, Nanao et al., 2014).

Previous studies suggest that ARF5/MP transcription factor can act as both a transcriptional activator (Cole et al., 2009, Konishi et al., 2015, Yamaguchi et al., 2013) as well as a repressor (Zhang et al., 2017, Zhao et al., 2010).

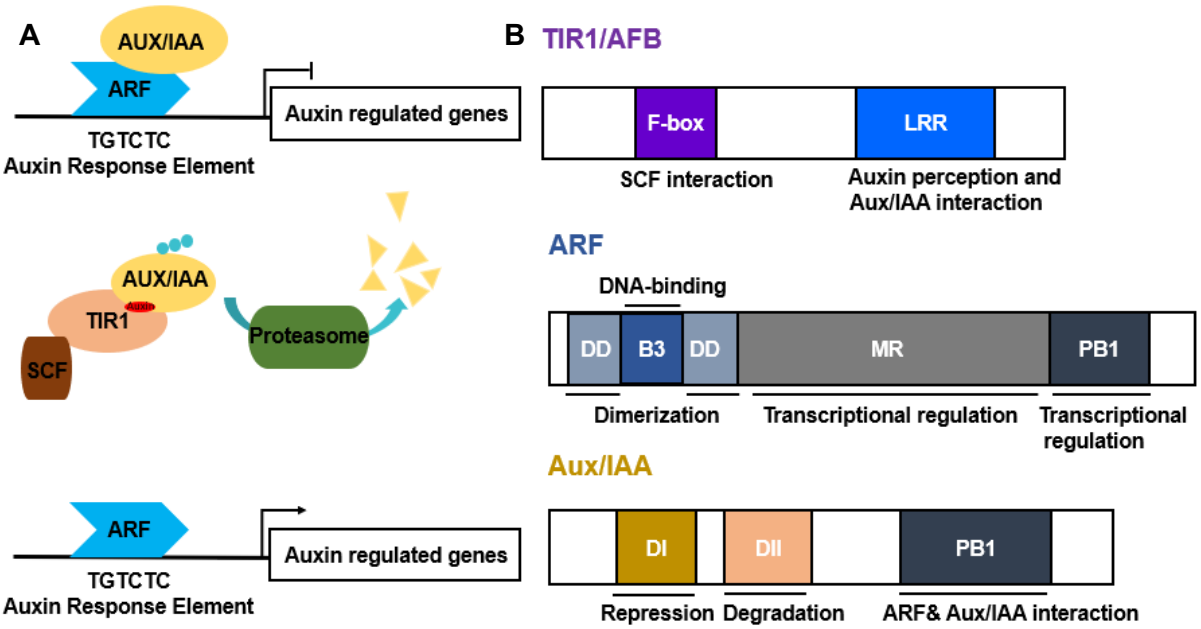

Fig. 7: Simplified model of auxin response genes activation by ARFs.

(A) Scheme of the auxin signaling through $SCF^{TIR1/AFB}$ pathway at low or high concentrations of auxin. At low auxin levels, Aux/IAA proteins interact with AUXIN RESPONSE FACTORS (ARFs) and inhibits the transcription of auxin regulated genes. At high auxin levels, auxin binds to the receptor complex SCF^{TIR1} this leads to the formation of complex with the Aux/IAA and the subsequent ubiquitination and degradation of AUX/IAA proteins. Aux/IAA degradation releases the ARF TF from inhibition to allows control of genes expression. **(B)** Structure of

TIR1/AFB, ARF and Aux/IAA proteins. Conserved domains and their roles in auxin signaling are indicated.

4.3.6. MONOPTEROS/AUXIN RESPONSIVE FACTOR 5 (MP/ARF5)

The most studied member of the ARF family is *MONOPTEROS*/*ARF5* (*MP*). MP plays a key role in in transducing the auxin signal in several developmental processes (Aida et al., 2002, Bhatia et al., 2016, Hardtke & Berleth, 1998). Plants lacking functional *MP* show severely defective developmental phenotypes such as rootless seedlings, variable arrangement and number of cotyledons and defects in vascular patterning within the leaves (Berleth & Jürgens, 1993, Hardtke & Berleth, 1998).

The expression of MP has been well described from early embryonic stages until during inflorescence and florescence meristem development. During embryogenesis MP is expressed from the globular stage until the torpedo stage, and is required for the ground tissue formation through promoting the transcription of SHR and SCR and for the direct activation of *DORNROSCHEN (DRN)* expression to regulates cotyledon development and *TARGET OF MP* (*TMO)* to promote embryonic root initiation (Cole et al., 2009, Möller et al., 2017, Schlereth et al., 2010, Weijers et al., 2006).

In the RAM, MP is expressed in the stele and in the columella cells (Hardtke & Berleth, 1998, Rademacher *et al.*, 2011), and regulates many auxin-mediated patterning processes (Hardtke *et al.*, 2004). In the SAM, MP was found to be highly expressed in the lateral organ primordia in the SAM, where it directly regulates the transcription of its targets, *LEAFY* (*LFY*), *AINTEGUMENTA* (*ANT*) and *AINTEGUMENTA LIKE 6* (*AIL6*), to promote lateral organ initiation development (Elliott et al., 1996, Hardtke & Berleth, 1998, Klucher et al., 1996, Vernoux et al., 2011b, Wu et al., 2015, Yamaguchi et al., 2013, Zhao et al., 2010).

4.3.7. Common regulatory modules in SAM and RAM

It is hypothesized that the RAM was evolved from the SAM, since the first appearance of roots are associated with the vascular plants. Consistent with this, the key gene regulatory networks that control stem cell niches maintenance in the SAM is relatively conserved in the RAM (Jiang & Feldman, 2005, Sarkar et al., 2007, Scott, 2003, Stahl et al., 2013).

Though tissue organization in the shoot is more complex and divergent compared to that fund in the root, the QC can be considered analogous to the organizing center in the shoot – both layers regulate the stem cell activity of the adjoining stem cell layers through expression of mobile homeobox proteins. Remarkably, the QC-expressed WOX5 is the closest homolog of

WUS that is expressed in the OC and their functions are at least partially exchangeable *in planta*, WUS can completely rescue *wox5* mutant root phenotypes when it is expressed in WOX5 domain and WOX5 partially restores the shoot meristem phenotype of *wus* mutant (Sarkar et al., 2007).

Furthermore, maintenance of stem cell activity in both SAM and RAM depends on the activities of CLE peptides that act through receptor-like kinases (RLK) such as CLV1, CLV2 and the pseudokinase CORYNE (CRN) (Berckmans et al., 2020, Ogawa *et al.*, 2008, Stahl et al., 2013). Additionally, the HAM TFs can form protein complexes with both WUS and WOX5 to maintain both SAM and RAM stem cell homeostasis respectively (Zhou et al., 2015). Thus, there is a need to examine, in detail, if RAM and SAM share other gene regulatory network. In this respect, the key regulators that control root meristem activity and patterning are of special interest since their functions in the shoot have not yet been studied.

5. Aims of this study

This study employs a combination of genetics, transgenesis and expression studies to investigate the role of the SHR regulatory network in coordination of shoot apical meristem (SAM) growth and initiation of lateral organ primordia (LOP). The major assumption underlying this approach was that core functions are conserved between root and shoot meristems, and that genes and gene regulatory networks responsible for root apical meristem (RAM) patterning also act in the SAM.

This work reveals that the SHR regulatory network is carries out key functions in SAM patterning. I could show that SHR expression is directly controlled by auxin dependent transcription factors within the different functional domains of the SAM. Using transcriptional and translational reporter lines, I found that the expression patterns of the four key actors of the SHR pathway, i.e., SHR, SCR, SCL23 and JKD, are covering all the functional domains of the SAM, and that the cell cycle regulator *CYCLIND6;1 (CYCD6;1)* is exclusively expressed where all 4 TFs are present.

Additionally, I found that the transcription factor SCL23, a target gene regulated by SHR, physically interacts with the stem cell regulating TF WUS to promotes stem cell homeostasis in the SAM, and that SCL23 expression is negatively regulated by the CLV signalling pathway. Together, these findings uncover a previously uncharacterised function of the SHR regulatory network in the regulation of Arabidopsis SAM growth and development, and provides new insights into the understanding of patterning in the SAM.

6. The SHR-SCR module coordinates shoot meristem development and auxin dependent organ initiation

This manuscript is in preparation for submission

Authors:

Elmehdi Bahfid[1], Imke Bradtmöller[1], Ann Marlene Thies[1], Thi Thuy Oanh Nicole Nguyen[1], Yvonne Stahl[1], Ikram Blilou[2], Rüdiger Simon[1]

Affiliation:

[1]Institute for Developmental Genetics, Heinrich Heine University, Building 26.14.00.071, 40225 Düsseldorf, Germany

[2]Laboratory of Plant Cell and Developmental Biology, Division of Biological and Environmental Sciences and Engineering, 4700 King Abdullah University of Science and Technology, Ibn Al Haytham Bldg.2, room 3274, Thuwal 23955-6900, Kingdom of Saudi Arabia

Author contributions:

Elmehdi Bahafid, Ikram Blilou and Rüdiger Simon initiated and designed the project. Elmehdi Bahafid conducted all experiments and data analyses, besides the following: Imke Bradtmöller, Ann Marlene Thies and Thi Thuy Oanh Nicole Nguyen performed part of the cloning (Fig.11 A; Suppl Fig. 7A) and the imaging (Fig.11 C; Suppl Fig. 7C).

Elmehdi Bahafid wrote the manuscript which was overworked by Rüdiger Simon.

6.1. Abstract

Unlike animals, plants maintain a capacity to produce new organs post-embryonically throughout their entire life cycle. This is due to stem cells present in the shoot and the root apical meristems (SAM and RAM, respectively). In the SAM, stem cells are located in the central zone (CZ) where they divide slowly. Stem cell daughters are displaced laterally and enter the peripheral zone (PZ). Here, their mitotic activity increases, and lateral organ primordia (LOP) are formed. How the spatial arrangement of these different domains is initiated and controlled during SAM growth and development, and how sites of LOP are determined in the PZ is not yet completely clear.

In the RAM, the GRAS family transcription factor SHORT-ROOT (SHR) acts as a master regulator of the signalling pathways that control maintenance of the root stem cell niche and formation of the ground tissue (GT) layers. We hypothesized that SHR could perform a similar role in the SAM, and show here that SHR, together with its target transcription factors SCARECROW (SCR), SCARECROW-LIKE23 (SCL23) and JACKDAW (JKD), controls shoot meristem size by regulating cell division rates, and promotes LOP formation. SHR, SCR, SCL23 and JKD are expressed in distinct patterns, with an overlapping area where they all physically interact to activate *CYCLIND6;1* (*CYCD6;1*) expression. Upregulation of *SHR* expression in the PZ depends on auxin acting through the transcription factor MONOPTEROS (MP) and auxin response elements in the *SHR* promoter. We find that the SHR target SCL23 physically interacts with WUS, a key regulator of stem cell maintenance. Both SCL23 and WUS expression is subject to negative feedback regulation from stem cells through the CLV pathway.

Together, we show here how SHR signaling can serve to link auxin dependent LOP initiation in the PZ with stem cell maintenance in the CZ of the SAM.

6.2. Introduction

In multicellular plants and animals, stem cells are the source of all tissues and organs. In contrast to most animals, plants can continuously produce new organs throughout their life span. This process depends on the activity of pluripotent stem cells embedded in their shoot and root apical meristems (SAM and RAM, respectively).

In the SAM, stem cells are located in the central zone (CZ) at the tip of the meristem. Directly underneath it lies the organizing center (OC), which is required for the stem cell maintenance. In the CZ stem cells have a low mitotic activity, and their descendants are continuously displaced into the peripheral zone (PZ). Here, they start dividing faster to provide the founder cells for lateral organ primordia (LOP) that will develop later at the flank of the SAM (Gaillochet et al., 2015). How the communication between these distinct functional domains is coordinated to balance stem cell proliferation in the center and organ formation at the periphery of the SAM is still not completely understood. This is in contrast to the RAM where the gene networks regulating the spatial arrangement of the different tissue types are better known.

In the RAM, a member of the plant-specific GRAS transcription factor (TF) family, SHORT-ROOT (SHR) has a key regulatory role in the maintenance of the root stem cell niche identity and tissue patterning (Pysh et al., 1999, Lee et al., 2008, Long et al., 2015b). Plants lacking functional SHR show a ‘short root´ phenotype with roots having only one ground tissue layer instead of the typical two (Di Laurenzio et al., 1996, Scheres et al., 1995, Pysh et al., 1999).

SHR is transcribed in the stele and moves one cell layer outward where it interacts with two other GRAS domain TFs SCARECROW (SCR) and SCARECROW-LIKE23 (SCL23), and with the BIRD/INDETERMINATE DOMAIN TF JACKDAW (JKD) (Long et al., 2015b, Long et al., 2017). The resulting complex promotes the asymmetric cell division (ACD) of the Cortex-Endodermis Initial/daughter (CEI/CEID) by directly activating the expression of *CYCLIND6;1* (*CYCD6;1*) to instruct ground tissue (GT) development (Long et al., 2015a, Long et al., 2015b, Long et al., 2017, Di Laurenzio et al., 1996, Helariutta et al., 2000, Nakajima et al., 2001).

Both *SHR* and *SCR* are expressed in the SAM, but little is known about their function in this context (Wysocka-Diller et al., 2000, Gardiner et al., 2011, Wang et al., 2011, Cui et al., 2014). Here, we asked if the SAM patterning is controlled by a similar mechanism present in the RAM to coordinate stem cell maintenance in the center with organ initiation in the periphery of the SAM.

In the SAM, stem cell maintenance depends on the homeodomain transcription factor, WUSCHEL (WUS) (Laux et al., 1996, Zhang et al., 2017). The expression of *WUS* transcript is limited to OC. While the transcript is immobile, WUS protein moves from the OC to the CZ,

where stem cells are located, via plasmodesmata to directly activate the transcription of the short signalling peptide CLAVATA3 (CLV3) (Mayer et al., 1998, Yadav et al., 2011, Daum et al., 2014). In turn, CLV3 acts to limit *WUS* expression to the OC via a system of receptor-like kinases and co-receptors: CLAVATA1 (CLV1), CLAVATA2 (CLV2), CORYNE (CRN) and BARELY ANY MERISTEM (BAM) (Bleckmann & Simon, 2009, Clark et al., 1997, Fletcher et al., 1999, Nimchuk et al., 2015, Ohyama et al., 2009). The resulting WUS-CLV3 negative feedback circuit controls stem cell homeostasis in the SAM (Brand et al., 2000, Schoof et al., 2000). Recently it was shown that WUS interacts with the GRAS family transcription factors HAIRY MERISTEM 1 and 2 (HAM1/2) to determine the apical-basal polarity of CLV3 expression in the CZ (Han et al., 2020).

At the flanks of SAM where the lateral organ primordia are initiated, this event is preceded by an establishment of a local maximum of the plant hormone auxin (Benková *et al.*, 2003, Heisler *et al.*, 2005, Vernoux *et al.*, 2011a). An auxin maximum is generated by the auxin efflux carrier PIN-FORMED1 (PIN1) through polar auxin transport (Friml et al., 2004, Gälweiler et al., 1998). The transcriptional auxin signaling is carried out by the Auxin/Indole-3-acetic acid (Aux/IAA) repressor proteins that under low auxin conditions dimerize with auxin response factors (ARFs) and repress their activity (Mockaitis & Estelle, 2008). ARFs bind DNA at the promoters of their target genes via an auxin response element (AuxRE) (Boer *et al.*, 2014). An increase in auxin levels triggers the formation of a complex between Aux/IAA and TIR1/AFB leading to the degradation of Aux/IAA and the release of the ARFs important for the regulation of the expression of auxin response genes (Paque & Weijers, 2016).

Auxin-dependent lateral organ initiation is mediated by AUXIN RESPONSE FACTOR 5/MONOPTEROS (ARF5/MP) (Berleth & Jürgens, 1993, Hardtke & Berleth, 1998). MP plays a crucial role in the initiation of flower primordia as the *mp* mutant lacks flowers and forms naked stem (Yamaguchi et al., 2013). MP directly induces the expression of its direct target gene *LEAFY (LFY)* a plant-specific transcription factor that plays a role in lateral organ primordia initiation and act as a key regulator for the organ primordium fate specification (Schultz & Haughn, 1991, Weigel et al., 1992, Yamaguchi et al., 2013, Wu et al., 2015). Additionally, the transcripts of *SHR* and *SCR* are strongly reduced in *mp* mutant embryo (Möller et al., 2017). These data suggest that MP regulates the expression of *SHR* and *SCR*.

Here, we provide insight that addresses the question of how organ initiation at the periphery is coordinated with stem cell maintenance in the center of the SAM. We present a detailed functional characterization of the SHR-SCR-SCL23-JKD regulatory network in the SAM. We show that SHR, SCR, SCL23 and JKD are expressed in the SAM in different expression domains with complementary and overlapping patterns and together, they cover all the

functional domains of the SAM. Interestingly, the overlapping region of the four TFs coincide with the expression of *CYCLIND6;1 (CYCD6;1).*

We further demonstrate that auxin acts upstream to SHR and SCR. It regulates SHR and SCR in the organ primordia by controlling the SHR expression via MP, and we also suggest that SHR may act upstream of *LFY* to promote lateral organ formation.

Finally, we reveal that the SHR-SCR-SCL23 regulatory network operates through elaborate communication among different functional domains of the SAM to coordinate primordium initiation at the periphery with stem cell maintenance in the center by interacting with the WUS-CLV3 circuit.

This work provides a new molecular framework in the SAM, where SHR regulatory network balances between lateral organ initiation and stem cell maintenance by controlling cell fate in the different domains within the SAM in an auxin level dependent manner.

6.3. Materials and methods

6.3.1. Chemicals

Tab. 1: Chemicals used in this study

Chemical	Manufacturer
17-β-Estradiol	Sigma Aldrich, Steinheim, Germany
6x DNA Loading Dye	Thermo Fisher Scientific, Braunschweig, Germany
Acetosyringon	Carbolution Chemicals, Saarbrücken, Germany
BASTA® (non-selective herbicide)	Bayer CropScience
BSA	New England Biolabs Inc., Ipswich, USA
Carbenicillin disodium salt	Carl Roth
D(+)-Saccharose	Carl Roth GmbH, Karlsruhe, Germany
DL-phosphinothricin (PPT)	Duchefa Biochemie bv
DNA Ladder GeneRµler 1 kb	Thermo Fisher Scientific, Braunschweig, Germany
Ethanol (EtOH)	Sigma Aldrich, Steinheim, Germany
Gentamicin sulfate	Sigma-Aldrich (Merck)
Glucose-Monohydrate	Caesar & Loretz, Hilden, Germany
Hygromycin B	Duchefa Biochemie bv
Hypochlorite acid (~37%)	Thermo Fischer Scientific
Isopropanol	Heinrich-Heine-Universität
Kanamycin monosulfate	Duchefa Biochemie bv
Magnesium chloride x 6H2O	Grüssig GmbH
Magnesiumchloride; Natriumchloride	VWR, Darmstadt, Germany
MES hydrate	SIGMA Aldrich, Steinheim, Germany
Murashige & Skoog medium	Ducheta Biochemie, Haarlem, Netherlands
my-Budget Standard Agarose	Bio-Budget Technologies GmbH, Krefeld, Germany
peqGreen	peqlab, Erlangen, Germany
Plant Agar	Duchefa Biochemie, Haarlem, Netherlands
Potassium hydroxide	Sigma-Aldrich (Merck)
Propidium iodide	Thermo Fischer Scientific
Rifampicin	TCI

Silwet	Heinrich-Heine-Universität
Sodium chloride	Carl Roth
Sodium dodecyl sulfate (SDS)	Sigma-Aldrich (Merck)
Spectinomycin HCl pentahydrate	Duchefa Biochemie bv
Tetracycline	Sigma-Aldrich (Merck)
Tryptone	gibco
Tween 20	Serva, Heidelberg, Germany

6.3.2. Kits

Tab. 2: Kits used in this study

Kit	**Producer**	**Use**
Luciferase® Reporter Assay System	Promega GmbH, Walldorf, Germany	Luciferase Assay
NucleoSpin® Plasmid	Thermo Fisher Scientific, Braunschweig, Germany	Plasmid extraction
peqGOLD Cycle-Pure Kit	PEQLAB Biotechnologie GmbH, Erlangen, Germany	Clean-up PCR products
peqGOLD Plasmid Miniprep	PEQLAB Biotechnologie GmbH, Erlangen, Germany	Plasmid extraction
Plasmid Midi-Kit	QIAGEN Hilden, Germany	Plasmid extraction
RNeasy Mini kit	QIAGEN Hilden, Germany	RNA extraction
Zero Blunt Cloning Kit	Thermo Fisher Scientific, Braunschweig, Germany	Cloning of pBlunt vectors

6.3.3. Enzymes

Tab. 3: Enzymes used in this study

Enzyme	Producer
BSA1 (ECORI)	Thermo Fisher Scientific, Braunschweig, Germany
Pfuμltra High-Fidelity DNA polymerase	Agilent, Santa Clara, USA
Phusion® High-Fidelity DNA Polymerase	Thermo Fisher Scientific, Braunschweig, Germany
T4-Ligase	Thermo Fisher Scientific, Braunschweig, Germany
Taq-DNA-Polymerase	Made in the lab according to (Pluthero, 1993)
Universal SYBR® Green Supermix	Bio-Rad

6.3.4. Molecular size standards

Tab. 4: Molecular size standards

Standard	Band size (bp)	Producer
GeneRuler™ 1kb DNA Ladder	10000, 8000, 6000, 5000, 4000, 3500, 3000, 2500, 2000,1500, 1000, 750, 500, 250 [bp]	Thermo Fisher Scientific, Waltham, USA
GeneRuler™ 50bp DNA Ladder	50, 100, 150, 200, 250, 300, 400, 500, 600, 700, 800, 900, 1031 [bp]	Thermo Fisher Scientific, Waltham, USA

6.3.5. Primers

Tab. 5: primers used for cloning.

Purpose	Primer	Sequence
SHR promoter cloning	EB-pSHR-F	AAAGGTCTCAACCTGAAGCAGAGCGTGGGGTTTC
	EB-pSHR-R	TTTGGTCTCATGTTTTTTAATGAATAAGAAAATGAATAGAAGAAAGGGGG
	EB-pSHR-BsaI-site-F	GTTCAAAAGTGGTCCCTTCTCTCTC
	EB-pSHR-BsaI-site-R	GAGAGAGAAGGGACCACTTTTGAAC
SHR CDS cloning	EB-SHR-CDS-F	AAAGGTCTCAGGCTTAATGGATACTCTCTTTAGACTAGTCAG
	EB-SHR-CDS-R	TTTGGTCTCACTGACGTTGGCCGCCACGCACTAG
SCR CDS cloning	EB-SCR-CDS-F	AAAGGTCTCAGGCTTAATGGCGGAATCCGGCGATTTC
	EB-SCR-CDS-R	TTTGGTCTCACTGAAGAACGAGGCGTCCAAGCTGAAG
	EB-SCR-CDS-BsaI-site-1-F	GCCATTATCAGGGACCTTATCC
	EB-SCR-CDS-BsaI-site-1-R	GGATAAGGTCCCTGATAATGGC
	EB-SCR-CDS-BsaI-site-2-F	GAAAATGGTATCTGCGTTTCAG
	EB-SCR-CDS-BsaI-site-2-R	CTGAAACGCAGATACCATTTTC
JKD CDS cloning	EB-JKD-CDS-F	AAAGGTCTCAGGCTTAATGCAGATGATTCCAGGAGATCC
	EB-JKD-CDS-R	TTTGGTCTCACTGAACCCAATGGAGCAAACCTTGCG
	EB-JKD-CDS-BsaI-site-F	GCCCTTGGTGACCTCACTGG
	EB-JKD-CDS-BsaI-site-R	CCAGTGAGGTCACCAAGGGC
SCL23 CDS cloning	EB-SCL23-F	AAAGGTCTCAGGCTTAATGACTACAAAACGCATAGACAG
	EB-SCL23-R	TTTGGTCTCACTGAATCGAACGGCTGAGATTTCC
MP CDS cloning	EB-MP-GG-F	AAAGGTCTCAGGCTTAATGATGGCTTCATTGTCTT
	EB-MP-GG-R	TTTGGTCTCACTGATGAAACAGAAGTCTTAAGATC
pSHR site-	EB-pSHRΔmAuxRE1-F	CTTTGTATCGAGCCAAACGAG

directed mutagen-esis	EB-pSHRΔmAuxRE1-R	CTCGTTTGGCTCGATACAAAG
	EB-pSHRΔmAuxRE2-F	TTCACATGGCTCTATGTTACTATG
	EB-pSHRΔmAuxRE1-R	CATAGTAACATAGAGCCATGTGAA
	EB-pSHRΔmAuxRE1-2-F	CTTTGTATCGAGCCAAACGAG
	EB-pSHRΔmAuxRE1-2-R	CTCGTTGTGCTCGATACAAAG
	EB-pSHRΔmAuxRE2-2-F	ATATTCACATGGGAGTATGTTACTATGTAAATG GTG ACC
	EB-pSHRΔmAuxRE2-2-R	GGTCACCATTTACATAGTAACATACTCCCATGTGA ATAT

Tab. 6: Primers used for qRT-PCR.

Primer name	**Sequence**
EB-RT-SHR-F	GATATCGAGTTTCCGACGGT
EB-RT-SHR-R	CGAAGCAAACCCTAAACCAT
EB-RT-SCR-F	GTAACCCAAATCTCGGTGCT
EB-RT-SCR-R	TTGCTGTTGTGGAGGAGAAG
EB-RT-JKD-F	ATCAACCTGGCACTCCAGA
EB-RT-JKD-R	GCAGATCTCGCACACGAAT
EB-RT-LFY-F	TGATGCTCTCTCCCAAGAAGA
EB-RT-LFY-R	CTTGACCTGCGTCCCAGTA
EB-SAND-F	AACTCTATGCAGCATTTGATCCACT
EB-SAND-R	TGATTGCATATCTTTATCGCCATC
EB-TIP41-F	GTGAAAACTGTTGGAGAGAAGCAA
EB-TIP41-R	TCAACTGGATACCCTTTCGCA

Tab. 7: primers used for genotyping.

Primer name	Sequence
EB-scl23-2-LP	ATGACTACAAAACGCATAGACAG
EB-scl23-2-RP	TTTGGTCTCACTGAATCGAACGGC
LBb1.3	ATTTTGCCGATTTCGGAAC
mp-S319-LP	CCTGGAAACTGATGAGCTGAC
mp-S319-RP	CCTTCTTCACTCATCTGCTGG
LBb1.3	ATTTTGCCGATTTCGGAAC
jkd-4-F	GGATGAAAGCAATGCAAAACA
jkd-4-R	AATGTCGGGATGATGAACTCC
RB	TCAAACAGGATTTTCGCCTGCT
scr-4F	CTGCTTCACCTACTGTATGGG
scr-4R	GGGTCAGAGGAAGAGGAAGG
	Restriction enzyme: *Eco*57M which should not cut in the mutant
shr-2-R	AAATCGAACTTGCGAATTCCT
shr-2-L	CGCTCAACGAGCTCTCTTCT
shr-2ins	CAGCAAGACAAGATGGGTCA
wus-7-F	CCGACCAAGAAAGCGGCAACA
wus-7-R	AGACGTTCTTGCCCTGAATCTTT
	Restriction enzyme: *Xm*NI which should cut in the mutant

6.3.6. Plasmids

Tab. 8: Entry plasmids used in this study.

Name	Description	Backbone	Reference
pSHR	SHR promoter 2.5 Kb upstream from transcription start	pBlunt	This study
SHR CDS	SHR coding sequence	pGGC000	This study
SCL23 CDS	SCL23 coding sequence	pGGC000	This study
linker NLS (pGGD007)	NUCLEAR LOCALIZATION SIGNAL	pGGD000	Lampropoulos et al., 2013
mVenus (pRD43)	mVenus	pGGD000	Rebecca Burkhart
FLUC	Firefly luciferase	pGGC000	Greg Denay
mVenus (pRD42)	mVenus	pGGC000	Rebecca Burkhart
GUS (pGGC051)	E. coli ß-GLUCURONIDASE	pGGC000	Lampropoulos et al., 2013
MP CDS	MP coding sequence	pGGC000	This study
35S promoter (pGGA004)	Cauliflower mosaic virus 35S promoter	pGGA000	Lampropoulos et al., 2013
RPS5A promoter (pGGA012)	RIBOSOMAL PROTEIN 5A promoter	pGGA000	Lampropoulos et al., 2013
UBIQ10 promoter (pGGA006)	UBIQUITIN10 promoter	pGGA000	Lampropoulos et al., 2013
d-dummy (pGGD002)	d-dummy	pGGD000	Lampropoulos et al., 2013
tCLV3	CLV3 terminator 1257 bp downstream of transcription stop	pGGE000	Jenia Schlegel
UBQ10 terminator (pGGE009)	UBQ10 terminator	pGGE000	Lampropoulos et
BastaR (pGGF008)	pNOS:BastaR:tNOS	pGGF000	Lampropoulos et al., 2013
GR (pRD64)	Hormone-binding domain of the glucocorticoid receptor	pGGD000	Rebecca Burkhart
pCLV3	CLV3 promoter 1480 bp upstream from transcription start	pGGA000	Jenia Schlegel

omega-element (pGGB002)	Omega- element	pGGB000	Lampropoulos et al., 2013

Tab. 9: Destination plasmids used in this study.

Name of construct	Promoter	N-Tag	CDS	C-Tag	Terminator	Resistance
pCLV3:SCL23-mVenus	pCLV3	Ω- element (pGGB002)	SCL23 CDS	mVenus	tCLV3	BastaR (pGGF008)
pRPS5A:SCL23-mVenus	pRPS5A	Ω- element (pGGB002)	SCL23 CDS	mVenus	tUBQ10 (pGGE009)	BastaR (pGGF008)
pUBIQ10:SCL23-mVenus	pUBIQ10	Ω- element (pGGB002)	SCL23 CDS	mVenus	tUBQ10 (pGGE009)	BastaR (pGGF008)
pUBIQ10:MP-GR	pUBIQ10	Ω- element (pGGB002)	MP CDS	GR	tUBQ10 (pGGE009)	BastaR (pGGF008)
p35S:GUS	p35S	Ω- element (pGGB002)	GUS	d-dummy (pGGD002)	tUBQ10 (pGGE009)	BastaR (pGGF008)
p35S:MP	p35S	Ω- element (pGGB002)	MP CDS	d-dummy (pGGD002)	tUBQ10 (pGGE009)	BastaR (pGGF008)
pSHR:mV-NLS	pSHR	Ω- element (pGGB002)	mVenus	linker NLS (pGGD007)	tUBQ10 (pGGE009)	BastaR (pGGF008)
pSHRΔmAuxRE1:mV-NLS	pSHRΔmAuxRE1	Ω- element (pGGB002)	mVenus	linker NLS (pGGD007)	tUBQ10 (pGGE009)	BastaR (pGGF008)
pSHRΔmAuxRE2:mV-NLS	pSHRΔmAuxRE2	Ω- element (pGGB002)	mVenus	linker NLS (pGGD007)	tUBQ10 (pGGE009)	BastaR (pGGF008)
pSHRΔmAuxRE1+2:mV-NLS	pSHRΔmAuxRE1+2	Ω- element (pGGB002)	mVenus	linker NLS (pGGD007)	tUBQ10 (pGGE009)	BastaR (pGGF008)
pSHRΔmAuxRE1-2:mV-NLS	pSHRΔmAuxRE1-2	Ω- element (pGGB002)	mVenus	linker NLS (pGGD007)	tUBQ10 (pGGE009)	BastaR (pGGF008)

pSHRΔmAuxRE2-2:mV-NLS	pSHRΔmAuxRE2-2	Ω- element (pGGB002)	mVenus	linker NLS (pGGD007)	tUBQ10 (pGGE009)	BastaR (pGGF008)
pSHRΔmAuxRE1-2+2-2:mV-NLS	pSHRΔmAuxRE1-2+2-2	Ω- element (pGGB002)	mVenus	linker NLS (pGGD007)	tUBQ10 (pGGE009)	BastaR (pGGF008)

Tab. 10: Destination plasmids used for luciferase assay.

Name of construct	Promoter	N-Tag	CDS	C-Tag	Terminator	Resistance
pSHR:FLUC	pSHR	Ω- element (pGGB002)	FLUC	d-dummy (pGGD002)	tUBQ10 (pGGE009)	BastaR (pGGF008)
pSHRΔmAuxRE1:FLUC	pSHRΔmAuxRE1	Ω- element (pGGB002)	FLUC	d-dummy (pGGD002)	tUBQ10 (pGGE009)	BastaR (pGGF008)
pSHRΔmAuxRE2:FLUC	pSHRΔmAuxRE2	Ω- element (pGGB002)	FLUC	d-dummy (pGGD002)	tUBQ10 (pGGE009)	BastaR (pGGF008)
pSHRΔmAuxRE1+2:FLUC	pSHRΔmAuxRE1+2	Ω- element (pGGB002)	FLUC	d-dummy (pGGD002)	tUBQ10 (pGGE009)	BastaR (pGGF008)
pSHRΔmAuxRE1-2:FLUC	pSHRΔmAuxRE1-2	Ω- element (pGGB002)	FLUC	d-dummy (pGGD002)	tUBQ10 (pGGE009)	BastaR (pGGF008)
pSHRΔmAuxRE2-2:FLUC	pSHRΔmAuxRE2-2	Ω- element (pGGB002)	FLUC	d-dummy (pGGD002)	tUBQ10 (pGGE009)	BastaR (pGGF008)
pSHRΔmAuxRE1-2+2-2:FLUC	pSHRΔmAuxRE1-2+2-2	Ω- element (pGGB002)	FLUC	d-dummy (pGGD002)	tUBQ10 (pGGE009)	BastaR (pGGF008)

6.3.7. Plants

Tab. 11: Mutants used in this study.

Lines	Reference
scr-4	Fukaki et al. 1998
jkd-4	Welch et al., 2007
scr-3	Fukaki et al., 1996b
shr-2	Nakajima et al. 2001
scl23-2	Lee et al.,2008
wus-7	Graf et al., 2010
wus-am	From Jan lohmann
mps-319	Schlereth et al., 2010
mp-b4149	Weijers et al., 2005
lfy-12	Huala and Sussex, 1992
clv3-9	Simon et al, 2003

Tab. 12: transgenic lines used in this study.

Lines	**Plant Resistance**	**Reference**
pSHR:mV-NLS	Basta	This study
pSHRΔmAuxRE1:mV-NLS	Basta	This study
pSHRΔmAuxRE2:mV-NLS	Basta	This study
pSHRΔmAuxRE1+2:mV-NLS	Basta	This study
pSHRΔmAuxRE1-2:mV-NLS	Basta	This study
pSHRΔmAuxRE2-2:mV-NLS	Basta	This study
pSHRΔmAuxRE1-2+2-2:mV-NLS	Basta	This study
pCLV3:SCL23-mVenus	Basta	This study
pRPS5A:SCL23-mVenus	Basta	This study
pUBIQ10:SCL23-mVenus	Basta	This study
pUBIQ10:MP-GR	Basta	This study
PlaCCI	Kanamycin	Desvoyes et al., 2020

pSHR:mScarlet-SHR	-	Ikram Blilou
pSHR:YFP-SHR	Basta	Long et al, 2017
pSCR:SCR-RFP	hyg	Long et al, 2017
pSCR:SCR-YFP	basta	Long et al, 2017
pSHR:SHR-YFP	Basta	Long et al, 2017
pJKD:mRFP-YFP	norf	Long et al, 2017
pJKD:JKD-YFP	Basta	Long et al, 2017
pSCL23:SCL23-YFP	Kanamycin	Long et al. 2015a
pSCL23:H2B-YFP	Kanamycin	Long et al. 2015a
pCYCD6;1:GFP	Basta	Sozzani et al., 2010
pSCR:H2B-YFP	Kanamycin	Heidstra et al, 2004
pPIN1:PIN1-GFP	Kanamycin	Benkova et al., 2003
pSHR:nTdTOMATO	-	Möller et al, 2017
pMP:MP-GFP	Kanamycin	Schlereth et al, 2010
pLFY:LFY-GFP	kanamycin	Wu et al., 2003
R2D2	kanamycin	Liao et al, 2015
pDR5v2:3xYFP-N7	Basta	Heisler et al, 2005
pWUS:3xVenus-NLS/pCLV3-mCherry-NLS	Kanamycin	Pfeiffer et al, 2016
pCYCD1,1-GFP	-	Ikram Blilou
pCYCD3,2-GFP	-	Ikram Blilou
pCYCD3,1-GFP	-	Ikram Blilou
pCYCD5,1-GFP	-	Ikram Blilou
pCYCD7,1-GFP	-	Ikram Blilou
pCYCD2,1-GFP	-	Ikram Blilou
pCYCD3,3-GFP	-	Ikram Blilou
pCYCB1,1-GFP	Kanamycin	Ikram Blilou

6.3.8. Plant material and growth conditions

Arabidopsis thaliana plants were grown on soil in climate chambers under long day (LD) conditions (16 h light / 8 h dark) at 21 °C. Most plants used in this study (Tab. 11 and Tab. 12) were in the Columbia (Col-0) background, except for: *scr-4* (WS) (Fukaki et al., 1998) and *wus*-7 (Graf et al., 2010) in *Landsberg Erecta* (Ler.) background.

6.3.9. Plasmid construction and plant transformation

The entry plasmids in this study (Tab. 8) were generated by gDNA or cDNA sequences that were amplified with Phusion High-Fidelity PCR polymerase using primers described in Tab. 3. All destination vectors in this study (Tab. 9 and Tab. 10) were generated using the GreenGate cloning system (Lampropoulos *et al.*, 2013).

Entry plasmid containing SHR promoter sequence (2.5 KB) was used as a template to create different promoter mutants using the QuikChange II kit according to manufacturer's protocol (Agilent Technologies). Mutagenic mismatch primers are listed in Tab. 5. all the clones were confirmed by sequencing.
Arabidopsis thaliana wildtype (Col-0) plants were transformed with *Agrobacterium tumefaciens* (strain GV3101 pMP90 pSoup) containing the respective destination vectors using the floral dipping method (Clough & Bent, 1998). Transgenic plants were initially selected on the appropriate antibiotic in the T1 generation. Homozygous T2 plants were identified through confirmation in the T3 generation. Several independent lines were analyzed and a representative line was selected for further work.
Nicotiana benthamiana plants were grown 4 – 5 weeks in the greenhouse and subsequently used for transient leaf epidermis cell transformation.

6.3.10. *Nicotiana benthamiana* infiltration

Agrobacterium tumefaciens strains (strain GV3101 pMP90 pSoup) harbouring relevant reporter constructs were cultured overnight with shaking at 28 °C in 5 ml dYT (double Yeast Tryptone, 1.6 % w/v tryptone, 1 % w/v yeast extract, 0.5 % w/v NaCl) with appropriate antibiotics. Cell cultures were adjusted to an optical density (OD_{600}) of 0.3 and then harvested by centrifugation at 4000 x g for 10 min. The pellet was resuspended in infiltration buffer (5 % w/v sucrose, 150 µM acetosyringone, 0.01 % v/v Silwet) and incubated for 2 h at 4 °C.

For coexpression of two transgenes, the corresponding transformed *A. tumefaciens* were mixed equally. The resuspensions were infiltrated into the abaxial leaf surface of the 3-4 weeks old *N. benthamiana* using a needle-less syringe. Plants transformed with constructs under the control of the 35S promotor were used for analyses 4 days after infiltration.

6.3.11. Chemical treatments

For hormone and dexamethasone treatments, plants were grown in soil. For RNA isolation experiments, *pSHR:SHR-YFP*, *pSCR:SCR-YFP* and *pCYCD6;1:GFP* expression analysis following auxin and auxin transport inhibitor treatment were performed by dipping 30-day-old plants inflorescence once in 10 µM (IAA or 2,4 D) once or with 100 µM NPA twice (at 0 hr and 7 hr). For dexamethasone treatment *pUBIQ1:MP-GR* inflorescence meristems were treated with 10 µM DEX only once and were imaged 5 hours after treatment.

6.3.12. Promoter mVenus activity in *Nicotiana benthamiana*

N. benthamiana leaves were co-transformed with different *pSHR:mVenus-NLS* and the effector plasmids *p35S:GUS* or *p35S:MP* (Tab. 9). Four days after infiltration, the leaves were processed for further analysis using imaging with a Zeiss LSM780 using same settings for all conditions.

6.3.13. Luciferase assay in *Nicotiana benthamiana*

The different reporter constructs with firefly luciferase reporter (FLUC) under the control of the different versions of *SHR* promoter (Tab. 10) were co-infiltrated into *N. benthamiana* leaves together with the effector plasmids *p35S:GUS* or *p35S:MP* (Tab. 9). Luciferase activities were measured four days after infiltration with the NightOwl luminescence system (Berthold). As substrate for the luciferase reaction, 5 mM D-Luciferin potassium salt solution was used.

6.3.14. Image acquisition and analysis

All confocal images were obtained by using a Zeiss LSM 780 confocal microscope (40× water immersion objective, Zeiss C-PlanApo, NA 1.2). For time series analysis, settings were established in the beginning on mock samples and were kept standard during the experiment. Shoot meristems were manually dissected by cutting of the stem, removing the flowers, and were stained with 1 mg/ml DAPI or 5mM propidium iodide (PI). Individual populations of 3 to 30 plants were analyzed.

Green fluorescence was excited with an argon laser at 488 nm and emission was detected at 490 – 530 nm, yellow was excited with an argon laser at 514 nm and emission was detected at 520 – 550 nm, and red was excited with Diode-pumped solid state (DPSS) lasers at 514 nm and detected at 570 – 650 nm. PI was excited at 561 nm by DPSS lasers and detected by PMTs at 590 – 650 nm. DAPI was excited at 405 nm with a laser diode and detected at 410 – 480 nm.

6.3.15. FRET-Acceptor-Photobleaching (APB)

N. benthamiana leaf epidermal cells were examined using a Zeiss LSM 780 confocal microscope (40× Water immersion objective, Zeiss C-PlanApo, NA 1.2). FRET was measured via mVenus fluorescence intensity increase after photobleaching of the acceptor mCherry (Bleckmann et al., 2010). The percentage change of the GFP intensity directly before and after bleaching was analyzed as E_{FRET}= (E_{FRET} = (mVenu $_{after}$ – $mVenus_{before}$)/$mVenus_{after}$ x 100. All photobleaching experiments were performed in the nucleus. The displayed data were obtained from at least 3 independent experiments.

6.3.16. FRET-FLIM interaction analysis in the SAM

In vivo FRET-FLIM experiments were measured using a Zeiss LSM 780 confocal microscope (40× Water immersion objective, Zeiss C-PlanApo, NA 1.2) equipped with a single-photon counting device (PicoQuant Hydra Harp 400) and a linear polarized diode laser (LDH-D-C-485).

YFP donor fluorophores was excited with a 485nm (LDH-D-C-485, 32MHz) pulsed polarized diode laser. Excitation power was adjusted to 1,5 µW. Emitted light was separated by a polarizing beam splitter Tau-SPADs (PicoQuant) and detected with a band-pass filter (520/35 AHF).

Images were acquired with a resolution of 256x256 pixel, zoom 8, a pixel size of 0.1µm and a dwell time of 12.6 µs. For each measurement 100 frames were taken and the intensity-weighted mean lifetimes τ (ns) were calculated using PicoQuant SymPhoTime64 software applying a bi-exponential fit. The displayed data were obtained from at least 5 independent experiments.

6.3.17. Quantitative real time PCR

For qRT-PCR, RNA was isolated from dissected inflorescence meristems using RNeasy Mini kit (Qiagen). First strand cDNA was synthesized with 1µg of RNA cDNA using the Superscript III Kit (Invitrogen). Quantitative real-time PCR was performed with 10-fold diluted cDNA using The SsoAdvancedTM Universal SYBR® Green Supermix (Bio-Rad). The mean and standard error were determined using three biological replicates with three technical replicates each. Expression levels were normalized to the references genes TIP41-like (At4g34270) and SAND-domain protein (AT2G28390) (Czechowski et al., 2005). Primers used are listed in Tab. 6. Calculation of the relative expression was performed according to Michael W. Pfaffl (Pfaffl, 2001).

6.3.18. Phenotypic analyses

Rosettes and plants were analyzed by taking photographs using Canon EOS 400D camera with an EF-S 60 mm Canon ZOOM lens) of plants growing on soil. Inflorescences were analyzed by taking pictures using stereo microscope (Nikon SMZ25). The inflorescence plastochron was obtained by calculating the average time separating the emergence of 2 successive flower above stage 15 emerging after plant bolting. For SAM area measurement, 30 DAG plants growing under LD conditions were used. The primary inflorescence was dissected and imaged using LSM 780. The SAM area measurement was done by Fiji.

6.3.19. Software

Microsoft Word, Excel, and PowerPoint software was used to organize experimental data. Images were analyzed and processed with ImageJ v 1.53c (Schneider et al., 2012) and Carl Zeiss ZEN 2011. All images were adjusted in “Brightness and Contrast”. Vector NTI (InvitrogenTM) was used for vector maps and sequence analysis. Databank gene research were performed on The Arabidopsis Information Resource (TAIR), (**http://www.arabidopsis.org/**). Indigo was used for the luciferase assay imaging. Statistical analyses and box plots were realized with GraphPad Prism v 8. For visualization.

Using the open-source software MorphoGraphX (MGX) software (**https://morphographx.org/**) (Barbier de Reuille et al., 2015) the surface of the meristem was extracted and the PI signal of the cell wall from layer 1 (L1) was projected and used for segmentation of the images to quantify number and size of cells. Cells were segmented manually. MorphographX analysis was performed according to standards defined in the user manual (Barbier de Reuille et al., 2015).

The visualisation and counting of nuclei expressing PlCCI (Desvoyes et al., 2020) was done with Imaris (version 9.1.2, Bitplane, Oxford Instruments plc).

Ratios for R2D2 were calculated as described previously (Bhatia et al., 2016). All Statistical analyses and data plotting were realized with GraphPad Prism v 8. All images for an experimental set were captured under identical microscope settings.

6.3.20. Transformation of *E. coli* and *A. tumefaciens*

Transformation of *Escherichia coli* (E. coli) was performed by heat shock at 42°C. Transformation of *Agrobacterium tumefaciens* (*A. tumefaciens*) was done with the thawing-freezing method as described by Hofgen and Willmitzer (Höfgen & Willmitzer, 1988).

6.3.21. Preparation of plasmid DNA

Plasmid DNA extraction from *E.coli* was performed with either the NucleoSpin® Plasmid or the peqGOLD Plasmid Mini Prep Kit 1 according to manufacturer's instructions.

6.3.22. Preparation of genomic DNA

Extraction of genomic DNA (gDNA) from *A. thaliana* was performed according to a modified protocol from Dellaporta, 1983 (Dellaporta et al., 1983).

6.3.23. Isolation of DNA fragments

Isolation and purification of DNA fragments was performed using peqGOLD Cycle-Pure Kit (Erlangen, Germany) according to manufacturer's instructions.

6.3.24. Isolation of total RNA from plant tissue

Isolation of total ribonucleic acid (RNA) from SAMs was performed with the RNeasy Plant Mini Kit according to manufacturer's instructions.

6.3.25. Synthesis of cDNA

Synthesis of complementary DNA (cDNA) from total RNA was performed with reverse transcription SuperScriptII according to manufacturer's instructions.

6.3.26. Measurement of DNA and RNA concentrations

Measurement of DNA and RNA concentrations was performed by absorption measurements with the spectrophotometer NanoDrop 2000c (Thermo Scientific).

6.3.27. Site directed mutagenesis

Site directed mutagenesis was performed with the QuikChangeII Site-Directed Mutagenesis Kit according to manufacturer's instructions.

6.3.28. Sterilization and stratification of seeds

Seeds in 1.5 ml tubes were surface sterilized with chlorine gas as described in Lindsey et al 2017 (Lindsey *et al.*, 2017). After sterilization seeds were then covered with 1 mL of 0,1 %

agarose and kept in the dark at 4°C for 2 days. After stratification, seeds were plated on GM in petri dishes to germinate and placed in the growth cabinet under continuous light at 21 °C.

6.3.29. Crossing of Arabidopsis plants

To generate multiple combinations of genotypes, flowers of the female plant were emasculated prior to fertility. Then pollen grains from the male plant was dusted on the stigma of the female plant.

6.3.30. Selection of transgenic Arabidopsis plants

Seeds of transformed *A. thaliana* plants were selected with antibiotics diluted in growth medium (BASTA 100 µg/ml, Hygromycin 20 µg/ml or Kanamycin 50 µg/ml).

6.4. Results

6.4.1. *SHR* and *SCR* regulate shoot meristem size and primordia initiation

In order to understand the regulatory roles of SHR and SCR in shoot meristem development, we analyzed the phenotypes of null mutant alleles of *SHR* (*shr-2*) and *SCR* (*scr-3* and *scr-4*). All mutants displayed a small rosette, dwarfed shoot phenotype and initiated fewer flowers compared to wild type (Fig. 1A-D; Suppl Fig. 1A-D). To assess the function of *SHR* and *SCR* in the SAM, we measured plastochrons and meristem sizes. The average time interval between the initiation of successive lateral organs (plastochron) were increased in the mutants (*shr-2, scr-3* and *scr-4*) compared to wild type, indicating a significant delay in the initiation of lateral organs in the mutants (Fig. 1M; Suppl Fig. 1A'-D'). Using confocal microscopy, we imaged the meristem of mutants and the WT (Fig. 1E-H) and measured the surface area of the SAM excluding organ primordia. We found it to be significantly reduced in the mutants (Fig. 1N). These results show that SHR and SCR may coordinate between cell division and lateral organ primordia initiation during SAM development.

To understand the cause for the reduction in SAM size, we analyzed both cell number and area on the surface of the SAM. Analysis of average cell surface areas showed no differences between mutants and wild type (Suppl Fig. 1E) however cell numbers were reduced in all mutants (Fig. 1O). Therefore, we investigated if there were any significant differences in cell proliferation rate between the wild type, *shr-2*, *scr-3* and *scr-4* at the SAMs contributing to the observed reduction in the SAM size. We used a plant cell cycle marker *PlaCCI* (Desvoyes et al., 2020) (Fig. 1I-L), an imaging tool combining the three reporters *pCDT1a:CDT1a-eCFP*, *pHTR13:HTR13-mCherry* and *pCYCB1;1:NCYCB1;1-YFP*, each of which individually marks the G1, S + G2 and mitotic (M) phases, respectively. In *shr-2*, *scr-3* and *scr-4* SAMs, the overall percentage of cells in G1 (labelled with CDT1a-CFP) was significantly increased compared to wild type (Fig. 1P; Suppl Fig. 1F), indicating a delay in progression through the cell cycle.

These results suggest that the lower cell division rate caused by delayed cell cycle progression during the loss of *SHR* or *SCR* function could account for the observed reduction in SAM size and delay in organ initiation in the peripheral zone of the meristem.

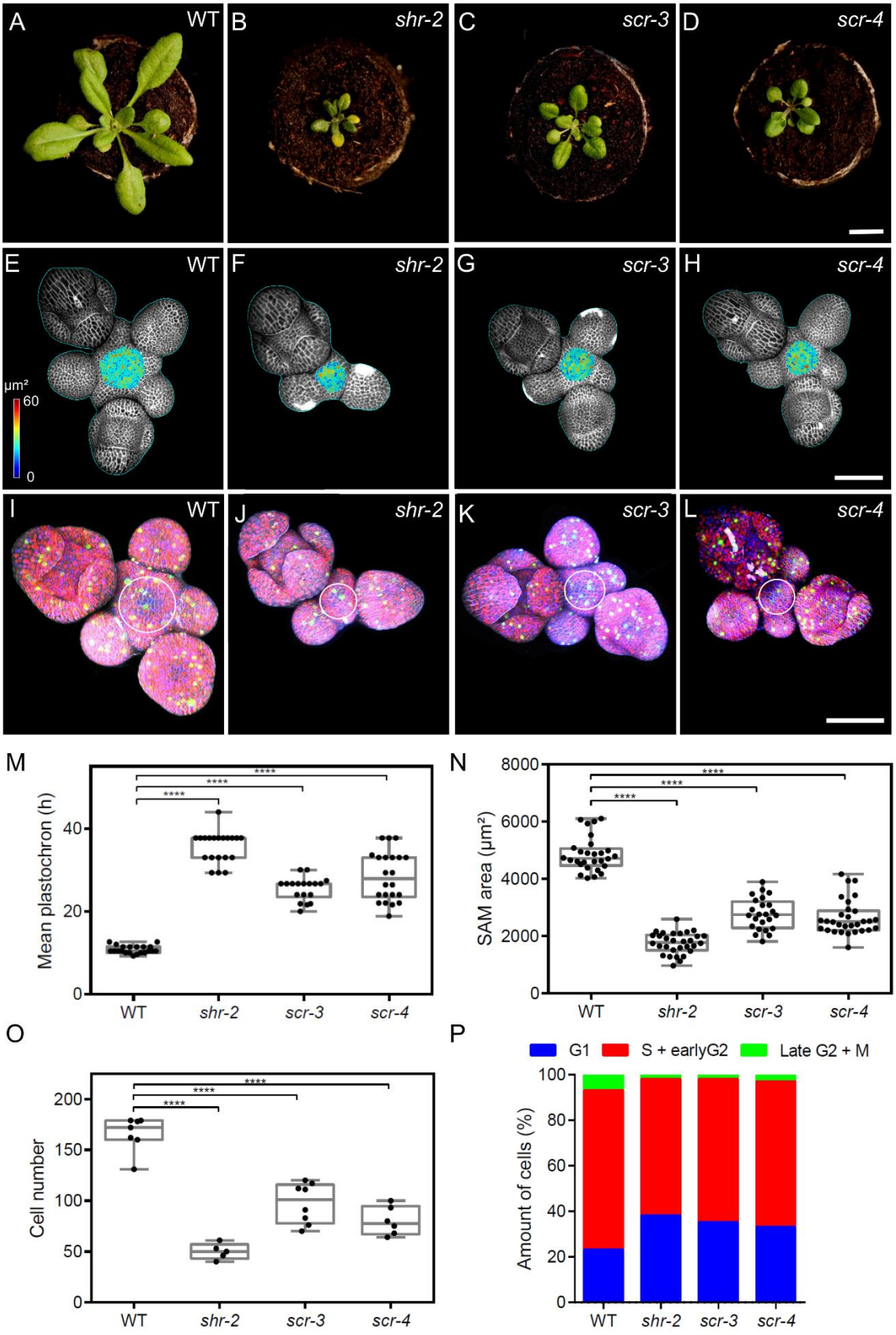

Fig . 1: The *shr* and *scr* mutants phenotypes.

(A-D) Top view of 21-day-old rosettes from WT (col-0) **(A)**, *shr-2* mutant **(B)**, *scr-3* mutant **(C)** and *scr-4* mutant **(D)**. Scale bar represents 1cm. **(E-H)** Heat-map quantification of the cell area in the meristem region at 5 weeks after germination from WT (n=7) **(E)**, *shr-2* mutant (n=5) **(F)**, *scr-3* mutant (n=8) **(G)** and *scr-4* mutant (n=6) **(G)**. Cell walls were stained with PI (gray). Scale bar represents 50 µm. **(I-L)** Representative 3D projection of shoot apical meristems at 5 weeks after germination expressing the three PlaCCI markers: *pCDT1a:CDT1a-eCFP* (blUE), *pHTR13:pHTR13-mCherry* (red), and *pCYCB1;1:NCYCB1;1-YFP* (green) in WT (n=11) **(I)**, *shr-2* mutant (n=4) **(J)**, *scr-3* mutant (n=7) **(K)** and *scr-4* mutant (n=6) **(L)**. White circles in **(I)**, **(J)**, **(K)** and **(L)** mark the meristem region. Cell walls were stained with DAPI (gray). Scale bar represents 50 µm. **(M)** Quantification of shoot apical meristem size at 5 weeks after germination from WT (n=28), *shr-2* mutant (n=30), *scr-3* mutant (n=24) and *scr-4* mutant (n=30). **(N)** Mean inflorescence plastochron in WT (n=21), *shr-2* mutant (n=20), *scr-3* mutant (n=18), and *scr-4* mutant (n=22). **(O)** Quantification of epidermal cell number in the meristem region of WT (n=11), *shr-2* mutant (n=4), *scr-3* mutant (n=7) and *scr-4* mutant (n=6). **(P)** Quantification of cells in different cell cycle phases in the meristem region (area surrounded by white circles in **(I)**, **(J)**, **(K)** and **(L)**) of WT (n=11), *shr-2* mutant (n=4), *scr-3* mutant (n=7) and *scr-4* mutant (n=6). Asterisks indicate a significant difference (****=$p < 0.0001$; statistically significant differences were determined by Student's *t*-test).

6.4.2. SHR and SCR function modulate auxin signalling in the SAM

Since organ initiation sites are determined by auxin accumulation and signaling (Vernoux et al., 2011b), we asked if auxin accumulation is affected by loss of *SHR* or *SCR* functions, which would explain the observed delayed lateral organ initiation effects in *shr* and *scr* mutants (Fig. 1M). We introduced the auxin transcriptional output reporter *pDR5v2:3xYFP-N7* (Heisler et al., 2005) into the *shr-2* and *scr-4* mutants and assessed the number of domains with auxin output maxima compared to wild type (Fig. 2A-C, arrowheads). We found that the average number of *DR5* positive domains in SAMs of *shr-2* and *scr-4* was significantly reduced compared to wild type (Fig. 2G). These results show that SHR and SCR functions interfere with auxin signaling in the SAM.

To closely evaluate how the distribution of auxin was affected in the SAM during the loss of SHR and SCR activities, we further evaluated auxin levels in the different meristem domains using the R2D2 auxin input sensor (Liao et al., 2015). R2D2 is a degron-based ratiometric auxin reporter consisting of an auxin-dependent degradation domain II (DII) of an Aux/IAA protein fused to Venus, and a mutant auxin nondegradable domain II (mDII) fused to tdTomato. The ratio of the fluorescence intensities between Venus and tdTomato represents a proxy for the level of auxin in every cell, with high intensity indicating a low auxin level and vice versa. We observed that the domains of low auxin in meristems of *shr-2* and *scr-4* mutants were expanded, which sometimes extended beyond the lateral organ boundary into the primordia (Fig. 2D-F, arrowheads).

Altogether, these results show that the interplay between SHR and SCR functions and auxin signaling is required to maintain the proper distribution of auxin within the SAM. This safeguards the regular generation of auxin maxima in the peripheral zone, which is a prerequisite for organ initiation.

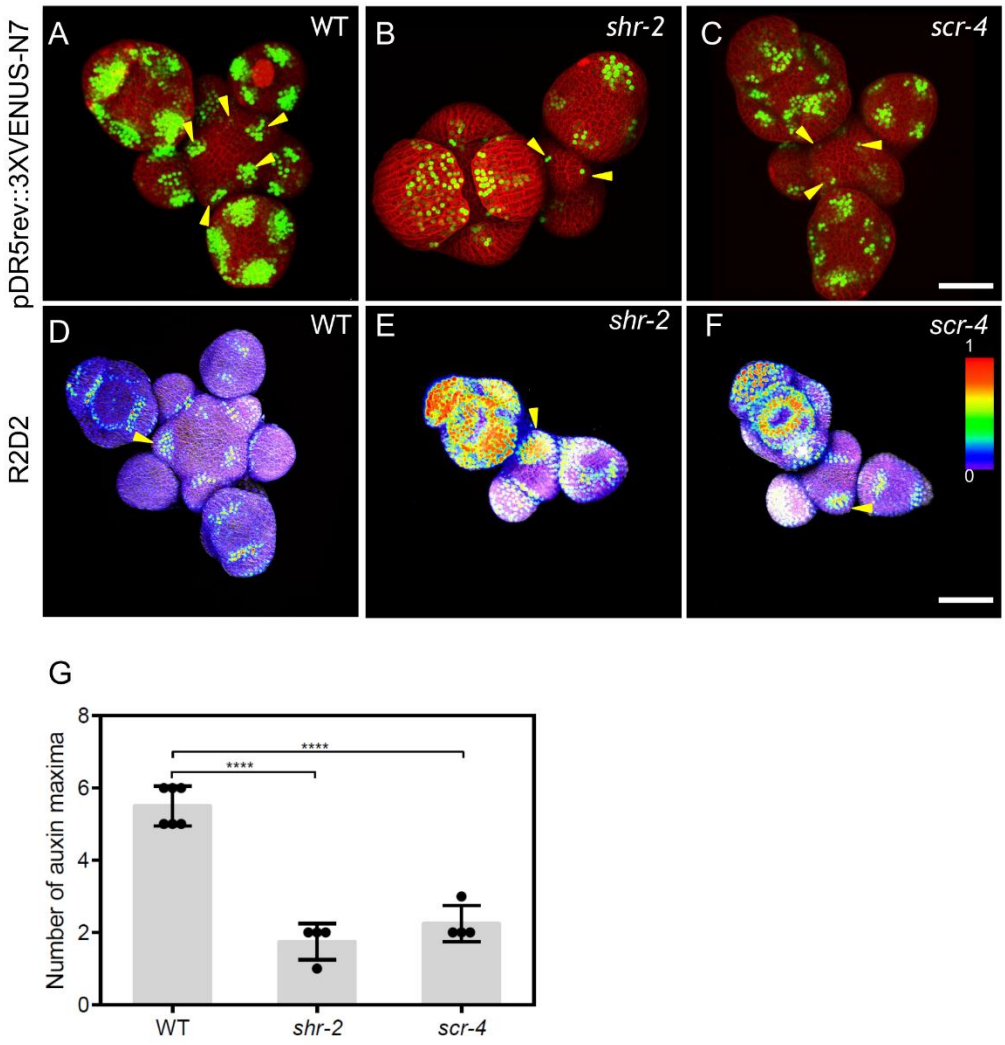

Fig. 2: SHR and SCR functions modulate auxin signalling in the shoot apical meristem.

(A-C) Representative 3D projection of shoot apical meristems at 5 weeks after germination expressing the auxin response reporter *pDR5rev:3XVENUS-N7* in WT (Col-0) (n=6) **(A)**, *shr-2* mutant (n=4) **(B)** and *scr-4* mutant (n=4) **(C)**. Yellow arrowheads in **(A)**, **(B)** and **(C)** show primordia with pDR5rev:3XVENUS-N7 expression. Cell walls were stained with PI (red). Scale bar represents 50 µm. **(D-F)** Representative 3D projection of shoot apical meristems at 5 weeks after germination expressing the auxin input sensor R2D2 showing DII/mDII ratio intensity in WT (Col-0) (n=4) **(D)**, *shr-2* mutant (n=4) **(E)** and *scr-4* mutant (n=3) **(F)**. Yellow arrowheads in **(D)**, **(E)** and **(F)** show primordia with low auxin. Cell walls were stained with DAPI (gray). Scale bars represents 50 µm. Fluorescence intensities were coded blue to red corresponding to increasing intensity. **(G)** Quantification of auxin maxima in WT (n=6), *shr-2* mutant (n=4) and *scr-4* mutant (n=4). Asterisks indicate a significant difference (****=$p < 0.0001$; statistically significant differences were determined by Student's *t*-test). Error bars display SD.

6.4.3. SHR and SCR expression in the shoot and flower meristems

To decipher how SHR and SCR mediate the observed strong meristem developmental defects in SAM, we decided to investigate their expression patterns during shoot development. We used established translational reporter lines which were previously shown to be active and to complement the corresponding *shr* or *scr* mutants (Long et al., 2017). Using confocal microscopy, we imaged *pSHR:YFP-SHR* transgenic plant meristems and observed SHR expression in the inflorescence meristems at 36 DAG. We observed that YFP-SHR was localized at primordia of both SAM and flower meristems. At the SAM, YFP-SHR protein was detected in initiating lateral organ primordia (Fig. 3A) and in flower organs.

During root development, *SHR* mRNA is only found in the stele, but SHR protein moves from the stele to the adjacent cell layer where it interacts with SCR in the nucleus. Limiting SHR movement and preventing its interaction with SCR was shown to restrict the number of root ground tissue cell layers. We asked if SHR and SCR can also interact in the SAM, and if SHR is mobile between shoot meristem tissue layers. Upon observing the transcriptional pattern of *SHR* using the transcriptional reporter *pSHR:ntdTomato* (Möller et al., 2017), we found its transcriptional activity to be localized from P1 onwards in the third meristematic cell layer (L3) and, weakly, in the L2 of older primordia (Fig. 3C; Suppl Fig. 2A). No *SHR* expression was observed in the center of the SAM or floral meristems (Fig. 3A, inset), or stem cell domains (Fig. 3A, inset, asterisks).

We then used the translational reporter *pSHR:YFP-SHR* to observe SHR protein localization (Fig. 3A and D). SHR protein localized throughout L3 cells and appeared to be preferentially confined to the nuclei in L2 cells and also in L1 cells, where *SHR* is normally not expressed (Fig. 3C). Based on the combined observation of SHR transcriptional activity and the protein localization, we conclude that SHR, similar to its activity in RAM, acts as a mobile transcription factor moving from the inner cell layers to the outermost cell layers of the organ primordia to mediate proper SAM development.

We then addressed the expression of *SCR* in the shoot meristem. A transcriptional reporter for *SCR* (*pSCR:YFP*) was previously described to be expressed in the QC and the root endodermis (Heidstra *et al.*, 2004). In the SAM, we found fluorescent signal only in differentiated vasculature of the shoot, and in a patchy pattern in some flower primordia (Suppl Fig. 2B, inset). Since the transcriptional *SCR* reporter might lack control elements that contribute to the native *SCR* expression pattern, we used a translational reporter line, *pSCR:SCR-YFP* that was previously shown to complement the *scr* mutant phenotypes (Long et al., 2017). We observed SCR-YFP fluorescence in the nuclei of L1 cells in the central zone

of the SAM and further extended into the deeper meristem layers specifically of the peripheral zone and lateral organ primordia (Fig. 3B, inset). Notably, SCR-YFP was lacking in the deeper regions of the meristem center and the rib meristem. In lateral organ primordia, *SCR* expression starts from the L1 and L2, and extends into deeper regions during further development. Stronger expression was found in the boundary region that separates lateral organ primordia from the remainder of the SAM (Fig. 3E). Thus, SHR and SCR proteins are expressed in partially overlapping domains during lateral organ primordia development. Importantly, *SHR* is missing from the SAM center, where *SCR* is expressed in the L1 (compare Fig. 3A, inset, with Fig. 3B, inset).

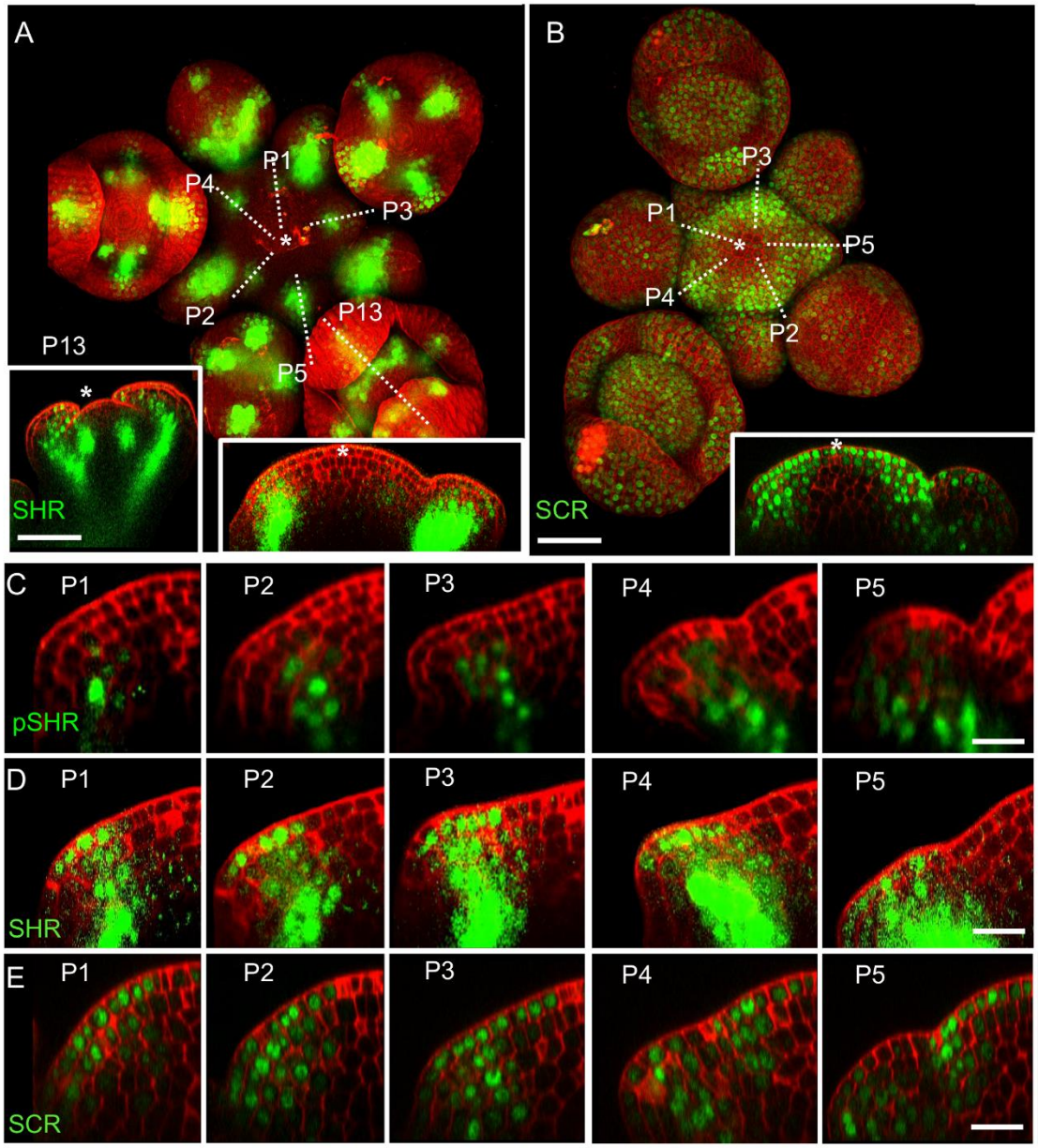

Fig. 3: The expression patterns of SHR and SCR in the shoot apical meristem.

(A) Representative 3D projection of shoot apical meristem at 5 weeks after germination expressing *pSHR:YFP-SHR* reporter (green) (n≥6). The lower right inset shows a longitudinal

optical section through the middle of the SAM. The lower left inset shows a longitudinal optical section through the middle of primordia 13 (representative section orientation shown by dotted line). Cell walls were stained with DAPI (red). Scale bar represents 50 µm. **(B)** Representative 3D projection of shoot apical meristem at 5 weeks after germination expressing *pSCR:SCR-YFP* reporter (green) (n≥10). The lower right inset shows longitudinal optical section through the middle of the SAM. Cell walls were stained with PI (red). Asterisks in **(A)** and **(B)** indicate the center of shoot apical meristem or floral meristem. Scale bars represent 50 µm. **(C)** Longitudinal optical sections through the middle of five successive primordia expressing *pSHR:ntdTomato* reporter (green) (representative section orientation shown by dotted line in Suppl Fig. 2A). Cell walls were stained with DAPI (red). Scale bar represents 20 µm. **(D and E)** Longitudinal optical sections through the middle of five successive primordia expressing *pSHR:YFP-SHR* reporter (green) **(C)** and *pSCR:SCR-YFP* reporter (green) **(D)** (representative section orientation shown by dotted line in **(A)** and **(B)**, respectively). Scale bars represent 20 µm. P= Primordium.

6.4.4. SHR and SCR form protein complexes in the SAM

As SHR and SCR localize in an overlapping domain during lateral organ development (Fig. 3D and E), we wanted to closely observe their precise intracellular localization. We saw that SCR and SHR co-localized predominantly in nuclei of cells in the L1 and L3 of lateral organ primordia (Fig. 4A and C).

Previously, using *in vivo* FRET-FLIM, Long et al demonstrated an interaction between SHR and SCR in the RAM (Long et al., 2017). Owing to their confined nuclear co-localization in SAM, we investigated if SHR and SCR also interacted in the SAM. We tested it using FRET-FLIM method with YFP-SHR serving as fluorescent donor and SCR-RFP as acceptor. Reductions in the fluorescence lifetime of YFP, which can then be recorded as a quantitative readout for FRET, is indicative of protein-protein interaction. We used SAMs at 36 DAG for FRET measurements between YFP-SHR and SCR-RFP in lateral organ primordia, petal primordia and sepal primordia. As a negative control for non-interacting proteins, we used SAMs from plants coexpressing *pSCR:SCR-YFP* with *pSCR:SCR-RFP*, since SCR proteins do not homodimerize (Long et al., 2017) (Fig. 4B and D). The YFP-SHR donor-only sample showed a fluorescence lifetime of ~3 ns (Fig. 4E), which significantly decreased by approximately 0.3 ns in all samples where SCR-RFP was coexpressed (Fig. 4E), whereas samples with SCR-RFP and SCR-YFP coexpression showed no significant changes in mean fluorescence lifetime compared to the SCR-YFP donor-only control (Fig. 4F).

These results show that the *SHR* and *SCR* genes are not only expressed in partially overlapping domains, but also that the SCR and SHR proteins physically interact in the SAMs of Arabidopsis.

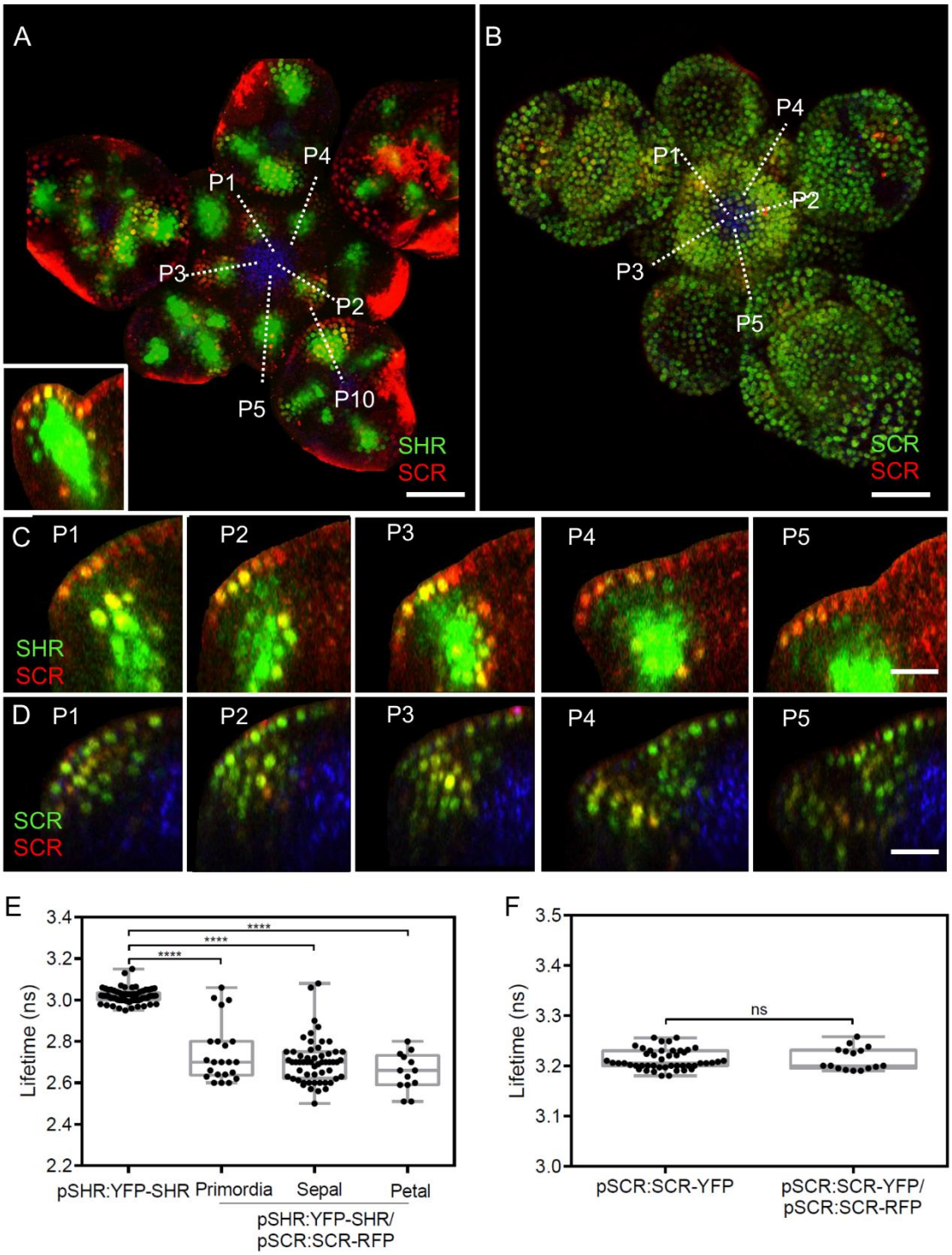

Fig. 4: *In vivo* FRET–FLIM quantification of SHR–SCR association in the shoot apical meristem.

(A-B) Representative 3D projection of shoot apical meristem at 5 weeks after germination coexpressing *pSHR:YFP-SHR* reporter (green) and *pSCR:SCR-RFP* reporter (red) **(A)** (the lower left inset shows a longitudinal optical section through the middle of primordia 10; representative section orientation shown by dotted line) and *pSCR::SCR:YFP* reporter (green) and *pSCR::SCR:RFP* reporter (red) **(B)**. Chlorophyll (blue). Scale bars represent 50 µm. **(C-D)** Longitudinal optical sections through the middle of five successive primordia coexpressing *pSHR:YFP-SHR* reporter (green) and *pSCR:SCR-RFP* reporter (red) **(C)**, and *pSCR::SCR:YFP* reporter (green) and *pSCR::SCR:RFP* reporter (red) **(D)** (representative

section orientation shown by dotted line in **(A)** and **(B)** respectively). Chlorophyll (blue). Scale bars represent 20 µm. **(E)** Average lifetime of YFP-SHR when expressed alone (pSHR:YFP-SHR (*n* =75)), or coexpressed together with SCR-RFP (pSHR:YFP-SHR/pSCR:SCR-RFP) in lateral organ primordia (n=22), sepal primordia (n=55) and petal primordia (n=13) in the shoot meristem. **(E)** Average lifetime of SCR-YFP when expressed alone (pSCR:SCR-YFP (n=49)), or coexpressed together with SCR-RFP (pSCR:SCR-YFP/pSCR:SCR-RFP(n=16)) in shoot meristem. Asterisks indicate a significant difference (****=p < 0.0001; ns= no significant difference; statistically significant differences were determined by Student's *t*-test). P= Primordium.

6.4.5. SHR-SCR heteromer regulates expression of *SCR* in lateral organ primordia

In the Arabidopsis root, SHR protein moves from the stele to outer cell layers and promotes expression of *SCR* in the QC and endodermis (Nakajima et al., 2001). SHR and SCR proteins form heteromers and control a critical formative cell division in the cortex-endodermis-initial (CEI) (Long et al., 2015b, Nakajima et al., 2001).

Given that both *shr* and *scr* mutants display smaller shoot meristems due to delayed progression through the cell cycle, and that organ initiation in the meristem periphery is compromised, we hypothesized that the regulatory hierarchies between *SHR* and *SCR* act also in the SAM. We first tested if SHR regulated *SCR*. We compared the SCR protein localization; using *pSCR:SCR-YFP* reporter line in WT and *shr-2* mutant background. SCR protein level remained unaffected in the central zone of the SAM, where *SHR* is normally not expressed (Fig. 5B, C and G). However, in the lateral organ primordia, SCR protein level was strongly reduced in *shr-2*, compared to wild type, but there were no significant differences starting from the meristem until the organ boundary (Fig. 5D, E and H). Analysis of *SCR* transcript levels by qRT-PCR corroborated a significant decrease in *shr-2* mutants (Fig. 5I). This result suggests that SHR acts as a transcriptional activator of *SCR* in the SAM, but that *SCR* expression in the meristem center is *SHR*-independent. Importantly, the expression pattern of *pSHR:ntdTOMATO* does not entirely overlap with the expression pattern of *pSCR:SCR-YFP*, indicating again that SHR acts as a mobile protein also in the SAM (Suppl Fig. 6A and D).

Previously, it was demonstrated that SCR restricts movement of SHR protein by nuclear retention (Cui et al., 2007, Long et al., 2015b, Long et al., 2015a). We tested if this was also the case in the SAM lateral organ primordia. Analysis of SAMs coexpressing *pSHR:SHR-YFP* and *pSCR:SCR-RFP* showed that SHR-YFP is enriched in the nuclei of cells coexpressing SCR-RFP at the lateral organ primordia (Fig. 5A inset and F). This enrichment entraps the SHR in the nuclei, thus restricting its further intercellular movement.

Altogether these results prove a hierarchical interaction between *SHR* and *SCR*, where SHR induce *SCR* expression in lateral organ primordia. Then SHR further physically interacts with SCR and enriches its nuclear presence, further restricting its mobility.

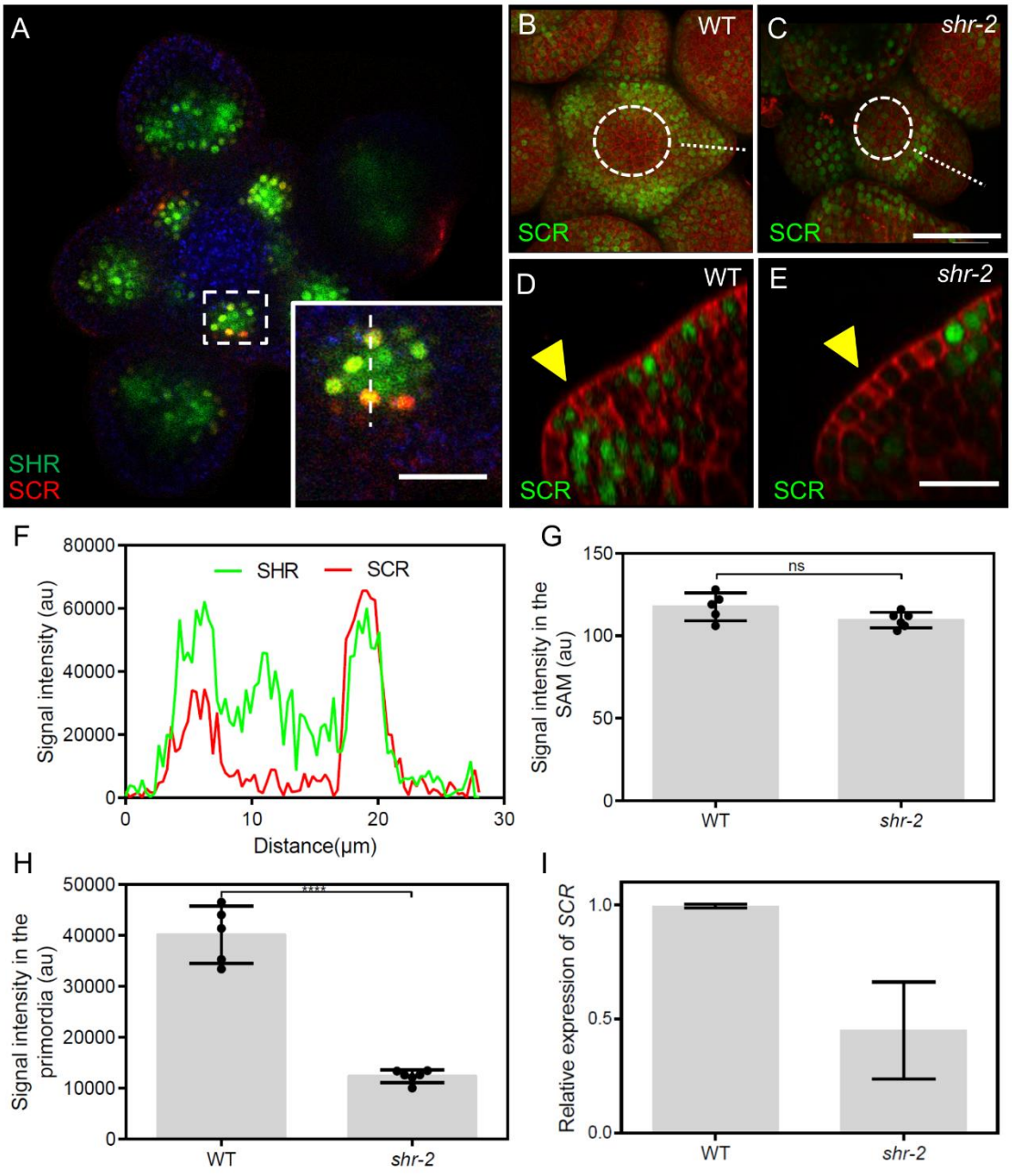

Fig. 5: SHR regulates *SCR* expression in the shoot apical meristem.

(A) Representative transversal confocal image of shoot apical meristem at 5 weeks after germination coexpressing the *pSHR:SHR-YFP* reporter (green) and the *pSCR:SCR-RFP* reporter (red) (n=4). Chlorophyll (blue). The lower right inset shows an optical section view with high magnification of the area surrounded by white dashed rectangle in **(A)**. Scale bar represents 50 μm. **(B and C)** Representative 3D projection of shoot apical meristems at 5 weeks after germination expressing the *pSCR:SCR-YFP* reporter (green) in WT (n=5) **(B)** and *shr-2* mutant (n=6) **(C)**. Cell walls were stained with PI (red). Scale bar represents 50 μm. **(D and E)** Longitudinal optical sections through the middle of primordia shown by dotted line in **(B)** and **(C)** respectively. Yellow arrowheads in **(D)** and **(E)** show primordia with SCR-YFP expression. Scale bar represents 20 μm. **(F)** Intensity plot profile of SHR-YFP (green) signal

and the SCR-RFP (red) signal in the area crossed by white dashed line in **(A)** inset. **(G and H)** Quantification of SCR-YPF signal intensity in the meristem center **(G)** (area surrounded by white dashed circles in **(B)** and **(C)**) and in the primordia **(H)**. **(I)** Quantitative real-time PCR analysis showing the relative expression levels of *SCR* in WT and *shr-2* mutant SAMs. The expression level in Col-0 is set to 1. Expression levels were normalized using AT4G34270 and AT2G28390. Asterisks indicate a significant difference (****=p < 0.0001; ns= no significant difference; statistically significant differences were determined by Student's *t*-test). Error bars display SD.

6.4.6. Expression pattern and functions of *JKD* in the SAM

In the root meristem, SHR and SCR form cell type-specific protein complexes with the BIRD-family transcription factor JACKDAW (JKD). JKD acts together with SCR in restricting the mobility of SHR, and this complex then defines the positioning of formative cell divisions. In the *jkd* mutants, SHR expands into the cortex and creates a third ground tissue layer (Long et al., 2015b, Long et al., 2017, Welch et al., 2007). We wanted to investigate if JKD plays any role in SAM development, as well. We compared the SAM development of *jkd-4* mutants with WT and found a significant increase in SAM size. Further analysis revealed that the observed increase was due to a significant rise in cell number (Fig. 6A-C and K), not due to increase of average cell surface areas (Suppl Fig. 3A). This shows that, as in the RAM, JKD also regulates the SAM development.

We then conducted expression studies using the transcriptional reporter *pJKD:YFP-RFP* and the translational *pJKD:JKD-YFP* reporter that has been previously shown to complement the *jkd-4* mutant phenotype (Long et al., 2017). *JKD* was expressed in the outer regions of primordia (Fig. 6D and E). The expression patterns of both reporter lines were mostly identical, indicating that *JKD* RNA and protein are found in the same cells, and that JKD protein is not mobile. We further observed that JKD is first expressed in adaxial cells in P1, and this expression domain slightly expanded in lateral organ primordia at later stages (Fig. 6H). At P7, JKD was found in a ring-like pattern in sepals, and at later flower developmental stages, in stamen and carpel primordia (Fig. 6E-G).

Based on the observed JKD expression (Fig 6 D and E), we wanted to examine if JKD localization directly correlates with sepal development. To do this, we used the strong *lfy-12* mutant where the florescence meristem fails to produce proper flower organs and instead generates sepal-like organs (Weigel et al., 1992), and the *clv3-9* mutant, which has an excessively enlarged SAM and flowers with additional organs (Schlegel et al., 2021). JKD was confined to sepal primordia of *clv3-9* mutants and to the sepal-like organs of *lfy-12* mutants like in the WT (Suppl Fig. 3C-D).

Since JKD has been shown to function together with SCR and SHR in the RAM (Welch et al., 2007, Long et al., 2015b, Long et al., 2017), we examined the molecular interaction of JKD with SCR in SAM *in vivo* using FRET-FLIM. SAMs coexpressing pJKD:JKD-YFP and pSCR:SCR-RFP showed significant fluorescence lifetime reductions of up to 0.17 ns (Fig. 6I and J). This indicates a direct interaction between JKD and SCR proteins in the SAM.

As we showed before, SCR also interacts with SHR in the SAM (Fig. 4E), Therefore, we propose that SHR-SCR-JKD form a multimeric complex in lateral and in floral organ primordia. Taken together, these data show that, as in RAM, proper localization of JKD and possibly its interaction and complex formation with SHR and SCR are vital to promote organ initiation and SAM growth. The observed JKD interaction might be conducive in restricting and/or respecifying SHR or SCR functions.

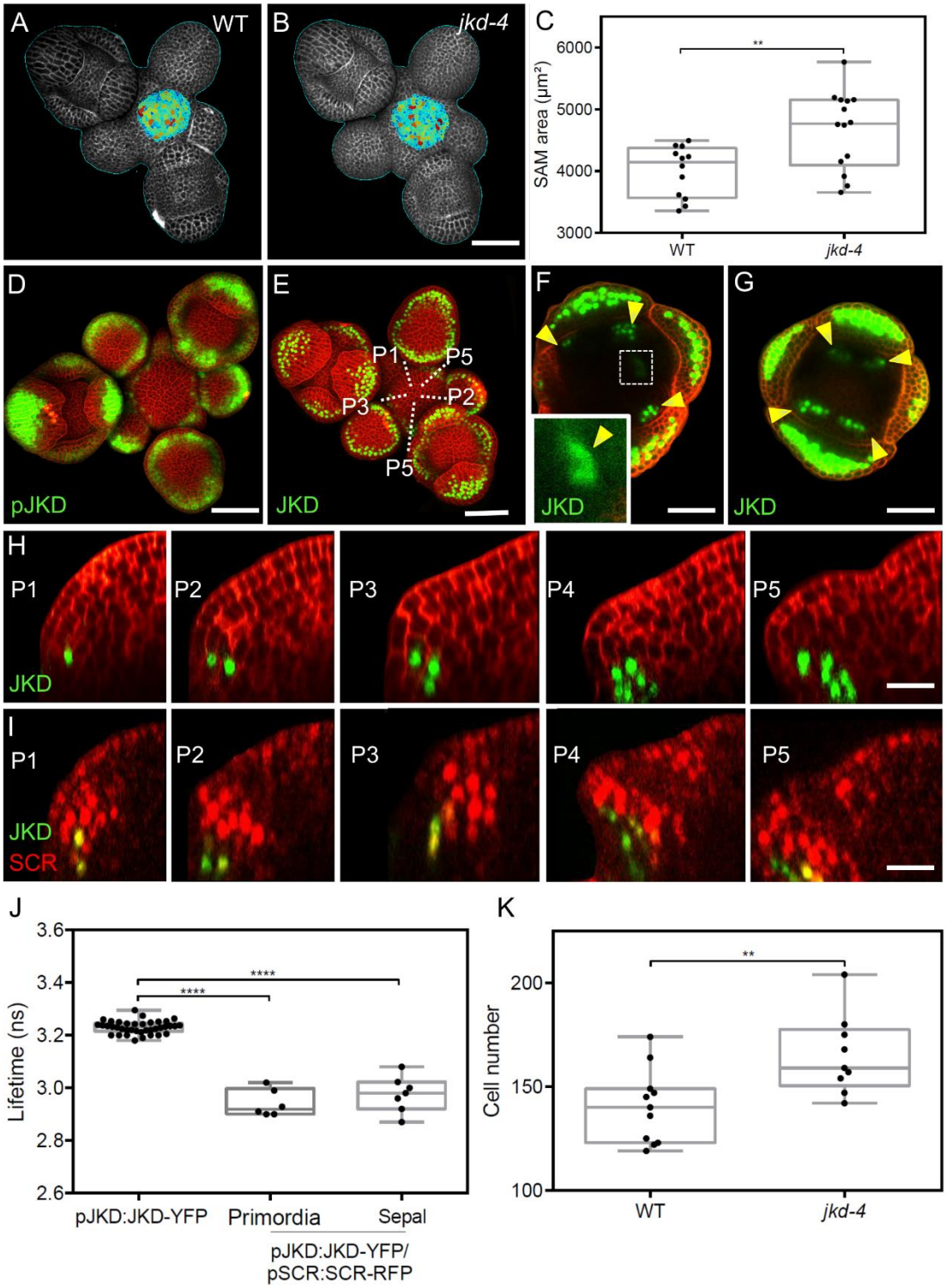

Fig. 6: JKD functions and expression pattern in the shoot apical meristem.

(A and B) Heat-map quantification of the cell area in the meristem region at 5 weeks after germination from WT **(A)** (n=10) and *jkd-4* mutant **(B)** (n=10). Cell walls were stained with PI (gray). Scale bar represents 50 µm. **(C)** Quantification of shoot apical meristems size at 34 days after germination (DAG) from WT (n=12) and *jkd-4* mutant (n=14). **(D and E)** Representative 3D projection of shoot apical meristems at 5 weeks after germination expressing *pJKD:YFP-RFP* reporter (green) (n≥4) **(D)** and *pJKD:JKD-YFP* reporter (green) (n≥20) **(E)**. Cell walls were stained with PI (red). Scale bars represent 50 µm. **(F and G)** Transversal optical through the primordia 16 from inflorescence apex of *pJKD:JKD-YFP* reporter (green). Yellow arrowheads in **(F)** and **(G)** show petal primordia with pJKD:JKD-YFP

expression. The lower left inset shows an optical view with high magnification of area surrounded by white dashed rectangle in **(F)**. Cell walls were stained with PI (red). **(H)** Longitudinal optical sections through the middle of five successive primordia (representative section orientation shown by dotted line in **(A)**) expressing *pJKD:JKD-YFP* reporter (green). Cell walls were stained with PI (red). Scale bar represents 20 µm. **(I)** Longitudinal optical sections through the middle of five successive primordia (representative section orientation shown by dotted line in Suppl Fig. 4F) coexpressing *pJKD:JKD-YFP* reporter (green) and *pSCR:SCR-RFP* reporter (red). Scale bar represents 20 µm. **(J)** Average lifetime of JKD-YFP when expressed alone (pJKD:JKD-YFP (n =38)), or coexpressed together with SCR-RFP (pJKD:JKD-YFP/pSCR:SCR-RFP) in lateral organ primordia (n=6) and sepal primordia (n=7) in the shoot meristem. **(K)** Quantification of epidermal cell number in the meristem region of WT **(A)** (n=10) and *jkd-4* mutant **(B)** (n=10). Asterisks indicate a significant difference (****=p < 0.0001; **=p < 0.001; statistically significant differences were determined by Student's *t*-test). P= Primordium.

6.4.7. The SHR-SCR-JKD complex triggers cell division in lateral organ primordia by regulating *CYCD6;1* expression

Lateral organ initiation in the SAM periphery is controlled by the *CYCLIN* genes through the regulation of cell division (Dewitte et al., 2003), and the main target of SHR-SCR-JKD complex in the root is *CYCD6;1*. We therefore asked if a similar regulatory pathway, where the SHR-SCR-JKD complex acts through transcriptional regulation of *CYCLIN* genes, might be active in the SAM.

We examined the expression of *pCYCD1;1:GFP, pCYCD2;1:GFP, pCYCD3;2:GFP, pCYCD3;3:GFP, pCYCD5;1:GFP, pCYCD6;1:GFP, pCYCD7;1:GFP* and *pCYCB1;1:CYCB1;1-GFP*. Amongst them only *CYCD1;1*, *CYCD3;2*, *CYCD3;3*, *CYCD6;1* and *CYCB1;1* were expressed in the SAM (Suppl Fig. 4A-D and G). *CYCD1;1*, *CYCD3;2* and *CYCB1;1* exhibited a patchy expression pattern in sepal primordia (Suppl Fig. 4D), while *CYCD3;3* was more uniformly distributed with an enrichment in lateral organ primordia (Suppl Fig. 4C). *pCYCD6;1:GFP* expression was detected in lateral organ primordia and floral organs in sepal primordia from all stages, but not at the center of the SAM (Fig. 7A, C, E, L and O). Notably, *CYCD6;1*, was expressed in the region where the expression of SHR, SCR and JKD overlapped. (Suppl Fig. 4E-S). This shows that *CYCD6*;1 may act as a downstream target of the SHR-SCR-JKD protein complex, similar to that reported in the RAM to regulate asymmetric cell divisions during primordia formation in the shoot and flower meristems.

Given that the SAMs in *shr* and *scr* mutants have reduced cell divisions rate and that *CYCD6*;1 expression overlaps with the SHR-SCR-JKD expression domain, we asked if expression of *pCYCD6;1:GFP* is affected when *SHR* function is compromised. We observed a strong reduction in *pCYCD6;1:GFP* expression level in the sepal primordia of *shr-2* and its complete

absence from lateral organ primordia in *shr-2* mutant, while in the WT *pCYCD6;1:GFP* was detected in the L3 of lateral organ primordia (Fig. 7A-F).

CYCD6;1 controls periclinal cell division resulting in the formation of new tissue layers (Long et al., 2015b). Therefore, we asked if the asymmetric cell divisions mediated *CYCD6;1* controls lateral primordia formation at the SAM. We compared the number of cell layers in the L3 at the lateral organ primordia between WT and *shr-2* mutant and observed a significant reduction in the mutant (Fig. 7G-I). We conclude that the core function of the SHR-SCR-JKD complex is the induction of periclinal cell divisions through CYCD6 expression, which is conserved between RAM and SAM.

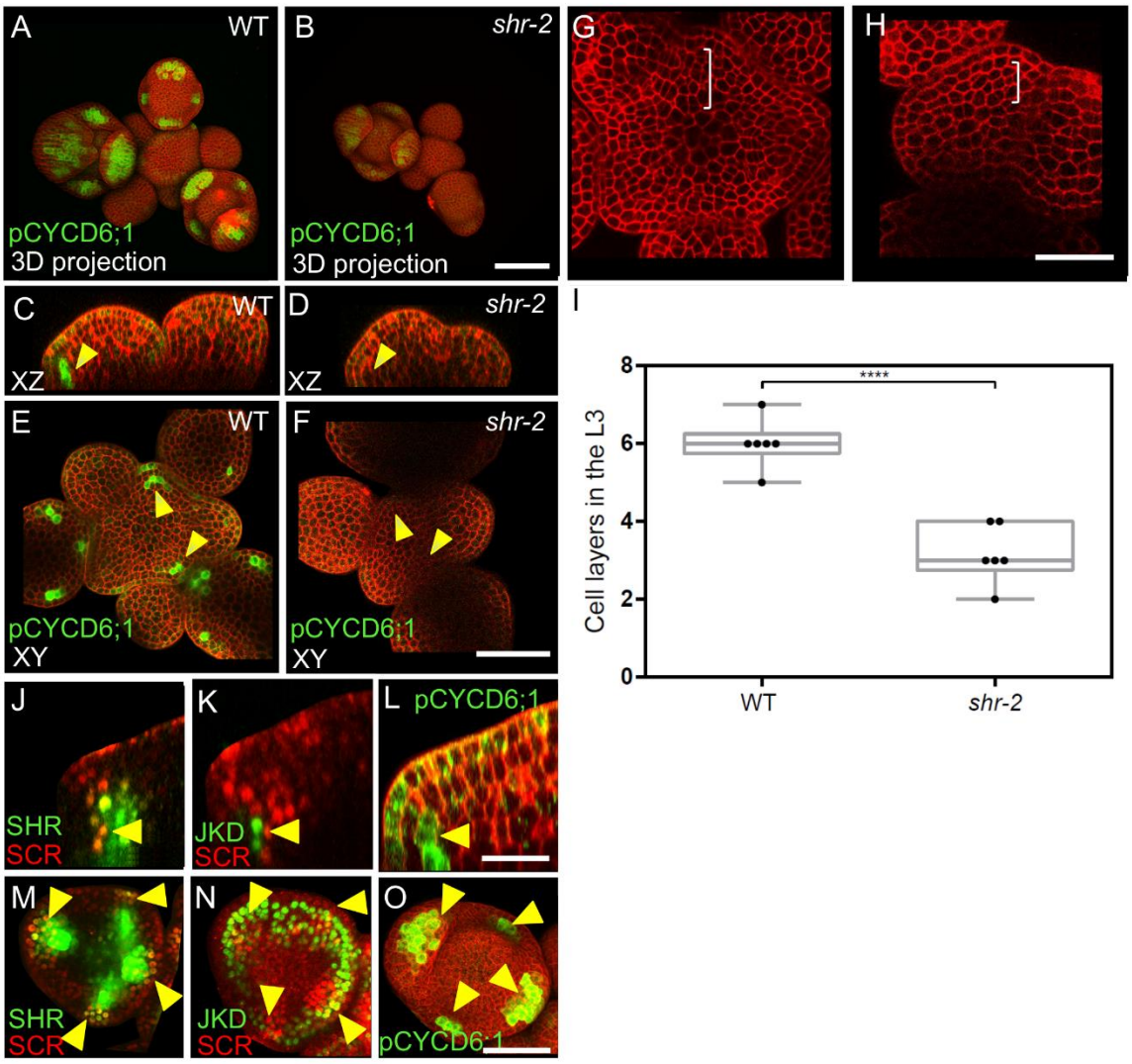

Fig. 7: SHR regulates *CYCD6;1* expression in the shoot apical meristem.

(A and B) Representative 3D projection of shoot apical meristems at 5 weeks after germination expressing *pCYCD6;1:GFP* reporter (green) in WT (n=5) **(A)** and *shr-2* mutant (n=6) **(B)**. cell walls were stained with PI (red). Scale bar represents 50 µm. **(C and D)** Longitudinal optical sections of **(A)** and **(B)** respectively. **(E and F)** Transversal optical sections of **(A)** and **(B)** respectively. Yellow arrowheads in **(C)**, **(D)**, **(E)** and **(F)** indicate the region where lateral organ

primordia initiate and pCYCD6;1:GFP expression. Scale bar represents 50 µm. **(G and H)** Transversal optical sections of the inflorescence apex at 5 weeks after germination from WT **(G)** and *shr-2* mutant **(H)**. **(I)** Quantitative comparison of cell files within the L3 in transversal optical sections of the inflorescence apex from WT (n=6) and *shr-2* mutant (n=6) shown by a bracket in **(G)** and **(H)** respectively. **(J-L)** lateral organ primordia showing (yellow arrowheads) coexpression of *pSHR:SHR-YFP* reporter (green) and *pSCR::SCR-RFP* reporter (red) **(J)**, *pJKD:JKD-YFP* reporter (green) and *pSCR::SCR-RFP* reporter (red) **(K)** and *pCYCD6;1-GFP* reporter (green) **(L)**. Scale bar represents 20 µm. **(M-O)** Florescence meristem stage 4 of flower development showing coexpression of *pSHR:SHR-YFP* reporter (green) and *pSCR::SCR-RFP* reporter (red) **(M)**, *pJKD:JKD-YFP* reporter (green) and *pSCR::SCR-RFP* reporter (red) **(N)** and *pCYCD6;1-GFP* reporter (green) **(O)**. Scale bar represents 20 µm. Asterisks indicate a significant difference (****$p < 0.0001$; **$p < 0.001$; analyzed by Student's t test).

6.4.8. Auxin induces *SHR* and *SCR* expression in the SAM

Since we observed that *SHR* and *SCR* control SAM size and lateral organ initiation, we investigated their interaction with auxin distribution and/or signaling. We wanted to first examine if SHR and SCR expression pattern correlated with that of auxin distribution using the functional *pPIN1:PIN1-GFP* reporter (Heisler et al., 2005). PIN1 is an auxin efflux transporter, which controls the flow and the distribution of auxin across the SAM (Benková et al., 2003). Analysis of the PIN1-GFP localization shows that PIN1 is localized from the L1 up to L3 within the lateral organ primordia (Suppl Fig. 6F).

The expression patterns of SHR and SCR in the primordia strongly overlapped with that of PIN1 during primordia initiation and development (Fig. 3A-D; Suppl Fig. 6A-F). This indicates that *SHR* and *SCR* might act downstream in response to auxin signaling. To that end, we performed an *in silico* analysis of the *SHR* promoter sequence. The analysis revealed the presence of two putative auxin-response element (AuxRE) core motifs (TGTCTC) within the DNA sequence (Fig. 8A). This motif is thought to be sufficient for recruitment of ARF transcription factors (Schlereth et al., 2010, Zhao et al., 2010, Ulmasov et al., 1999), which are the downstream TFs released after auxin dependent degradation of TIR1/AFB receptors (Paque & Weijers, 2016). This suggests that SHR is likely induced by ARF upon auxin signaling.

We then directly tested if auxin regulates expression of *SHR* and *SCR* in the SAM. We treated wildtype inflorescences with 10 µM indole-3-acetic acid (IAA). Within 12 h of hormone application, the expression levels of both *SHR* and *SCR* increased to about 300% of untreated control levels. *SHR* expression increased slightly earlier than that of *SCR*, further confirming our previous observation that *SHR* activates *SCR* expression (Fig. 5B-E; Fig. 8H; Suppl Fig. 13E).

To uncover the spatial distribution of *SHR* and *SCR* in response to exogenous auxin application, we analyzed SAMs expressing *pSHR:SHR-YFP* and *pSCR:SCR-YFP* after treatment with 10 µM of the synthetic auxin analogue 2,4-D, a form of auxin that can diffuse into cells. We found that expression visibly increased within 2-5 h after the start of the hormone treatment (Fig. 8B-G). Importantly, the expression patterns of both *SHR* and *SCR* were not strongly affected.

Since we observed an overlap of auxin expression domain with that of SHR and SCR and also established that auxin induced SHR and SCR expression, we tested if changes in auxin transport and local distribution in turn affected SHR and SCR expression pattern. Next, we asked if *SHR* and *SCR* expression patterns depend on the transport and local distribution of auxin in the SAM. We inhibited polar auxin transport and hence its distribution in tissues using the auxin transport inhibitor N-1-naphthylphthalamic acid (NPA). The mock control SAMs expressing *pPIN1:PIN1-GFP* showed a wide distribution of PIN1-GFP, which relocated into a ring-shaped domain in deeper regions of the meristem 3 d after treatment with 100 µM NPA (Fig. 8Q-T). Concomitantly, the expression pattern of SHR-YFP changed from being associated with primordia into a ring-shaped domain, reflecting the rearrangement of the *PIN1* expression domain (Fig. 8I-L). Similar changes in expression pattern were found for *SCR* upon NPA treatment (Fig. 8M-P). In addition, NPA treatment resulted in enlarged expression domains for *pCYCD6;1:GFP*, a key target gene of the SHR-SCR-JKD complex (Suppl Fig. 5A-D). Based on all these observations, we conclude that, in the SAM, *SHR* and *SCR* levels and expression pattern are to a large extent coordinated by auxin levels and distribution.

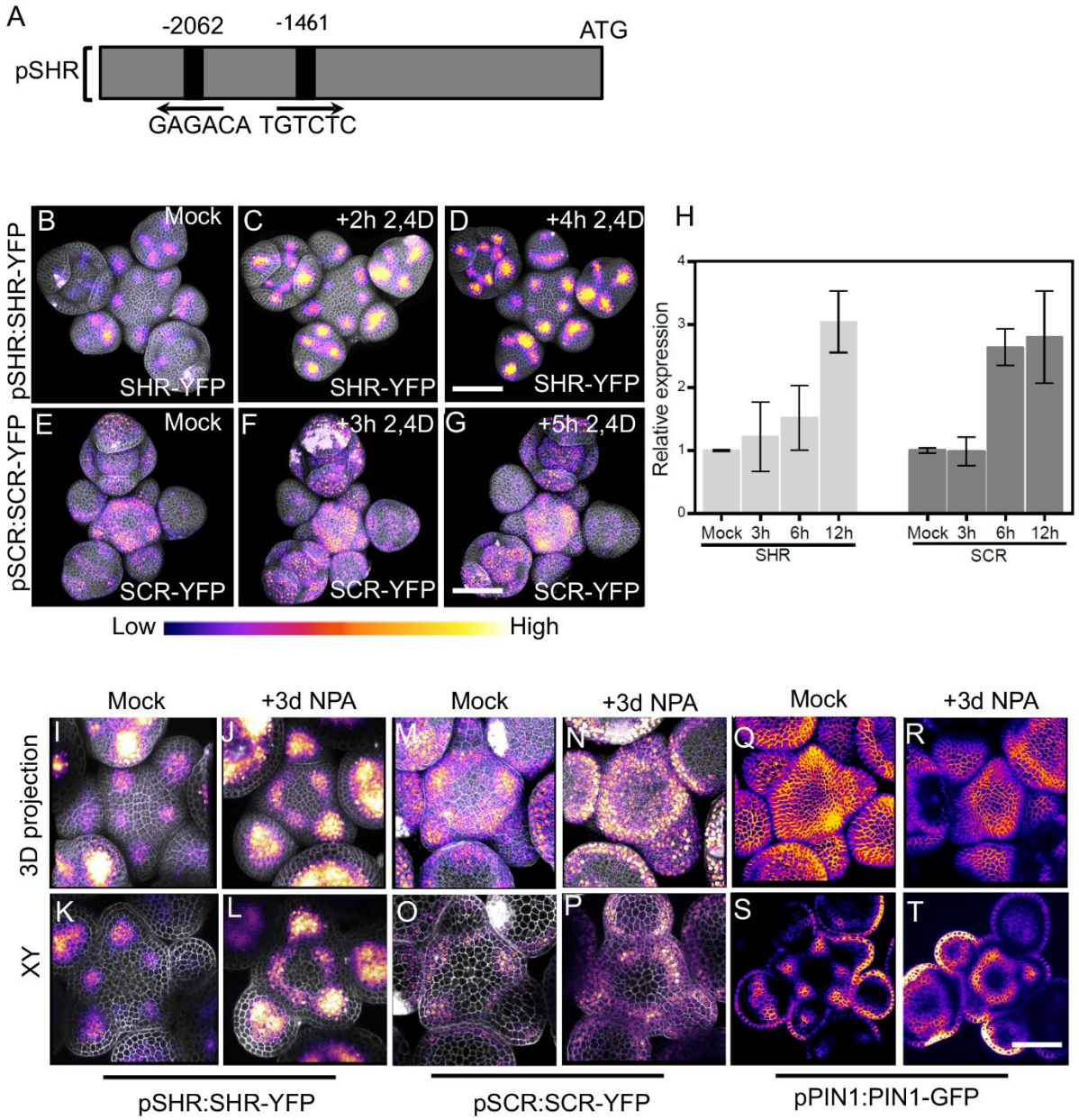

Fig. 8: SHR and SCR expressions respond to auxin.

(A) Schematic representation of the *SHR* promoter. The positions of two auxin response elements (GAGACA and TGTCTC) are shown. **(B-D)** Representative 3D projection of shoot apical meristems at 5 weeks after germination expressing *pSHR:SHR-YFP* reporter (magenta) in mock **(B)** (n=4), after 2 hours 10 µM 2,4D treatment (n=3) **(C)** and after 4 hours 10 µM 2,4D treatment (n=3) **(D)**. Fluorescence intensities were coded blue to yellow corresponding to increasing intensity. Scale bar represents 50 µm. **(E-G)** Representative 3D projection of shoot apical meristems at 5 weeks after germination expressing *pSCR:SCR-YFP* reporter (magenta) mock **(E)** (n=4), after 3 hours 10 µM 2,4D treatment (n=2) **(F)** and after 5 hours 10 µM 2,4D treatment (n=2) **(G)**. Fluorescence intensities were coded blue to yellow corresponding to increasing intensity. Scale bar represents 50 µm. **(H)** Quantitative real-time PCR analysis showing the relative expression levels of *SHR* and *SCR* expression in response to auxin (10 µm IAA) in WT shoot apical meristems. The expression level in Col-0 is set to 1 and error bars show standard deviation. Expression levels were normalized using AT4G34270 and AT2G28390. **(I and J)** Representative 3D projection of shoot apical meristems at 5 weeks after germination expressing *pSHR:SHR-YFP* reporter (magenta) three days after mock (n≥6) **(I)** or 100 µM NPA treatment (n≥6) **(J)**. **(K and L)** Transversal optical sections of **(I)** and **(J)**

respectively. **(M and N)** Representative 3D projection of shoot apical meristems at 5 weeks after germination expressing *pSCR:SCR-YFP* reporter (magenta) three days after mock (n≥6) **(M)** or 100 µM NPA treatment (n≥6) **(N)**. **(O and P)** Transversal optical sections of **(M)** and **(N)** respectively. **(Q and R)** Representative 3D projection of shoot apical meristems at 5 weeks after germination expressing *pPIN1:PIN1-GFP* reporter (magenta) three days after mock (n≥3) **(Q)** or 100 µM NPA treatment (n≥3) **(R)**. **(S and T)** Transversal optical sections of **(Q)** and **(R)** respectively.

6.4.9. MONOPTEROS regulates *SHR* and *SCR* expression in the SAM

We have shown that auxin regulates *SHR* expression likely through ARFs (Fig 8A). MP is one of the key ARFs acting in Arabidopsis embryos and meristems, and previous studies have shown that MP is required to promote expression of *SHR* and *SCR* in the early embryo (Möller et al., 2017). We investigated if MP also regulates *SHR* and *SCR* expression in the SAM. When we observed their expression pattern, we saw a strong overlap in MP and SCR and SHR expression domains (Fig. 3D and E; Suppl Fig. 6A; B and E).

We then analyzed the expression of *pSHR:nTdTomato* in *mp-B4149,* a loss-of-function mutant for *MP*. In the wildtype vegetative meristem at 7DAG, *SHR* was expressed in the deeper region of the young leaf primordia, where the vasculature will eventually develop. *SHR* was expressed in a similar pattern in the *mp-B4149* mutants, albeit at lower levels (Fig. 9A and B), indicating that *MP* is required for normal *SHR* expression levels post embryogenesis.

We used the hypomorphic allele *mp-S319* to study later stages of development, since *mp-B4149* mutants fail to develop beyond the early seedling stage. *mp-S319* mutants display weaker phenotypes than *mpB-4149* null mutants and initiate an inflorescence meristem with, occasionally, some lateral organ primordia. We used a transcriptional reporter, *pSHR:nTdTOMATO* and a translational reporter, *pSHR:SHR-YFP* to distinguish between effects of auxin on the *SHR* promoter activity and posttranscriptional effects leading to protein localization. Compared to the wild type, *pSHR:nTdTOMATO* expression was strongly reduced in the *mp-S319* inflorescences (Fig. 9C-F). Similar results were observed for the translational reporter *pSHR:SHR-YFP*, and weak expression in a ring-shaped domain was found in cross sections through the inflorescence stem (Fig. 9K-N). Similarly, on following the SCR localization using *pSCR:SCR-RFP*, we observed a reduced expression in the meristem periphery in *mp-S319*, thus overall resembling the SHR expression pattern (Fig. 9G-J). We therefore conclude that MP induces *SHR* and *SCR* expression in the meristem periphery and primordia.

We then tested whether *MP* could promote *SHR* expression throughout the meristem. We examined the regulation of *SHR* under controlled MP expression through inducible MP-GR fusion protein from the ubiquitin-10 promoter (*pUBQ10:MP-GR*). Treatment of these plants

with dexamethasone (DEX) allows the nuclear entry of MP-GR. Within 4 h of DEX treatment, ubiquitously expressed MP resulted in increased expression levels of *pSHR:SHR-YFP* while retaining its wildtype expression domain (Fig. 9O-P; Suppl Fig. 8Q and R), indicating that MP can increase *SHR* expression levels, but is not sufficient to control the precise expression pattern in the absence of additional auxin. Thus, MP possesses a quantitative regulatory control over *SHR* expression with increasing levels of MP correspondingly increasing SHR levels.

To better understand the distinct roles of *SHR* and *MP* in organ initiation, we generated double mutants of *mp-S319* and *shr-2*. Unlike *mp-S319* that forms fewer flower than the wild type, the phenotype of the double mutant *mp-S319 shr-2* was severe with naked inflorescences that lacked all organ primordia (Fig. 10A-D''). These data suggest that *SHR* acts downstream of *MP* to promote flower initiation.

In summary, MP induces SHR and SCR expression. And MP regulation of *SHR* expression occurs likely through its binding to the identified AuxRE motifs in *SHR* promoter region (Fig. 9A-P).

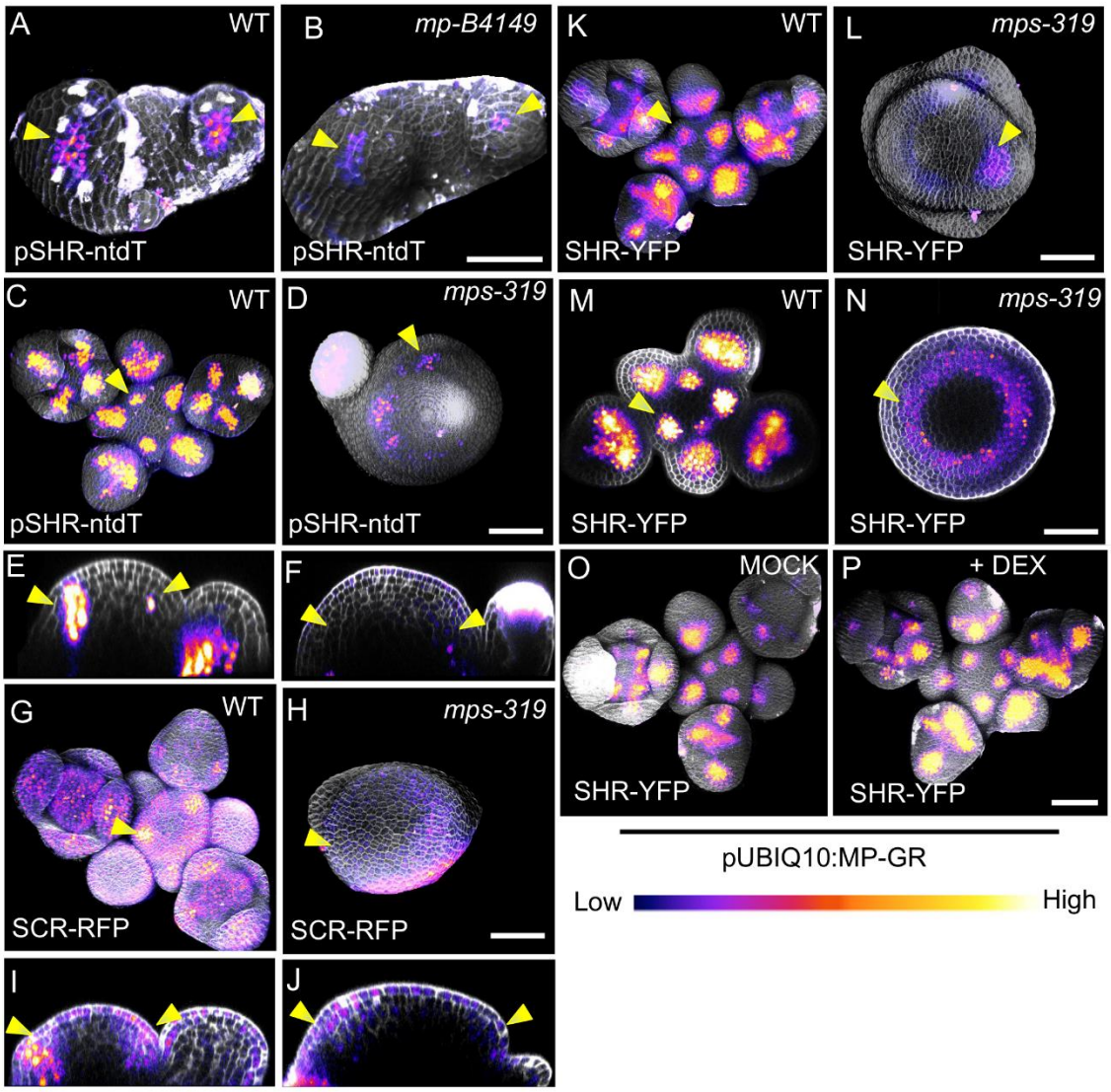

Fig. 9: SHR and SCR act downstream of MP in the shoot apical meristem.

(A and B) Representative 3D projection of shoot apical meristems at 5 weeks after germination expressing *pSHR-ntdTomato* reporter (magenta) in WT (n=4) **(A)** and *mp-B4149* (n=4) **(B)** mutant vegetative meristems. Yellow arrowheads in **(A)** and **(B)** indicate the region where lateral organ primordia initiate and pSHR-ntdTomato expression. Scale bar represents 50 µm. **(C and D)** Representative 3D projection of shoot apical meristems at 5 weeks after germination expressing *pSHR-ntdTomato* reporter (magenta) in WT (n=5) **(C)** and *mps-319* mutant (n=5) **(D)**. **(E and F)** Longitudinal optical section of **(C)** and **(D)** respectively. Yellow arrowheads in **(C)**, **(D)**, **(E)** and **(F)** indicate the region where lateral organ primordia initiate and pSHR-ntdTomato expression. Scale bar represents 50 µm. **(G and H)** Representative 3D projection of shoot apical meristems at 5 weeks after germination expressing *pSCR:SCR-RFP* reporter (magenta) in WT (n=4) **(G)** and *mps-319* mutant (n=4) **(H)**. **(I and J)** Longitudinal optical section of **(G)** and **(H)** respectively. Yellow arrowheads in **(G)**, **(H)**; **(I)** and **(J)** indicate the region where lateral organ primordia initiate and pSCR:SCR-RFP expression. Scale bar represents 50 µm. **(K and L)** Representative 3D projection of shoot apical meristems at 5 weeks after germination expressing *pSHR:SHR-YFP* reporter (magenta) in WT (n=4) **(K)** and *mps-319* mutant (n=3) **(L)**. **(M and N)** Transversal optical section of **(K)** and **(L)** respectively. Yellow arrowheads in **(K)**, **(L)**; **(M)** and **(N)** indicate the region where lateral organ primordia initiate and pSHR:SHR-YFP expression. Scale bar represents 50 µm. **(O and P)** Representative 3D projection of shoot

apical meristems at 5 weeks after germination expressing *pSHR:SHR-YFP* reporter (magenta) in *pUBIQ10:MP-GR* plants 4 hr after mock (n=5) **(O)** and 4 hr after DEX treatment (n=5) **(P)**. Fluorescence intensities were coded blue to yellow corresponding to increasing intensity. Scale bar represents 50 µm.

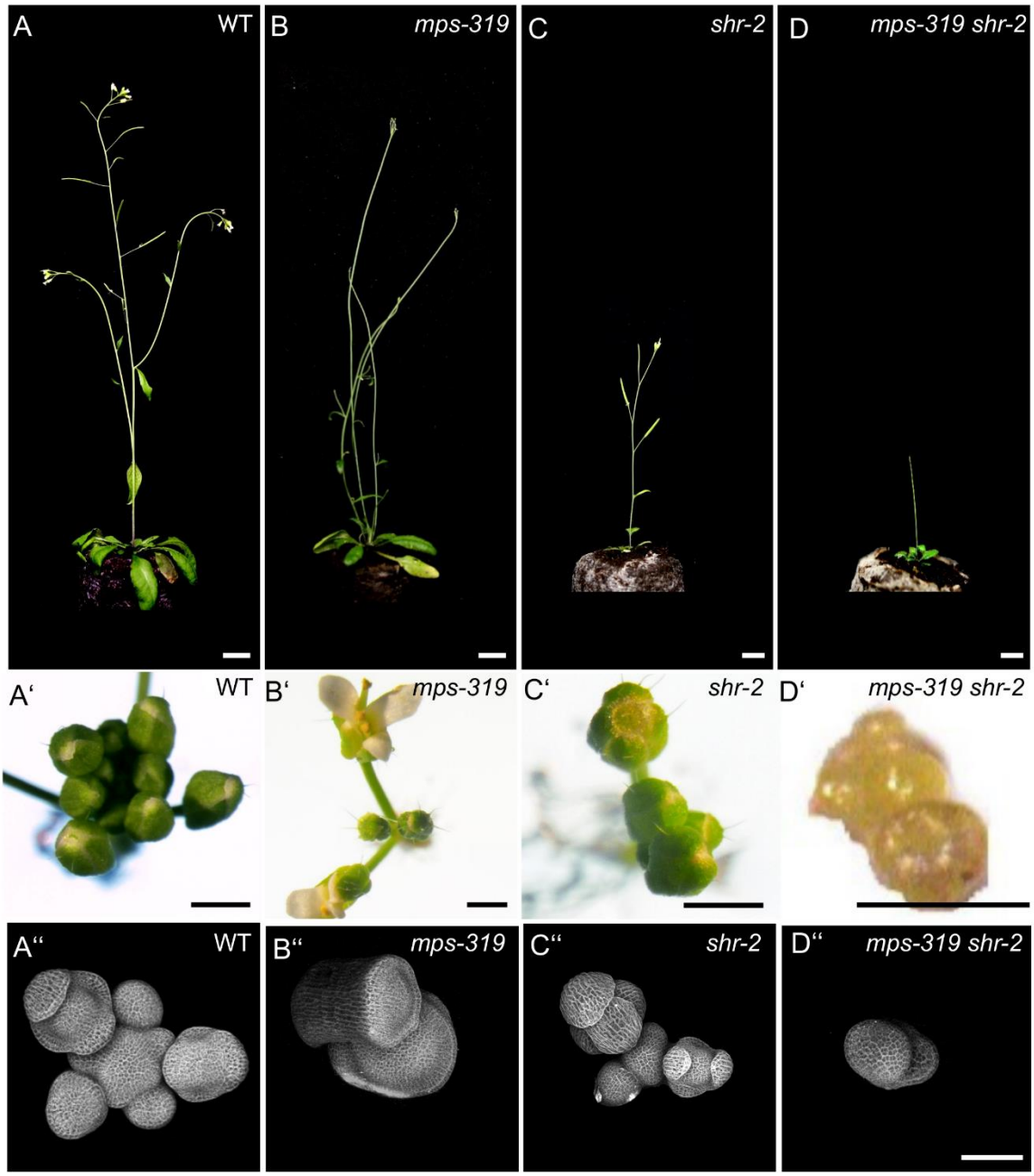

Fig 10: *shr* mutant and *shr mps-319* double-mutant phenotypes.

(A-D) Plant phenotypes of 42-day-old WT **(A)**, *mps-319* mutant **(B)**, *shr-2* mutant **(C)** and *mps-319 shr-2* double mutant **(D)**. Scale bar represents 1 cm. **(A'-D')** Top view of 31-day-old inflorescences of WT **(A')**, *mps-319* mutant **(B')**, *shr-2* mutant **(C')** and *mps-319 shr-2* double mutant **(D')**. Scale bars represent 2 mm. **(A''-D'')**. Representative 3D projection of shoot apical meristems at 5 weeks after germination from WT **(A'')**, *mps-319* mutant **(B'')**, *shr-2* mutant **(C'')** and *mps-319 shr-2* double mutant **(D'')**. Scale bar represents 50 µm.

6.4.10. Mutation of the AuxRE motifs within *SHR* promoter results in low promoter activity

SHR expression has been shown to be induced by the ARF TF, MP (Fig: 9A-P). To that end, we wanted to understand if MP regulation of *SHR* occurs by MP binding to the AuxRE motifs of the SHR promoter. We first functionally analyzed the two AuxREs (AuxRE1 and AuxRE2) in the *SHR* promoter for transcriptional activation. We tested the ability of the *SHR* promoter, with or without these AuxREs, to control the expression of mVenus or luciferase upon transient expression in *Nicotiana benthamiana* leaves after Agrobacterium infiltration. mVenus under control of the wild-type *SHR* promoter was co-infiltrated with *p35S:MP*, or *p35S:GUS* as a negative control. We observed strong *mVenus* expression from the wild-type *SHR* promoter in the presence of *p35S:MP*, which was about 6 fold higher than upon coexpression of *p35S:GUS* (Fig. 6B). Converting AuxRE1 from “GAGACA” to “GAGCCA” (mAuxRE1) or “GTGCTC” (mAuxRE1-2) and AuxRE2 from “TGTCTC” to “TGGCTC“ (mAuxRE2) or TGGAGA (mAuxRE2-2) drastically reduced the response to *p35S:MP* coexpression, and mutating both AuxREs had an additive effect, resulting in no significant response to overexpression of *MP* (Fig. 11B-J; Suppl Fig. 7B-J). Similar results were obtained using a Luciferase assay system (Suppl Fig. 8A-H), indicating that MP interacts with AuxRE elements in the *SHR* promoter to regulate *SHR* expression.

We then investigated if these elements also contribute to *SHR* expression pattern in the Arabidopsis SAM, we generated transgenic plants using either the wild-typic *SHR* promoter, or the mutant versions carrying base changes in one or both AuxREs. At least ten independent transgenic lines were analyzed for each promoter construct. Expression of the wild-typic *pSHR:mVenus-NLS* produced a strong expression in lateral organ primordia and floral meristems. However, mutations in AuxRE1 (mAuxRE1 or mAuxRE1-2) or AuxRE2 (mAuxRE2 or mAuxRE2-2) led to decreased mVenus expression in all organ primordia stages and the floral meristem (Fig. 11K-M; Suppl Fig 7K-M). And when both AuxREs (mAuxRE1+2 or mAuxRE1-2+2-2) were mutated, mVenus expression was barely detectable in the *SHR* promoter version (Fig. 11N; Suppl Fig 7N), showing a stronger reduction in expression. This shows that both AuxRE motifs function parallelly in an additive manner during ARF-dependent activation of *SHR* expression in the SAM. Notably, consistent with the expression in the SAM, mutations in AuxREs motifs in the *SHR* promoter also led to a decreased mVenus expression in RAM compared to the wild-typic *pSHR:mVenus-NLS* where *SHR* and *MP* expression overlap (Suppl Fig. 9A-H; Suppl Fig. 13B and C).

In conclusion, AuxRE motifs in *SHR* promoter are required for MP-dependent activation of SHR expression in in both SAM and RAM.

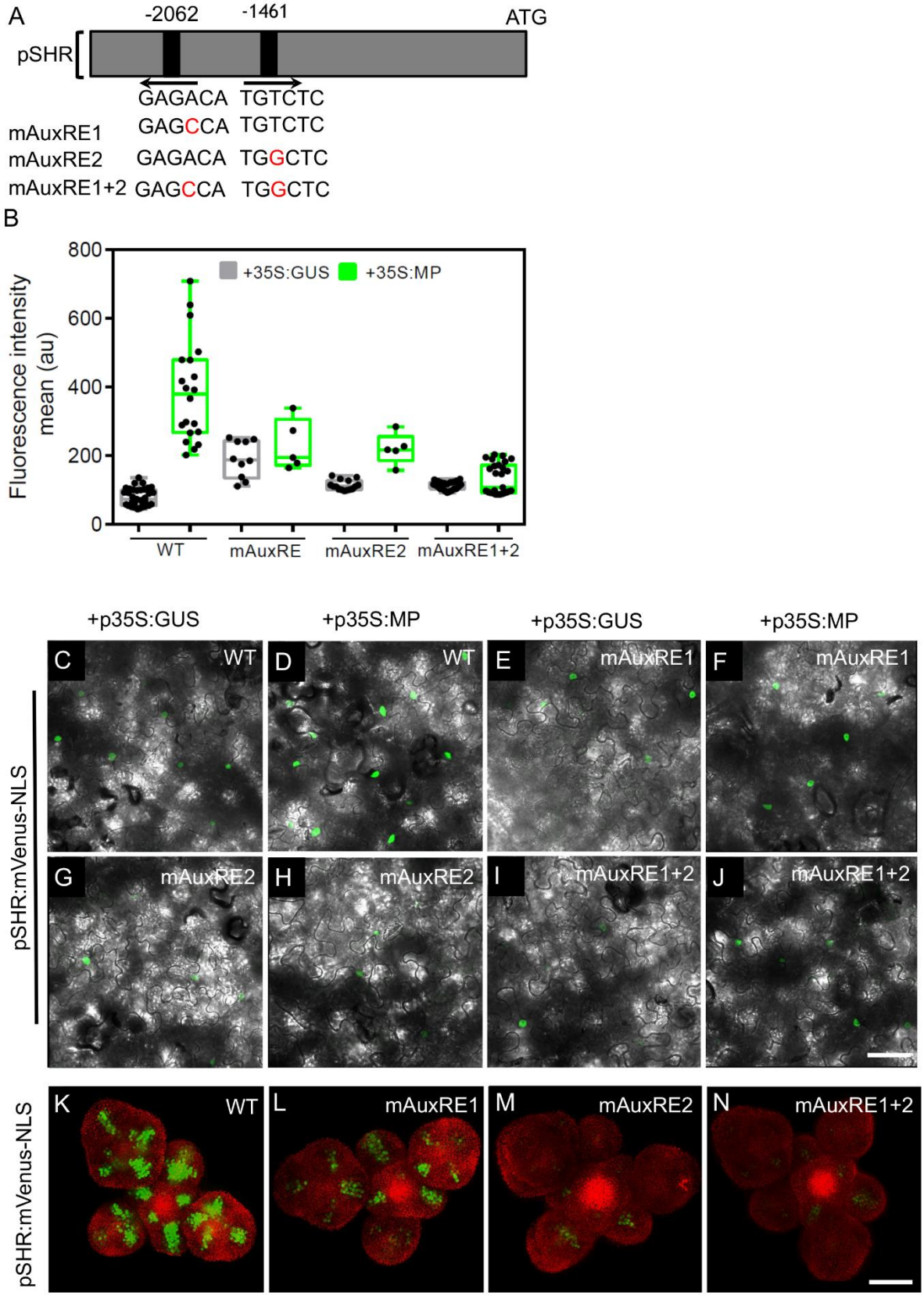

Fig. 11: MP Regulates *SHR* expression in the shoot apical meristem.

(A) Schematic representation of the *SHR* promoter. The positions of two auxin response elements are shown. Overview of mutated promoter versions of *pSHR*. AuxREs were mutated and multiple combinations of these mutated motifs were combined into a single promoter. The original AuxRE sequence GAGACA was mutated to GAGCCA (mAuxRE1), the original AuxRE sequence TGTCTC was mutated to TGGCTC (mAuxRE2). **(B)** Quantification of mVenus fluorescence signal intensity from leaves transiently transformed with mVenus-NLS under the control of the wild-type SHR promoter or under the control of the SHR promoter with mutations in AuxRE motifs in the presence of *p35S:GUS* or *p35S:MP*. **(C-J)** Leaves transiently transformed with mVenus-NLS under the control of the wild-type SHR promoter **(C and D)** or under the control of the SHR promoter with mutations in AuxRE motifs, mAuxRE1 **(E and F)** mAuxRE2 **(G and H)** and mAuxRE1+2 **(I and J)** together with *p35S:MP* or *p35S:GUS*. mVenus fluorescence signals were detected by confocal microscopy. Scale bar represents 50 µm. **(K–N)** Representative 3D projection of shoot apical meristems at 5 weeks after germination expressing mVenus-NLS under the control of the wild-type SHR promoter (n≥6) **(K)**, and under the control of the SHR promoter with mutations in AuxRE motifs mAuxRE1 (n≥5) **(L)** mAuxRE2 **(M)** and mAuxRE1+2 (n≥5) **(N)**; Chlorophyll (red). Scale bar represents 50 µm.

6.4.11. SHR regulates *LFY* expression in the SAM

It has been previously shown that *MP* directly activates *LFY* expression to confer floral identity to organ primordia (Yamaguchi et al., 2013). We further showed that MP induces *SHR* and *SHR* is required for normal flower initiation pattern and meristem development. We therefore asked if *SHR* and *LFY* activities are coordinated.

We then performed coexpression analysis of LFY, SHR and SCR. We observed that *SHR* and *SCR* were expressed two plastochrons prior to *LFY* in the primordia (Fig. 12A), we hypothesized that *SHR* might mediate MP-dependent *LFY* expression. We first tested whether *LFY* expression was altered in *shr-2* mutants. mRNA quantification via qRT-PCR from SAM and flower primordia up to stage 5 revealed that *LFY* RNA levels were downregulated by approximately 60% in *shr-2* compared to wild type levels (Fig. 12D). We further tested the LFY protein level and expression pattern using *pLFY:GFP-LFY* reporter (named *pLFY::GLFY* in Wu et al., 2003) (Wu et al., 2003). In the wild type, *LFY* was not expressed in the SAM, but at the flower primordia from stage 3 onwards. At later stages, *LFY* remained expressed in the adaxial side of sepals, and in the 2nd and 3rd floral whorls. In *shr-2* mutants, LFY-GFP fluorescence was barely visible at early stages and strongly decreased at later stages, compared to wild type (Fig. 12B-C). This indicates that *SHR* function is required for normal *LFY* expression patterns. However, analysis of *SHR* and *SCR* expression in *lfy-12* mutants revealed no obvious differences compared to wild type (Suppl Fig. 10A-D), and we therefore conclude that *LFY* does not feed-back to the *SHR-SCR* module.

In the *lfy-12* null-mutant, leaf-like bracts are generated from the inflorescence meristem and formation of flower meristems is delayed. Most floral organs are leaf-like and not arranged in regular whorls. Double mutants of *lfy-12 shr-2* were strongly retarded in growth and displayed dramatically enhanced floral primordium initiation defects (Fig. 12E-L). We conclude from this

analysis that the *SHR-SCR* module promotes *LFY* expression, and that it also promotes floral meristem development in a *LFY*-independent manner.

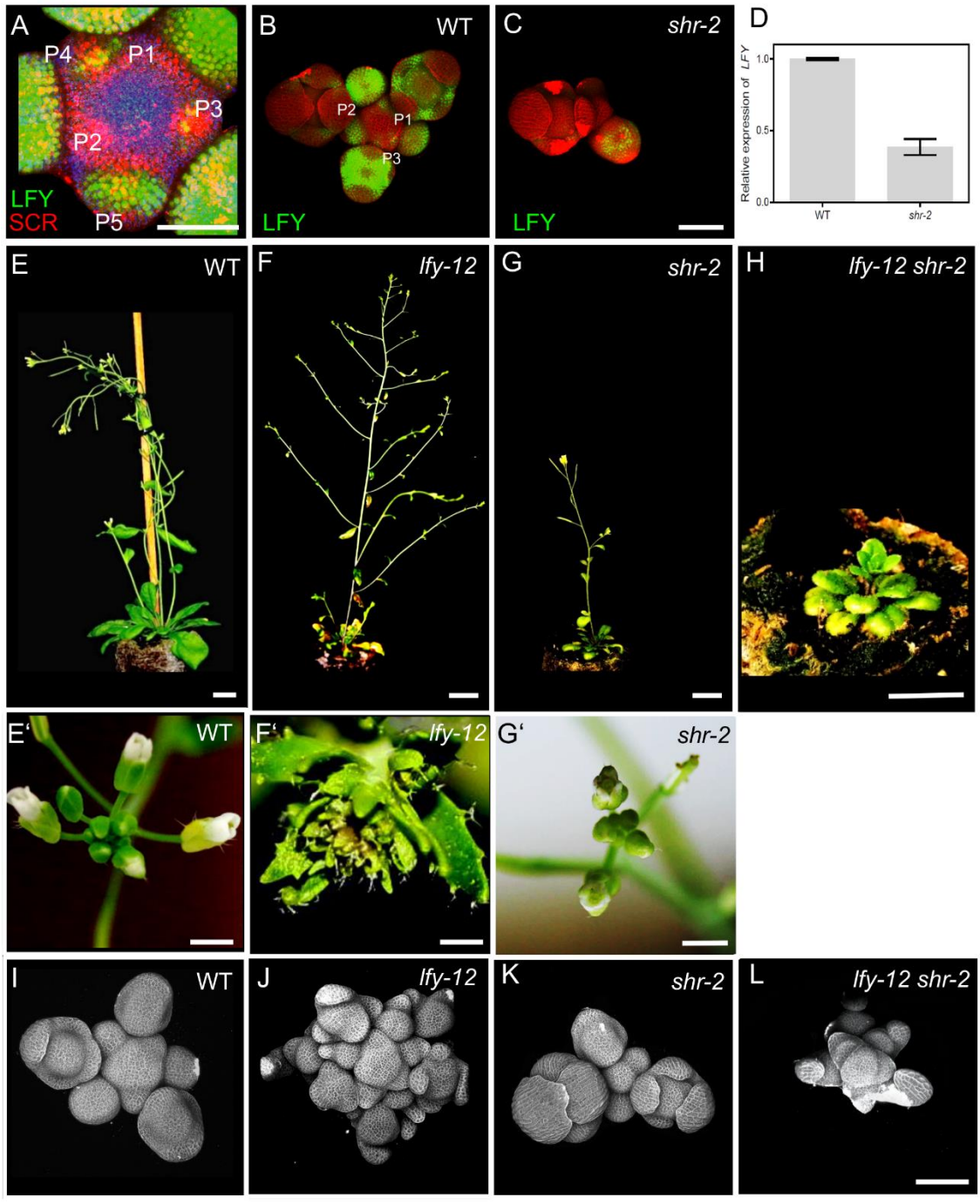

Fig. 12: *LFY* act downstream of SHR in the shoot apical meristem.

(A) Representative 3D projection of shoot apical meristems at 5 weeks after germination coexpressing *pLFY:LFY-GFP* (green) and *pSCR:SCR-RFP* (red) reporters. Chlorophyll (blue). Scale bar represents 50 µm. **(B and C)** Representative 3D projection of shoot apical meristems expressing *pLFY:LFY-GFP* reporter (green) in WT(n≥3) **(L)** and *shr-2* mutant (n≥3) **(M)**. Cell walls were stained with PI (red). Scale bar represents 50 µm. **(D)** Quantitative real-time PCR analysis showing the relative expression levels of *LFY* in WT and *shr-2* mutant shoot apical meristems. The expression level in Col-0 is set to 1 and error bars show standard deviation. Expression levels were normalized using AT4G34270 and AT2G28390. **(E-H)** Plant

phenotypes of 45-day-old WT **(E)**, *lfy-12* mutant **(F)**, *shr-2* mutant **(G)** and *lfy-12 shr-2* double mutant **(H)**. Scale bar represents 1 cm. **(E'-G')** Top view of 31-day-old inflorescences of WT **(E')**, *lfy-12* **(F')** mutant and *shr-2* mutant **(G')**. Scale bar represents 2 mm. **(I-L)** Representative 3D constraction of shoot apical meristems at 5 weeks after germination from WT **(I)**, *lfy-12* mutant **(J)**, *shr-2* mutant **(K)** and *lfy-12 shr-2* double mutant **(L)**. Scale bar represents 50 µm.

6.4.12. *SCL23* genetically interacts with SHR-SCR pathway and contributes to SAM size maintenance

The GRAS family TF SCL23, the closest homologue of SCR, interacts with the *SHR-SCR* module at several levels. SCL23 forms protein complexes with both SHR and SCR (Long et al., 2015a), and its expression is activated by SHR but gets repressed by SCR in the root. Interestingly, SCL23 was reported to be highly mobile, and to transcriptionally repress *SCR* (Long et al., 2015a). Taken together, this indicates that *SCL23* acts to fine-regulate expression and function of the *SHR-SCR* module in the root meristem. We therefore asked if *SCL23* exerts a similar function in the SAM.

To answer this, we first investigated the expression pattern of *SCL23* in the SAM using the transcriptional reporter *pSCL23:H2B-YFP*, and a functional translational reporter line expressing *pSCL23:SCL23-YFP* (Long et al., 2015a). The expression of the transcriptional reporter, *pSCL23:H2B-YFP* was found in the L3 of the SAM and floral meristems, and in floral organ primordia (Fig. 13A and C). The translational reporter *pSCL23:SCL23-YFP* showed a wider expression pattern than the transcriptional reporter (Fig. 13B and D), which was suggestive of SCL23 mobility. To make sure that the wider activity of translational line is not due to the presence of additional transcriptional control regions within the coding sequence of *SCL23*, we expressed SCL23-mVenus under the *CLV3* promoter, which confines the expression exclusively to the CZ. We, once again, observed SCL23 spreading from the CZ into the surrounding cells, which is consistent with SCL23 being mobile in the SAM (Fig. 13E and F).

We then tested the coexpression of SCL23 and SCR to investigate the regulatory dynamics among *SCL23*, *SCR* and *SHR*. A dual reporter line with *pSCR:SCR-RFP* and *pSCL23:SCL23-YFP* revealed that the expression patterns of both genes are mostly mutually exclusive, with SCL23 in a central domain of the SAM and in the inner cell layers of primordia, while SCR is concentrated to the PZ, the L1 of the CZ and the outer cell layers of lateral organ primordia (Fig. 13G and I). Some cells expressing both SCL23 and SCR were located deep inside lateral organ primordia (Fig. 13K). A similar coexpression analysis of *pSCL23:SCL23-YFP* with *pSHR:mScarlet-SHR* indicated an overlap of expression in the deep cell layers of lateral organ primordia (Fig. 13H, J and L). In *shr-2* mutants, *pSCL23:SCL23-YFP* remains only weakly

expressed in a pattern similar to wild type (Fig. 13M and N), indicating that SHR promotes expression of *SCL23* in the SAM, similar to the regulation observed in the RAM (Long et al., 2015a).

We then performed genetic interaction studies to understand the relationship between SCL23, SCR and SHR in the SAM. In *scl23-2* mutants, SAM size is significantly decreased compared to wild type, or to the complemented line *pSCL23:SCL23-YFP*/*scl23-2* (Fig. 13O-R). Using the PlaCCI marker to analyze cell division patterns, we found that similar to *shr-2* and *scr-3* or *scr-4* mutants, the percentage of cells in G1 phase increased, indicating delayed cell divisions in the SAM (Fig. 13S-U). Genetic analyses showed that *shr* mutants are epistatic to *scl23* mutants in double mutant combinations, and that *scr-3 scl23-2* double mutants and *shr-2 scr-3 scl23-2* triple mutants were additive with smaller plant rosettes and reduced plant stature (Suppl Fig. 11A-H') (Yoon et al., 2016) .

To further analyse *SCL23* function, we generated transgenic Arabidopsis plants overexpressing SCL23 from the pUBIQ10 (*pUBIQ10:*SCL23-mVenus) or pRPS5A (*pRPS5A*:SCL23-mVenus) promoter. Both UBIQ10 and RPS5A promoters are expected to drive high-level and widespread expression of the fused reporter gene. However, we observed SCL23-mVenus fluorescence confined to the lateral organ primordia and not in the meristem center, where normally pSCL23:SCL23-YFP is expressed. We found a similar scenario when we tried to overexpress SHR or SCR in the SAM, implying tight regulatory controls acting in the different domains in the SAM preventing excessive protein accumulation. However, excessive accumulation of these transcription factors was observed outside their normal expression domains (Suppl Fig. 12A-E). This shows that SCL23, SHR and SCR are under strict translational or post-translational control, for example due to the localised presence of miRNAs (Llave et al., 2002), and that meristem cells can therefore express only a set maximum amount of these GRAS protein family members.

Together, these results show that SHR is the upstream regulator of SCL23 and SCR, and the that the SHR-SCR-SCL23 regulatory pathway plays an important role in regulating the SAM development.

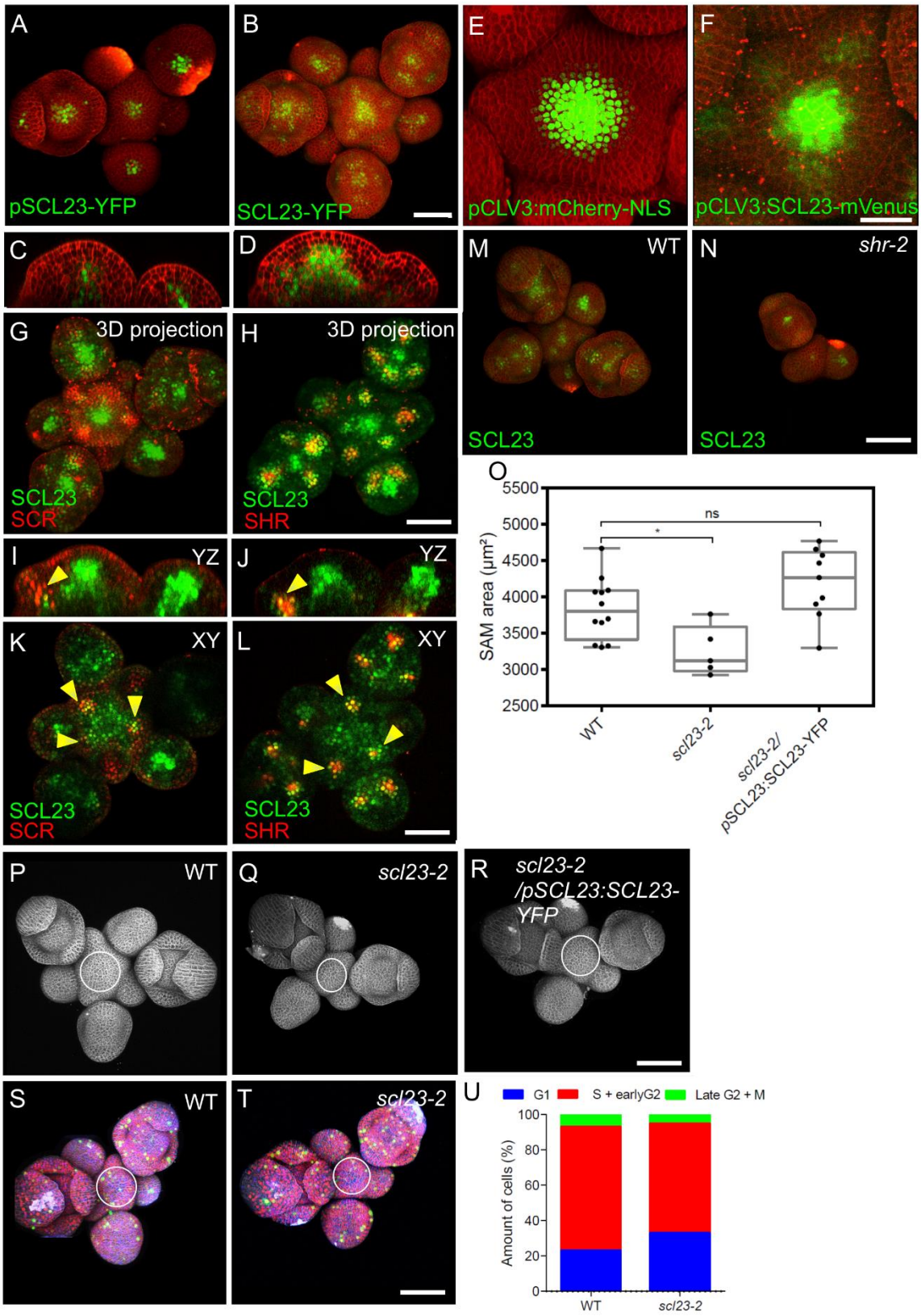

Fig. 13: SCL23, SCR and SHR proteins show spatially different patterns but perform similar functions in the shoot apical meristem.

(A and B) Representative 3D projection of shoot apical meristems at 5 weeks after germination expressing *pSCL23:H2B-YFP* reporter (green) (n≥3) **(A)** and *pSCL23:SCL23-YFP* reporter (green) (n≥10) **(B)**. Cell walls were stained with PI (red). Scale bar represents 50 µm. **(C and**

D) Longitudinal optical sections of **(A)** and **(B)** respectively. **(E and F)** Representative 3D projection of shoot apical meristems at 5 weeks after germination expressing *pCLV3-mCherry-NLS* reporter (green) (n≥5) **(E)** and the *pCLV3:SCL23-mVenus* reporter (green) (n≥4) **(F)**. Cell walls were stained with PI (red). Scale bar represents 50 µm. **(G and H)** Representative 3D projection of shoot apical meristems at 5 weeks after germination meristems coexpressing *pSCL23:SCL23-YFP* reporter (green) and *pSCR:SCR-RFP* reporter (red) (n≥3) **(G)** and *pSCL23:SCL23-YFP* reporter (green) and *pSHR:mScarlet-RFP* reporter (red) (n≥3) **(H)**. Scale bar represents 50 µm. **(I and J)** Longitudinal optical sections of **(G)** and **(H)** respectively. **(K and L)** Transversal optical sections of **(G)** and **(H)** respectively. Yellow arrowheads in **(I)** and **(K)** indicates the region where both *pSCL23:SCL23-YFP* reporter (green) and *pSCR:SCR-RFP* reporter (red) expression overlap. Yellow arrowheads in **(J)** and **(L)** indicates the region where both *pSCL23:SCL23-YFP* reporter (green) and *pSHR:mScarlet-SHR* reporter (red) expression overlap. **(M and N)** Representative 3D projection of shoot apical meristems at 5 weeks after germination expressing *pSCL23:SCL23-YFP* reporter (green) in WT (n=4) **(G)** and *shr-2* mutant (n=3) **(H)**. Cell walls were stained with PI (red). Scale bar represents 50 µm. **(O)** Quantification of shoot apical meristem size at 5 weeks after germination from Col-0 (n=12), *scl23-2* mutant (n=5) and *scl23-2*/*p*SCL23:SCL23-YFP (n=9). **(P-R)** Representative 3D projection of shoot apical meristems at 5 weeks after germination from WT **(P)**, *scl23-2* mutant **(Q)** and *scl23-2*/*p*SCL23:SCL23-YFP **(R)**. Cell walls were stained with PI (gray). Scale bar represents 50 µm. **(S and T)** Representative 3D projection of shoot apical meristems at 5 weeks after germination from WT (n=11) **(S)** and *scl23-2* (n=5) **(T)** coexpressing the three PlaCCI markers. *pCDT1a:CDT1a-eCFP* reporter (blue), *pHTR13:pHTR13-mCherry* reporter (red) and *pCYCB1;1:NCYCB1;1-YFP* reporter (green). Cell walls were stained with DAPI (gray). Scale bar represents 50 µm. **(U)** Quantification of cells in different cell cycle phases in the meristem region (area surrounded by white circles in **(S)** and **(T)**) of WT (n=11) and *scl23-2* (n=5). Asterisks indicate a significant difference (*=$p < 0.01$; ns= no significant difference; statistically significant differences were determined by Student's *t*-test).

6.4.13. SCL23 acts together with WUS to maintain stem cell homeostasis in the SAM

Our study of *SCL23* function so far showed that SCL23 promotes SAM development and acts from the meristem center (Fig. 13B and D). The related *GRAS* family transcription factors HAM1 and HAM2 were shown to physically interact with WUS to promote shoot stem cell proliferation and repress *CLV3* expression in the OC (Zhou et al., 2015). Since *SCL23* and *WUS* expression strongly overlap in the rib meristem (Fig. 14B and C), we wanted to examine if SCL23, like HAM1/2, could also interact with WUS. Therefore, we tested the *in vivo* interaction of WUS and SCL23 by determining FRET between fluorescent protein fusions after inducible transient expression in *Nicotiana benthamiana* leaves. SCL23-mVenus interacted with WUS-mCherry with a FRET efficiency similar to the FRET-positive control, a nuclear localized mVenus-mCherry fusion protein (Fig. 14A). SCL23 showed a much weaker tendency to form homomers, assayed by measuring FRET between SCL23-mVenus and SCL23-mCherry. SCL23-mVenus with the transcription factor AS2-mCherry served as negative control.

Given its interaction with WUS and its developmental role in the SAM, we asked if SCL23 expression is also subjected to regulation by the *CLV* signaling pathway. We first observed the expression pattern of SCL23 and CLV3. The dual reporter line with *pSCL23:SCL23-YFP* and *pCLV3:NLS-mCherry* showed that *SCL23* and *CLV3* were expressed in largely complementary patterns in the SAM. SCL23 was expressed in the rib meristem, but absent from L1 and L2 layers in the meristem center, while *CLV3* is highly expressed in the L1 and L2 layers and to a lesser level in the L3 layer (Fig. 14B and C). When introduced into the *clv3-9* mutant background, *pSCL23:SCL23-YFP* expression was strongly expanded and extended throughout the enlarged and sometimes fasciated meristems, similar to the altered expression domain of *WUS* in strong *clv*-mutants (Fig. 14F-G). This shows that *SCL23* expression is, like *WUS*, negatively regulated by the *CLV* signalling pathway.

To study the developmental role of SCL23 and WUS interaction, we conducted genetic interaction studies. While the SAM of *scl23-2* single mutant was smaller than wild type (Fig. 13O), the null allele *wus-am* had terminated SAM development at an early seedling stage but continued to initiate new shoot meristems from axillary positions (Fig. 15C). The *wus-am scl23-2* double mutants showed an enhanced phenotype with earlier arrest of SAM development (Fig. 14D). The hypomorphic *wus-7* mutants forms an inflorescence meristem similar to the wild type (Fig. 15G-G'') (Zhou et al., 2015), while the *wus-7 scl23-2* double mutants display premature termination of floral meristems (Fig. 15I-I''). These genetic data support our hypothesis that SCL23 and WUS function together in shoot meristem stem cell maintenance.

Taken together, the colocalization and interaction between SCL23 and WUS along with the genetic data strongly suggests that SCL23 and WUS function as partners in SAM maintenance.

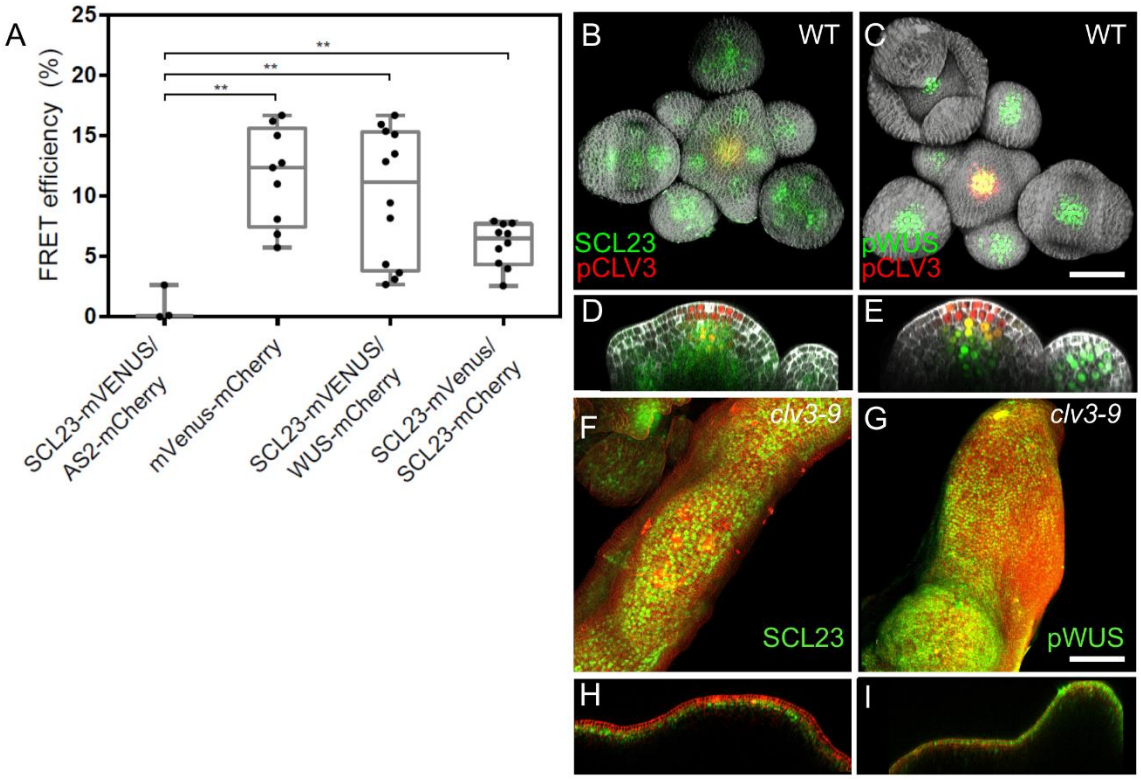

Fig. 14: SCL23 and WUS physically interact, and both are negatively regulated by CLV pathway in the shoot apical meristem.

(A) FRET efficiency measured in epidermis cells of *N. benthamiana* between SCL23-mVenus and WUS-mCherry (n=12) or SCL23-mCherry (n=10), compared with the negative control SCL23-mVenus and AS2-mCherry (n=3) and positive control mVenus-mCherry (n=9). **(B and C)** Representative 3D projection of shoot apical meristems at 5 weeks after germination coexpressing *pSCL23:SCL23-YFP* (green) and *pCLV3-mCherry-NLS* reporter (red) (n≥3) **(B)** and *pWUS:3xVenus-NLS* reporter (green) and *pCLV3-mCherry-NLS* reporter (red) (n≥6) **(C)**. Cell walls were stained with DAPI (gray). Scale bar represents 50 µm. **(D and E)** Longitudinal optical sections of **(B)** and **(C)** respectively. **(F and G)** Representative 3D projection of shoot apical meristems at 5 weeks after germination expressing *pSCL23:SCL23-YFP* reporter (green) in *clv3-9* mutant (n≥3) **(M)** and *pWUS:3xVenus-NLS* reporter (green) in *clv3-9* mutant (n≥3) **(N)**. Cell walls were stained with PI (red). Scale bar represents 50 µm. **(H and I)** Longitudinal optical sections of **(F)** and **(G)** respectively. Asterisks indicate a significant difference (**=$p < 0.001$; statistically significant differences were determined by Student's *t*-test).

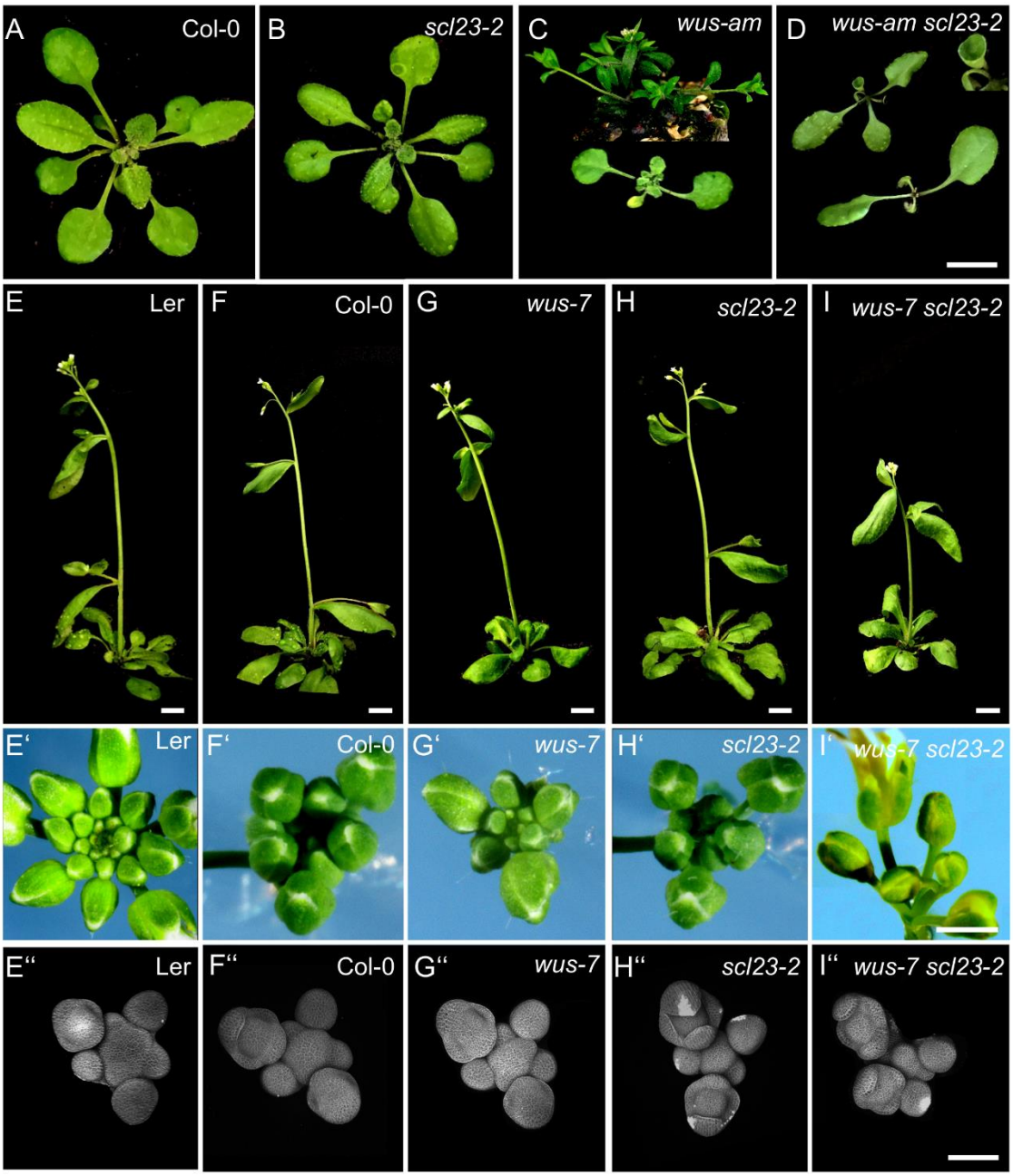

Fig. 15: WUS and SCL23 cooperatively control shoot stem cell homeostasis in the shoot apical meristem.

(A-D) Top view of 21-day-old rosettes of WT (Col-0) **(A)**, *scl23-2* mutant **(B)**, *wus-am* mutant **(C)** and *scl23-2 wus-am* double mutant **(D)**. Scale bar represents 1 cm. **(E-I)** Plant phenotypes of 36 old Ler **(E)**, Col-0 **(F)**, *scl23-2* mutant **(G)**, *wus-7* mutant **(H)** and *scl23-2 wus-7* double mutant (I). Scale bar represents 1 cm. **(E’-I’)** Top view of 35-day-old inflorescences of Ler **(E’)**, Col-0(F’), *scl23-2* mutant **(G’)**, *wus-7* mutant **(H’)** and *scl23-2 wus-7* double mutant **(I’)**. Scale bar represents 2 mm. **(E’’-I’’)** Representative 3D projection of shoot apical meristems at 5 weeks after germination from Ler **(E’’)**, Col-0 **(F’’)**, *scl23-2* mutant **(G’’)**, *wus-7* mutant **(H’’)** and *scl23-2 wus-7* double mutant **(I’’)**. Cell walls were stained with PI (gray). Scale bar represents 50 µm.

6.5. Discussion

Acquisition of cell identity within the different functional domains of the SAM is important for the postembryonic establishment of all above ground structures and the maintenance of plant shoot architecture. To better understand the mechanisms that form and maintain the multiple functional domains within the SAM, we asked if a well-characterized gene regulatory network responsible for ground tissue patterning in the RAM is conserved in the SAM.

Several previous studies showed how SHR, SCR, SCL23 and JKD act together to control key steps in root meristem development and tissue layer patterning (Scheres et al., 1995, Long et al., 2015a, Long et al., 2015b). However, their function in the SAM has so far not been explored.

Using quantitative live-cell imaging together with molecular and genetic approaches, we investigated the function of the GRAS TFs SHR, SCR, SCL23 and the BIRD TF JKD in the SAM. Our results revealed that the four TFs are expressed in the SAM and together their expression covers the complete SAM in a combination of complementary and overlapping domains.

We showed here that the functions of these TFs are responsible for the cell proliferation in the SAM through the transcriptional control of key cell division regulators. Our genetic analyses also demonstrated that SHR expression is regulated by a MP dependent auxin signalling pathway via a pair of AuxRE in the *SHR* promoter (Ulmasov et al., 1997a, Ulmasov et al., 1995, Ulmasov et al., 1997b). Mutations in these AuxRE core motifs led to a decline in the activity of the *SHR* promoter (Liao et al., 2015, Lieberman-Lazarovich et al., 2019). We further showed that SHR contributes to the regulation of its known target *CYCD6;1*, and the TF LFY in lateral organ primordia. Protein interaction studies showed that SCL23 interacts with WUS in the OC to maintain shoot stem cell homeostasis. Thus, similar to what was previously described for *WUS*, we showed that *SCL23* expression is negatively regulated by the CLV pathway.

Together, these results underline the importance of the SHR-dependent gene regulatory network during SAM development. Our data show how auxin-triggered primordia initiation in the peripheral zone of the SAM activates the SHR network, which promotes formative cell divisions and, at the same time, communicates with the stem cell regulatory system via direct interaction with WUS.

6.5.1. SHR, SCR, SCL23 and JKD control SAM size by regulating the rate of cell division.

The SAM sizes of *shr*, *scr* and *scl23* mutants were smaller than the wild type, and this reduction was caused by a decrease in cell division rate (Fig. 1E-H and I-L). These findings are consistent with the growth-promoting activities of *SHR* and *SCR* in leaves and roots (Dhondt et al., 2010, Long et al., 2015a, Scheres et al., 1995) and uncover a similar role for SCL23 in the SAM (Fig. 13O-R), while JKD acts to restrict growth in both roots and shoots (Fig. 6A-C and K) (Long et al., 2015b, Welch et al., 2007).

6.5.2. Transcriptional profiles and interdependences of SCR, SCL23 and JKD in the SAM

Our detailed expression analysis of transcriptional and translational reporters showed how SHR, SCR, SCL23 and JKD expression patterns are distributed within the SAM. Analysis of expression patterns of the four TFs genes allowed us to define their expression in the different domains of the SAM. We found here that the expression of SHR to be restricted to the primordia (Fig. 3A, C and D). SCR is expressed in the primordia, overlapping with SHR expression, and its expression is also enriched in the meristem periphery and in the L1, with a low expression in the L2 within the center of the SAM (Fig. 3A and E). The lateral organ primordia expression patterns of SHR and SCR closely resembles that of PIN1, MP and LFY in the primordia (Suppl Fig. 6A-F; Fig12A) (Yamaguchi et al., 2013). JKD expression was restricted to a few cells in the abaxial cells of the lateral organ primordia. This expression overlapped in a few cells with SHR and SCR (Fig. 3D; Fig. 6H and I; Fig. 7J and K). Interestingly, SCL23 expression had a broad expression pattern within the SAM, being expressed in the OC, rib meristem, PZ and in the L3 of lateral organ primordia (Fig. 13D and I). SCL23 expression overlapped with WUS expression in the OC and RZ, and with SHR, SCR, JKD in the primordia (Fig. 13G-L) and compliments with *CLV3* expression in the center of the SAM (Fig. 14B-E).

Together SHR, SCR, SCL23 and JKD cover all the functional domains of the SAM with an overlapping domain in the primordia, and that their expression pattern is either complementing or overlapping with some genes known as key regulators of SAM patterning and activity such as *WUS*, *CLV3*, *PIN1* and *MP*. This provides further evidence that, the SHR-SCR-SCL23-JKD network could act as an important gene regulatory network that mediates a communication between the different functional domains within the SAM, to coordinates stem cell proliferation in the center and lateral organ formation at the periphery via the conserved SHR signaling pathway.

In the RAM, SHR is expressed in the stele where it is maintained mainly in the cytoplasm by its direct downstream target SCL23, which is also a mobile TFs in the RAM (Nakajima et al., 2001, Long et al., 2015a). Once in the surrounding layer, SHR is restricted to the nucleus by SCR and JKD where they together promote the expression of SCR to specify ground tissue patterning (Welch et al., 2007, Long et al., 2015b). SCL23 is the closest homolog of SCR and was shown to physically interact with SHR and SCR (Lee et al., 2008, Long et al., 2015a, Yoon et al., 2016). It has been also reported that SHR-SCL23 and SHR-SCR complexes activate the transcription of SCL23 and SCR respectively by binding to their promoters (Yoon et al., 2016, Long et al., 2015b). Moreover, genetic studies have shown that all mutant combinations where SHR function is lost display phenotypes identical to those of the *shr* single mutant, which suggests that SHR acts as the master regulator of this regulatory network (Suppl Fig. 11A-H') (Yoon et al., 2016). SHR, SCR, SCL23 and JKD are all expressed in the root CEI from where GT initiates (Suppl Fig. 13) (Long et al., 2015a, Long et al., 2017). In line with all these findings, we show here that *SHR* and *SCL23* mRNA expression is found in a smaller domain than the protein indicating a non-cell-autonomous function of SHR and SCL23 also in the SAM (Fig. 3C and D; Fig. 13C and D). SCR expression in *shr* mutant was down regulated in the primordia where both are expressed, but interestingly, SCR expression level in the meristem center did not change in *shr* mutant (Fig. 5B-E, G and H). SHR was found to accumulate more in the nucleus of cells coexpressing SCR than in the cells where SCR is absent (Fig. 5A, inset and F). This could be explained by the nuclear retention of SHR through its interaction with SCR to restrict SHR movement and activate *SCR* expression.

We were also able to show here that the expression of SCL23 and SCR are complementary in the center of the SAM with an overlapping domain in the primordia where SHR and JKD are also expressed (Fig. 13G, I and K). In agreement with previously published data (Long et al., 2015a, Yoon et al., 2016), we found here too that SCL23 expression is down regulated in the *shr* mutant (Fig. 13M and N).

Our phenotypic analysis of the different combinations between *shr, scr* and *scl23* mutants showed that these TFs genetically interact during SAM development (Suppl Fig. 11). Together with their expression pattern in the SAM (Fig. 13J-L) and the protein interaction data (Long et al., 2015a, Long et al., 2017), this gives us an understanding about the spatial localization od the different complexes in the.

6.5.3. SHR, SCR and JKD interact to form protein complexes in SAM

Various studies, using different techniques, have shown that SHR, SCR and JKD physically interact to restrict SHR mobility and regulate the expression of their target genes within the cell layer surrounding the stele in the RAM (Long et al., 2017, Clark et al., 2016). The resulting SHR–SCR–JKD complex directly controls the expression of its downstream genes in a cell type-specific manner, such as CYCD6;1 in the CEI that activate asymmetric cell division leading to the formation of the ground tissue in the root (Cui et al., 2007, Sozzani et al., 2010, Long et al., 2015b, Long et al., 2017). In agreement with these results, we show here using *in vivo* FRET-FLIM analysis that similar to the RAM, SHR, SCR and JKD physically interact in the SAM including in a small domain in the primordia where *CYCD6;1* is expressed (Fig. 4E and F; Fig. 6J and K; Fig. 7J-O). Additionally, we found that *CYCD6;1* was not expressed in the lateral organ primordia of *shr* mutant. These results provide further evidence that SHR-SCR-JKD protein complex is conserved in the SAM, and it is also implicated in the asymmetric cell division by activating the expression of CYCD6;1 in the abaxial side of lateral primordia. The resulting cell proliferation within the abaxial side create a critical mass of cells in the L3 necessary for new lateral organ outgrowth.

6.5.4. SHR regulates the initiation of lateral organ primordia in an auxin dependent manner

By linking data from current and previous studies including, the correlation between meristem size and plastochron, overlapping expression between MP, PIN1, SHR and SCR during lateral organ primordia development (this study; Suppl Fig. 6A-F; Fig. 3A-E), in the RAM (Suppl Fig. 13), and leaf (Cui et al., 2014, Wenzel et al., 2012), the identification of AuxREs in promoter SHR (this study), the down regulation of SHR expression in *mp* mutant embryo (Möller et al., 2017) and the SHR coexpression with MP target gene ARABIDOPSIS THALIANA HOMEOBOX8 (ATHB8) during leaf formation (Gardiner et al., 2011), we hypothesized that auxin may control SHR expression in the lateral organ primordia via an MP-dependent pathway. The expression of both *pDR5v2:3xYFP-N7* and R2D2 auxin reporters in *shr* and *scr* mutants (Fig. 2A-G) showed a strong change in auxin distribution compared to the wild type, with a decrease in the number of auxin maxima in the mutants. These results suggest that the expression of *SHR* and *SCR* expression is linked to auxin and that auxin could regulate their expressions. Our studies with auxin inhibitors revealed that SHR and SCR expression respond to auxin distribution in the SAM and that the addition of exogenous auxin enhances their expression (Fig. 8B-T). We demonstrated here that SHR and SCR expression in the primordia is regulated by auxin resulting in activation of cell division in the flanks of the SAM.

In the primordia, high level of auxin release MP to activate the downstream auxin response genes. Previous studies have demonstrated that SHR and SCR are strongly reduced in the embryo of *mp* mutant (Möller et al., 2017), thus likely reflecting MP as the probable link between auxin and SHR expression. In this study, we demonstrate that MP acts as a positive regulator of SHR. Here we found that the expression of SHR and SCR in *mp* mutant SAMs were dramatically decreased, as what was shown earlier in the embryo (Fig. 9A-N) (Möller et al., 2017). Additionally, SHR expression was increased after MP-GR activation in the SAM (Fig. 9O and P). Moreover, our genetic study showed that *shr* mutant enhance the primordium initiation defects of a hypomorph *mp* mutant (Fig. 10A-D'').

It was shown recently by Luo et al., that mutating the AuxRE motifs by exchanging one nucleotide reduced *DRN* promoter activity in the SAM (Luo et al., 2018). We therefore mutated the two AuxRE motifs in *SHR* promoter by substituting one or four nucleotides of these motifs and found that modification in the AuxRE motifs in *SHR* promoter leads to a severe reduction of the promoter activity and no enhancement of *pSHR:mVenus-NLS* expression upon p35S:MP in *N. benthamiana* leaves (Fig. 11; Suppl Fig. 7; Suppl Fig. 8). These results suggest that both AuxRE motifs have roughly equal contributions in the transcriptional regulation of *SHR*. Together our results provide evidence that *SHR* is required for lateral organ initiation and that its expression is regulated in an MP-dependent pathway.

In an effort to identify other SHR targets in the SAM primordia, we investigated possible interactions between *LFY* and the SHR-SCR module. *SHR* and *SCR* begin to be expressed at P1 stage of primordia while LFY expression starts in P3 (Fig. 12A), and therefore the possibility exists that *LFY* might function downstream of *SHR*. We thus assessed *LFY* expression in *shr* mutant and found that it was strongly reduced (Fig. 12B-D). The double mutant *lfy12 shr-2* showed a delay in inflorescence transition and a strong defect in shoot growth (Fig. 12E-L). Together these findings suggest that *SHR* is needed for normal expression level of LFY.

6.5.5. WUS-SCL23 heteromeric complex acts to maintain stem cell in the SAM.

The homeodomain transcription factor WUS acts as a major component in regulating SAM activity (Laux et al., 1996). WUS is expressed in the OC and migrates to the central zone where stem cells are located to activate the expression of its negative regulator CLV3 (Daum et al., 2014, Yadav et al., 2011). The resulting WUS-CLV3 negative feedback loop maintains the balance between stem cell numbers and differentiation rates of stem cell progenitors (Daum et al., 2014). A null mutation in *WUS* causes premature termination of the inflorescence meristem (Laux et al., 1996).

A previous publication reported that WUS physically and genetically interacts with HAM1 and HAM2 to confine the CLV3 expression domain to the stem cells niche in the CZ (Zhou et al., 2015, Zhou et al., 2018). Since SCL23 and the HAMs (HAM1 and HAM2) belong to the same family of GRAS TFs (Cenci & Rouard, 2017, Sidhu et al., 2020), we investigated the interactions between WUS and SCL23. Because SCL23 is strongly expressed in the OC and RZ where it is overlapping with WUS (Fig. 14B-E), it is possible that SCL23 and WUS physically interact to form heteromers. We therefore performed FRET-FLIM to examine the interaction and found that indeed SCL23 forms a protein complex with WUS (Fig. 14A).

Next, to address the role of SCL23-WUS complex in the SAM, we generated a double mutant, *scl23-2 wus-am* and found that *scl23-2* mutation enhances the vegetative shoot meristem termination in *wus-am* (Fig. 15A-D). In combination with the hypomorphic allele *wus-7*, which displays higher floral meristem activity compared to *wus-am*, *scl23-2 wus-7* double mutant caused a premature termination of the inflorescence meristem (Fig. 15E-I''). In addition, similar to *HAM1* and *WUS, SCL23* is negatively controlled by the CLV signaling, as SCL23 is expressed throughout *clv3-9* SAMs (Fig. 14F-I). Overall, these results imply that *SCL23* acts together with *WUS* to regulate the maintenance of stem cell homeostasis in the SAM.

6.5.6. Model for SHR-SCR-SCL23-JKD regulatory network in the SAM

Based on previous publications and our findings, we propose the pathways regulating the SAM and the RAM patterning, in which conserved gene regulatory networks together with auxin regulate inter-domain/layer communication to maintain the identity of the different functional domains/layers within both meristems (Fig. 16A-D).

In the SAM, within the organizing center (OC), where auxin levels are low, WUS and SCL23 physically interact to form a heteromeric complex that maintains the homeostasis of stem cells populations in the centrale zone (CZ). In the periphery zone, SCL23 and SCR may act together to maintain the boundary. Finally in the primordia auxin promote SHR expression in MP-dependent manner and then SHR physically interacts with SCR, SCL23 and JKD to activate the expression of their target genes such as *CYCD6;1* to promote cell division leading to lateral organ primordia outgrowth (Fig. 16A-C).

In the RAM, *SHR* is transcribed in the stele by MP in an auxin dependent manner and then SHR protein physically interacts with SCL23 and directly promote *SCL23* expression. SHR protein moves from stele to the cortex/endodermis initial (CEI) and the quiescent center (QC). In the CEI, SHR binds to SCR, SCL23 and JKD to activates and restricts *CYCD6;1* expression to the CEI. In the QC, SHR interacts with JKD and SCR to maintain QC through regulation of WOX5 (Fig. 16B-D).

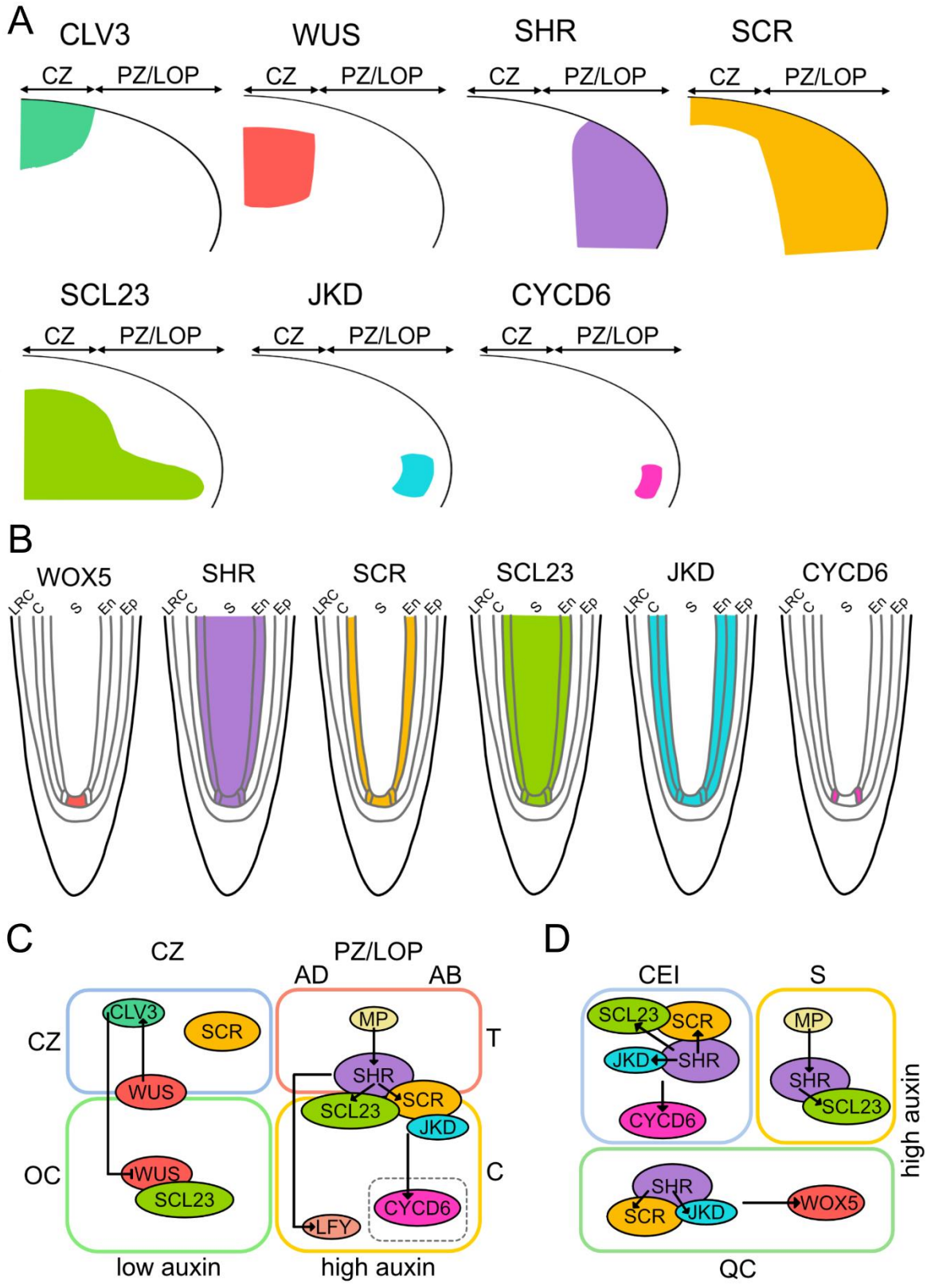

Fig 16: Proposed model for SHR-SCR-SCL23-JKD regulatory network function in the SAM and the RAM.

(A and B) Schematic representation of observed expression patterns of *CLV3*, *WUS*, SHR, SCR, SCL23, SHR and JKD showing typical expression domains in the SAM **(A)** and the RAM **(B)**.

(C and D) Schematic molecular models for SHR-SCR-SCL23-JKD gene regulatory network function in the SAM **(C)** and the RAM **(D)**, genes with genetic and/or biochemical interactions are indicated. Lines with arrows depict positive regulation, and with bars depict negative regulation. Overlap between circles describe protein–protein interactions.

(C) The SHR transcription is regulated by MP in the PZ/LOP (orange box and yellow box). In the PZ/LOP, SHR activates SCR and SCL23 transcription. Then SHR-SCR-SCL23-JKD protein complex induces periclinal cell division that leads to the outgrowth of lateral organ primordia through the activation of *CYCLIND6;1* (*CYCD6;1*) in a small domain within the corpus in the PZ/LOP (white dashed rectangle). SHR also regulates the expression of *LFY* within the corpus in the PZ/LOP (yellow box) leading to lateral organ initiation. In the organizing center (green box), SCL23 interacts with WUS to maintain a stem cell homeostasis in the central zone (CZ) (blue) where CLV3 is expressed.

(D) In the RAM, SHR is transcribed in the stele (yellow box) then the proteins move to the CEI (blue box). In the CEI, SHR activates *SCR*, *SCL23* and *JKD* expression, and together form protein complex to induce the formative division via activation the expression of *CYCD6;1*. High levels of auxin in the CEI also contribute to *CYCD6;1* activation. In the QC (green box), the SHR-SCR-SCL23-JKD protein complex positively regulates expression of *WOX5*.

T= Tunica, C= Corpus. CZ= Central zone. OC= Organizing center. PZ/LOP= Peripheral zone/lateral organ primordia. LRC= Lateral root cap. C= Cortex. S= Stele. En= Endodermis. Ep= Epidermis. CEI= Cortex/endodermis initial. QC= Quiescent center

6.6. Perspectives

We describe here a new mechanism that coordinates between the cell production domain in the center of the SAM and their final destination in lateral organ primordia. However, the exact mechanism of their regulation remains to be investigated.

Our experiments demonstrate the relationship between auxin and SHR regulatory network to maintain the proper development of the SAM. Similar approaches can be used to analyze the link between this gene regulatory network and other phytohormones that are important for SAM stem cell homeostasis such as cytokinin. These will provide a deeper understanding of how the SHR signalling pathway functions during SAM development and would provide more insights into phytohormone-mediated meristem activities to adjust the progression of cell fate acquisition within the different functional domains of the SAM.

Furthermore, it will be important to investigate how this novel gene regulatory network relates to the various pathways already characterised in the SAM. This will help to uncover how the relationships between these different signaling pathways are integrated to achieve communication between the spatially distinct domains of the SAM.
Our analysis identifies some known and new targets of the SHR regulatory pathway, and it will be important to further identify other targets of the SHR developmental pathway in the different domains of the SAM using new approaches with a higher resolution, like single-cell transcriptomic.

It will also be important to unravel relationships between environmental responses and SHR regulatory pathway function in the SAM. These could help uncover the mechanisms of developmental plasticity in the shoot meristem.

As the genes studied here have homologues in important crop plants such as rice and maize, a knowledge of the gene regulatory networks in Arabidopsis could be translated to such crops. This increased understanding could enable us to engineer the plants through to improve crop yields.

6.7. Supplemental information

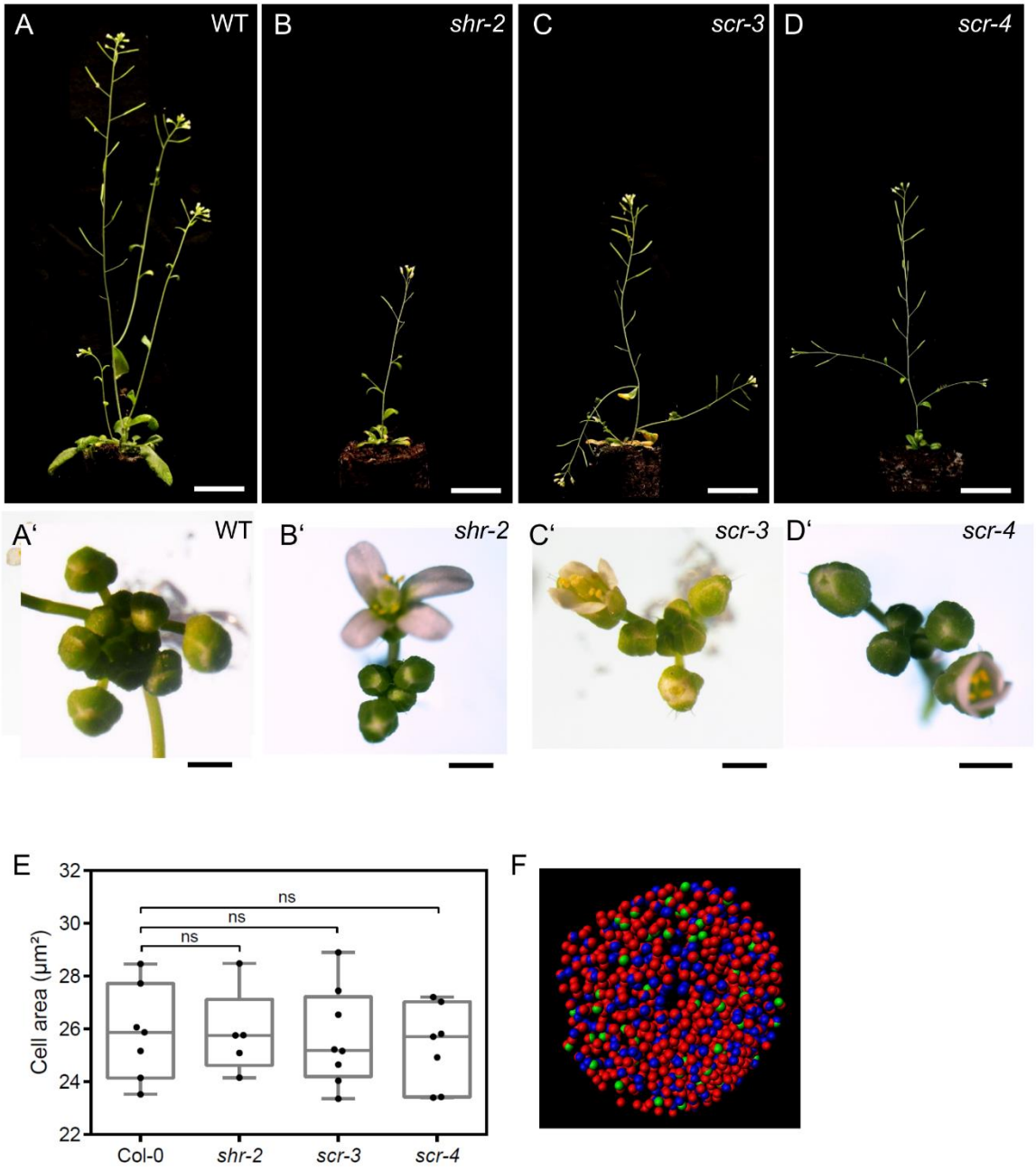

Suppl Fig. 1: The *shr* and *scr* mutants phenotypes.

(A-D) Plant phenotypes of 42-day-old WT **(A)**, *shr-2* mutant **(B)**, *scr-3* mutant **(C)** and *scr-4* mutant **(D)**. Scale bar represents 1cm. **(A'-D')** Top view of 31-day-old inflorescences of WT (n> 30) **(A')**, *shr-2* mutant (n>35) **(B')**, *scr-3* mutant **(C')** and *scr-4* mutant **(D')**. Scale bars represent 2 mm. **(E)** Quantification of the epidermal cell area in the meristem region of WT (n=11), *shr-2* mutant (n=4), *scr-3* mutant (n=7) and *scr-4* mutant (n=6). **(F)** Example of visualisation and quantification of cells in different cell cycle phases in the meristem region coexpressing the three PlaCCI markers. *pCDT1a:CDT1a-eCFP* (blue), *pHTR13:pHTR13-mCherry* (red), and *pCYCB1;1:NCYCB1;1-YFP* (green) using Imaris. ns= no significant difference; statistically significant differences were determined by Student's *t*-test.

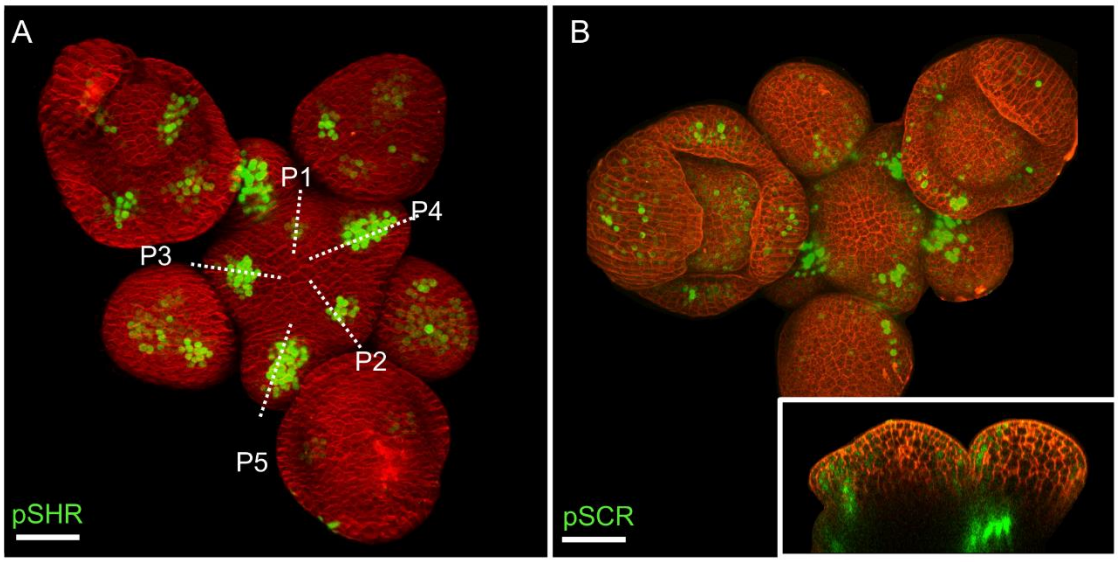

Suppl Fig. 2: The expression pattern of SHR and SCR in the shoot apical meristem.

(A) Representative 3D projection of shoot apical meristem at 5 weeks after germination expressing *pSHR:ntdTomato* reporter (green). Cell walls were stained with DAPI (red) (n≥5). Scale bar represents 50 µm. **(B)** Representative 3D projection of shoot apical meristem at 5 weeks after germination expressing *pSCR:YFP* reporter (green). Cell walls were stained with PI (red) (n≥3). The Lower right inset shows an optical longitudinal section through the middle of the SAM. Scale bar represents 50 µm.

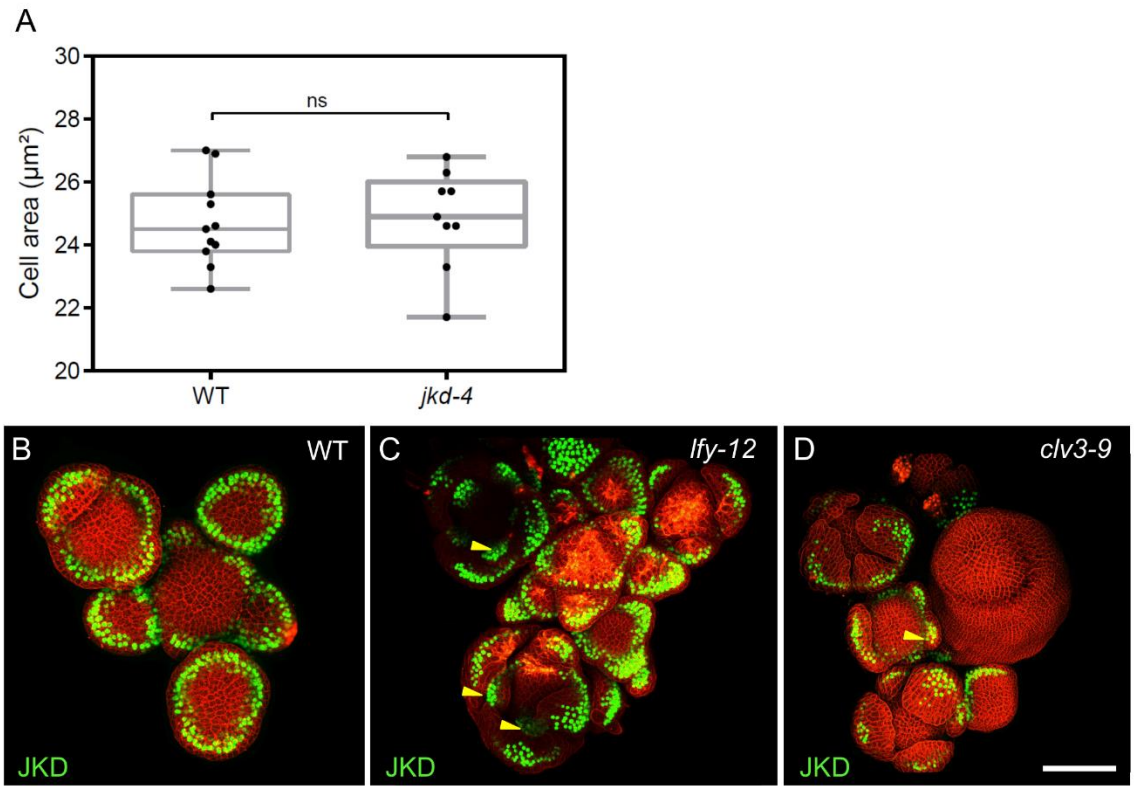

Suppl Fig. 3: The expression pattern of JKD in *lfy* and *clv3* mutants shoot apical meristem.

(A) Quantification of the epidermal cell area in the meristem region of WT (n=10) and *jkd-4* mutant (n=10). **(B-D)** Representative 3D projection of shoot apical meristems at 5 weeks after germination expressing *pJKD:JKD-YFP* reporter (green) in WT (n=5) **(B)**, *lfy-12* mutant (n=3) **(C)** and *clv3-9* mutant (n=2) **(D)**. Yellow arrowheads in **(C)** and **(D)** show sepal primordia with pJKD:JKD-YFP expression. Cell walls were stained with PI (red). Scale bar represents 50 µm. difference. ns= no significant; statistically significant differences were determined by Student's *t*-test.

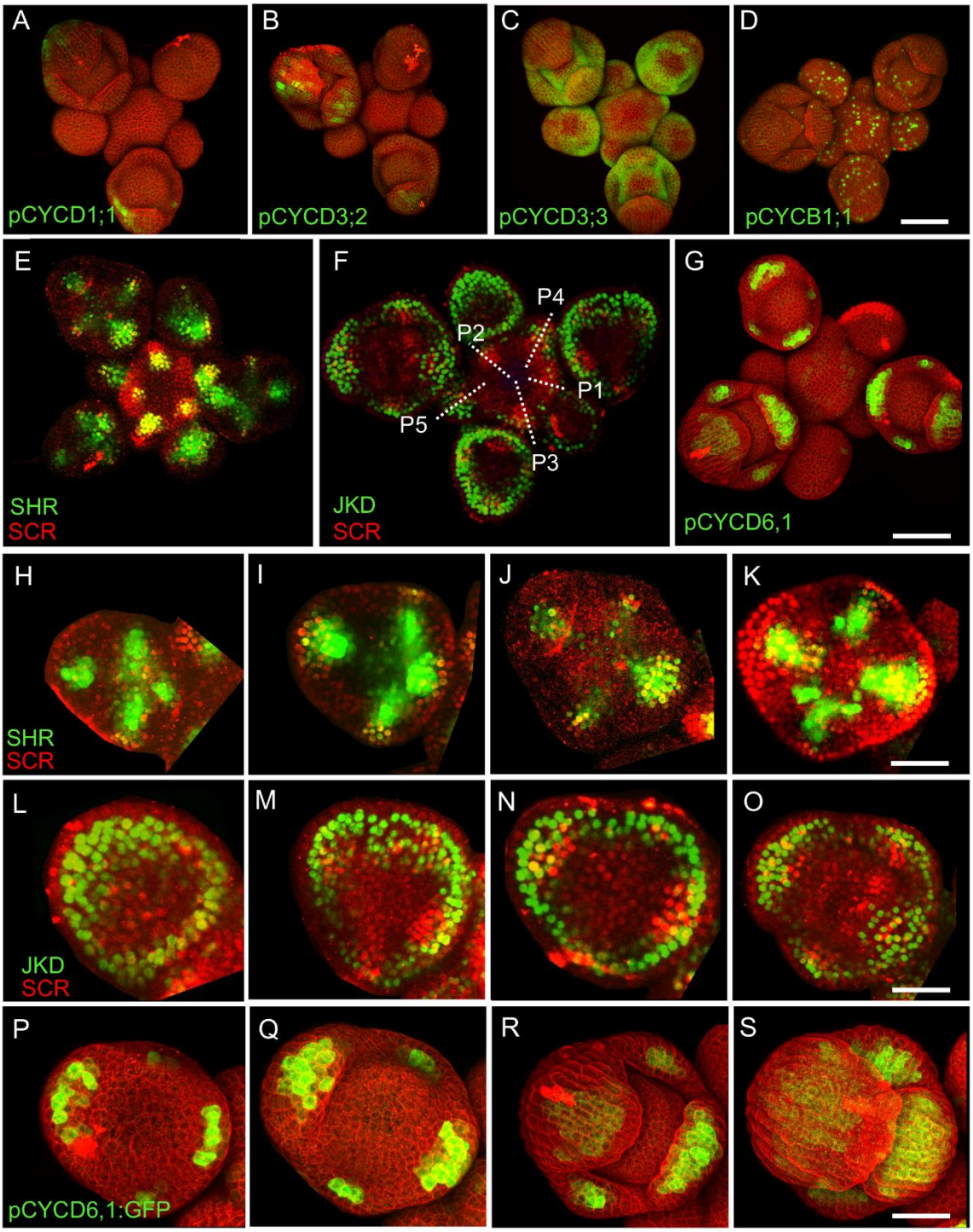

Suppl Fig. 4: The colocalization of the expression patterns of SHR, SCR, JKD and CYCD6;1 in the shoot apical meristem.

(A-D) Representative 3D projection of shoot apical meristem at 5 weeks after germination expressing *pCYCD1;1-GFP* reporter (green) (n=2) **(A)**, *pCYCD3;2-GFP* reporter (green) (n=2) **(B)**, *pCYCD3;3-GFP* reporter (green) (n=5) **(C)** and *pCYCB1;1:CYCB1;1-GFP* reporter (green) (n=2) **(D)**. Cell walls were stained with PI (red). Scale bars, 50 µm. **(E and F)** Representative 3D projection of shoot apical meristems at 5 weeks after germination coexpressing *pSHR:SHR-YFP* reporter (green) and *pSCR:SCR-RFP* reporter (red) (n=3) **(E)** and *pJKD:JKD-YFP* reporter (green) and *pSCR:SCR-RFP* reporter (red) (n=3) **(F).** Scale bar represents 50 µm. **(G)** Representative 3D projection of shoot apical meristems expressing *pCYCD6;1:GFP*

(green) reporter (n≥5). Cell walls were stained with PI (red). Scale bar represents 50 µm. **(H-S)** Expression of SHR, SCR, JKD and *CYCD6;1* during early stages of flower development. expression is observed at the sepal primordia in the florescence meristem stage 3 **(H, L and P)**, stage 4 **(I, M and Q)**, stage 5 **(J, N and R)** and stage 6 **(K, O and S)**. Scale bar represents 20 µm.

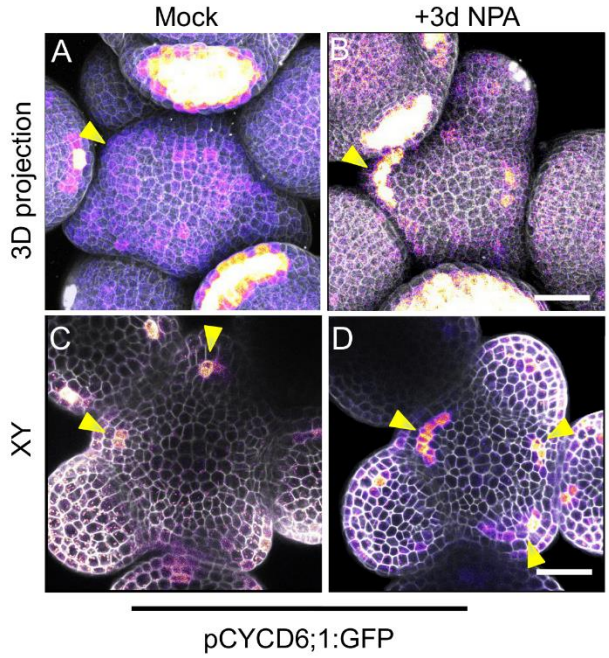

Suppl Fig. 5. *CYCD6;1* expression responds to auxin.

(A and B) Representative 3D projection of shoot apical meristems at 5 weeks after germination expressing *pCYCD6;1:GFP* reporter (magenta) three days after mock (n≥3) **(M)** or 100 µM NPA treatment (n≥6) **(N)**. **(C and D)** Transversal optical sections of **(A)** and **(B)** respectively. Yellow arrowheads in **(A)**, **(B)**, **(C)** and **(D)** show primordia with pCYCD6;1:GFP expression. Cell walls were stained with DAPI (gray). Scale bar represents 50 µm.

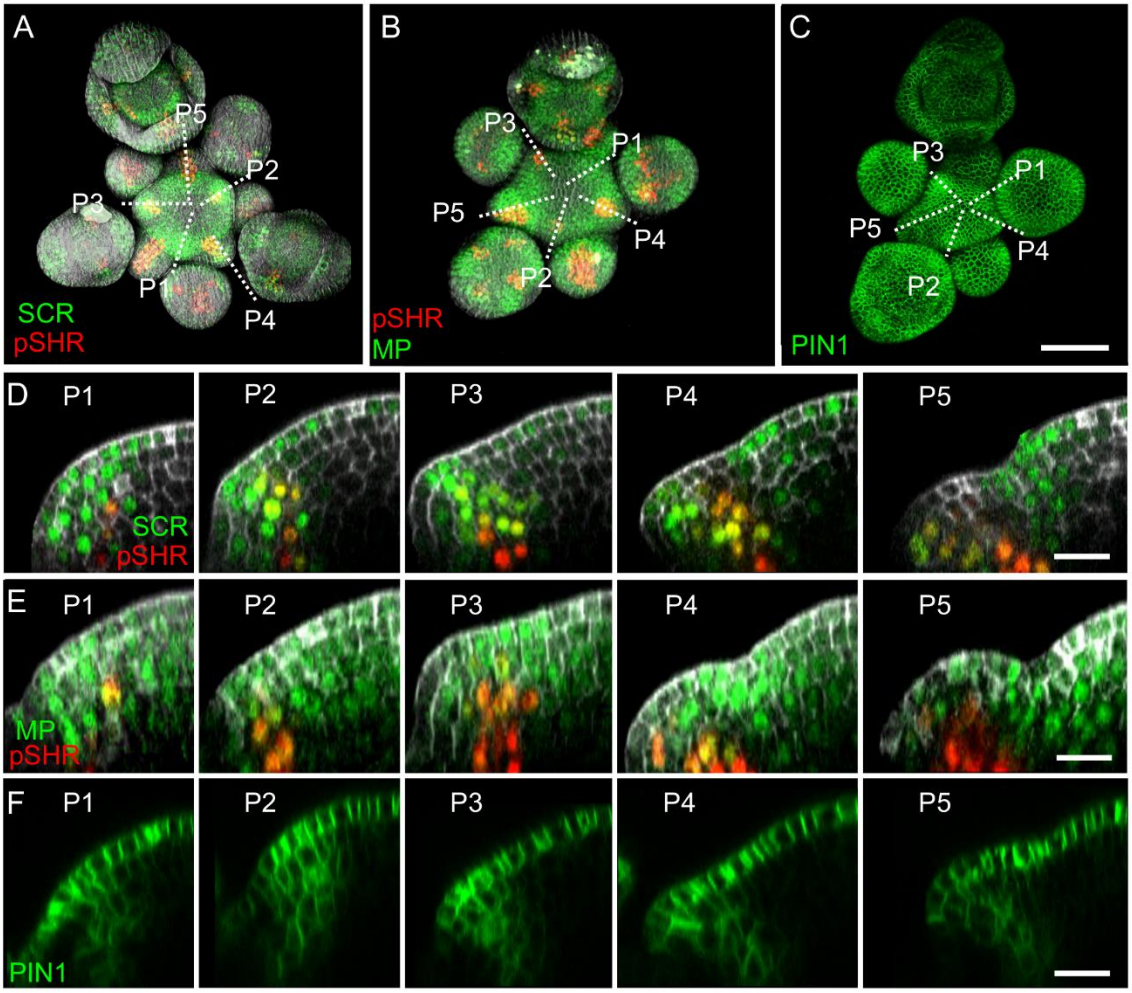

Suppl Fig. 6: The expression patterns of SHR, SCR, MP and PIN1 in the shoot apical meristem.

(A and B) Representative 3D projection of shoot apical meristems at 5 weeks after germination coexpressing *pSCR:SCR-YFP* reporter (green) and *pSHR:ntdTomato* reporter (red) (n≥3) **(A)** and the *pMP:MP-GFP* (green) and *pSHR:ntdTomato* (red) reporters (n≥2) **(B)**. Cell walls were stained with DAPI (gray). Scale bar represents 50 µm. **(C)** Representative 3D projection of shoot apical meristems at 5 weeks after germination expressing *pPIN1:PIN1-GFP* reporter (green) (n≥3). Scale bar represents 50 µm. **(D-F)** Longitudinal optical sections through the middle of five successive primordia (representative section orientation shown by dotted line in **(A)**, **(B)** and **(C)** respectively). Scale bar represents 20 µm.

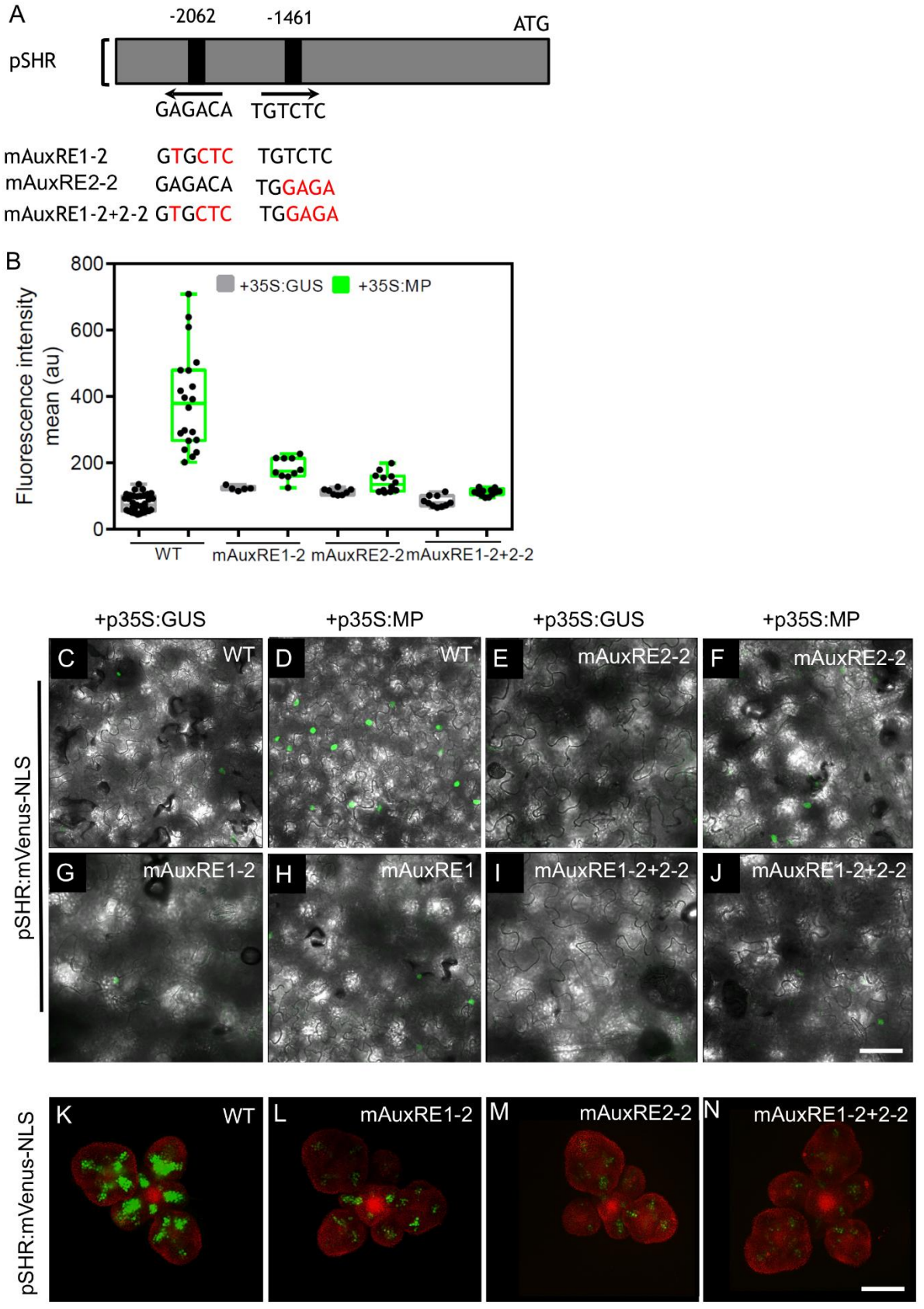

Suppl Fig. 7: MP Regulates *SHR* expression in the shoot apical meristem.

(A) Schematic representation of the *SHR* promoter. The positions of two auxin response elements are shown. Overview of mutated promoter versions of *pSHR*. AuxREs were mutated

and multiple combinations of these mutated motifs were combined into a single promoter. The original AuxRE sequence GAGACA was mutated to GTGCTC (mAuxRE1), the original AuxRE sequence TGTCTC was mutated to TGGAGA (mAuxRE2-2). **(B)** Quantification of mVenus fluorescence signal intensity from leaves transiently transformed with mVenus-NLS under the control of the wild-type SHR promoter or under the control of the SHR promoter with mutations in AuxRE motifs in the presence of *p35S:GUS* or *p35S:MP*. **(C-J)** Leaves transiently transformed with mVenus-NLS under the control of the wild-type SHR promoter **(C and D)** or under the control of the SHR promoter with mutations in AuxRE motifs, mAuxRE1-2 **(E and F)** mAuxRE2-2 **(G and H)** and mAuxRE1-2+2-2 **(I and J)** together with *p35S:MP* or *p35S:GUS*. mVenus fluorescence signals were detected by confocal microscopy. Scale bar represents 50 µm. **(K–N)** Representative 3D projection of shoot apical meristems at 5 weeks after germination expressing mVenus-NLS under the control of the wild-type SHR promoter (n≥5) **(K)**, and under the control of the SHR promoter with mutations in AuxRE motifs mAuxRE1-2 (n≥5) **(L)** mAuxRE2-2 (n≥4) **(M)** and mAuxRE1-2+2-2 (n≥4) **(N)**; Chlorophyll (red). Scale bar represents 50 µm.

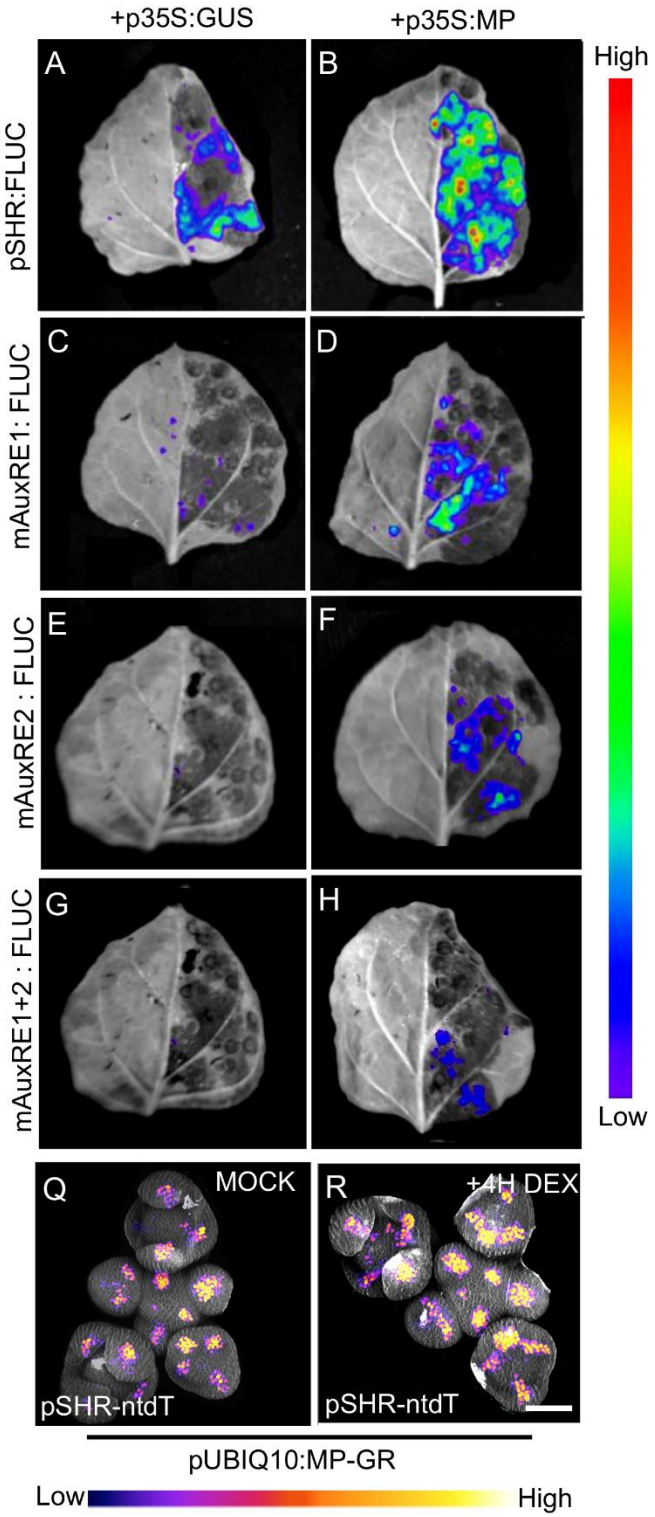

Suppl Fig. 8: MP induces the expression of SHR *in planta*

(A-H) (A-H) Representative images of leaves transformed with pSHR variants (pSHR (A and B), mAuxRE1 **(C and D)**, mAuxRE2 **(E and F)** and mAuxRE1+2 **(G and H)** draving the reporter gene firefly luciferase (FLUC) together with *p35S:MP* or *p35S:GUS*. D-luciferin was used as the substrate of FLUC**.** No luminescence could be detected without the substrate D-Luciferin. Color code indicate relative signal intensities (red: high; violet: low). **(Q and R)** Representative 3D projection of shoot apical meristems at 5 weeks after germination expressing *pSHR:ntdTomato* reporter (magenta) in *pUBIQ10:MP-GR* plants 4 hr after mock **(Q)** (n = 4)

and 4 hr after DEX treatment **(P)** (n = 4). Cell walls were stained with DAPI (gray). Scale bar represents 50 µm.

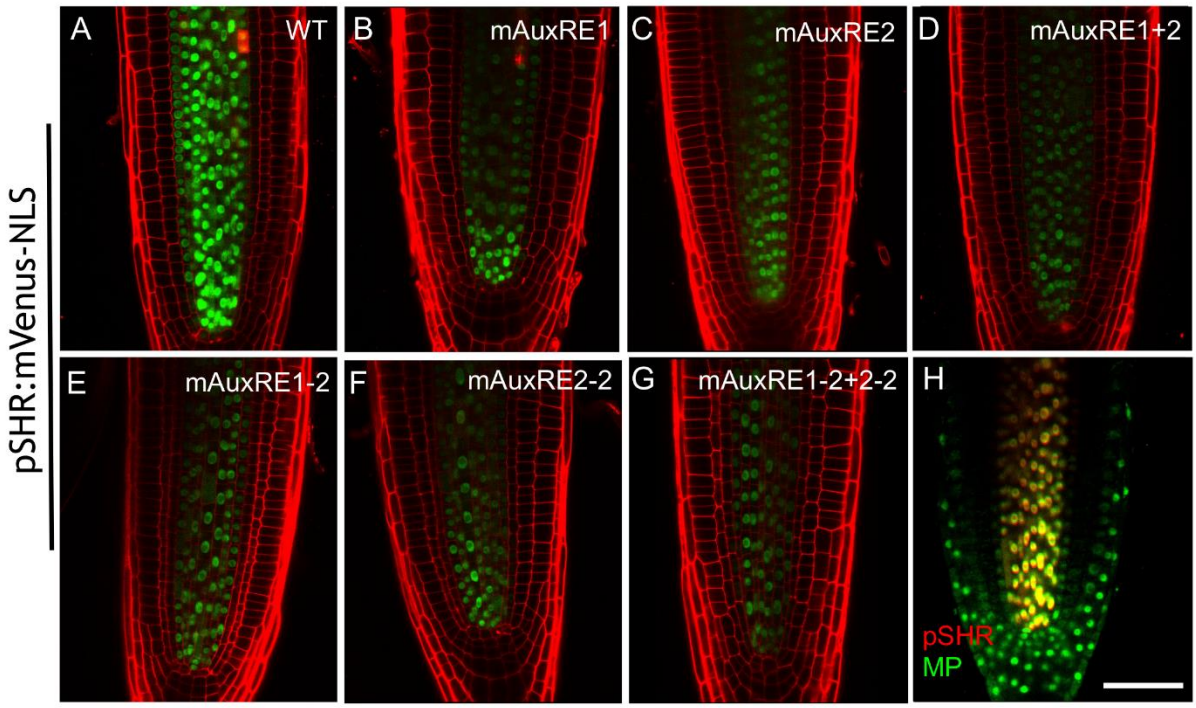

Suppl Fig. 9: The expression pattern of the different promoter versions of *SHR* in the root apical meristem.

(A–G) Representative images of root apical meristem at 5 days after germination expressing mVenus-NLS driven by the wild-type SHR promoter (n≥8) **(A)**, and the SHR promoter with mutations in AuxRE motifs mAuxRE1 (n≥8) **(B)**, mAuxRE2 (n≥8) **(C)**, mAuxRE1+2 (n≥8) **(D)**, mAuxRE1-2 (n≥8) **(E)**, mAuxRE2-2 (n≥8) **(F)** and mAuxRE1-2+2-2 (n≥8) **(G)**. **(H)** Representative images of 5-d-old root tips that coexpressing the *pMP:MP-GFP* reporter (green) and *pSHR:ntdTomato* reporter (red). Cell walls were stained with PI (red) (n≥2). Scale bar represents 50 µm.

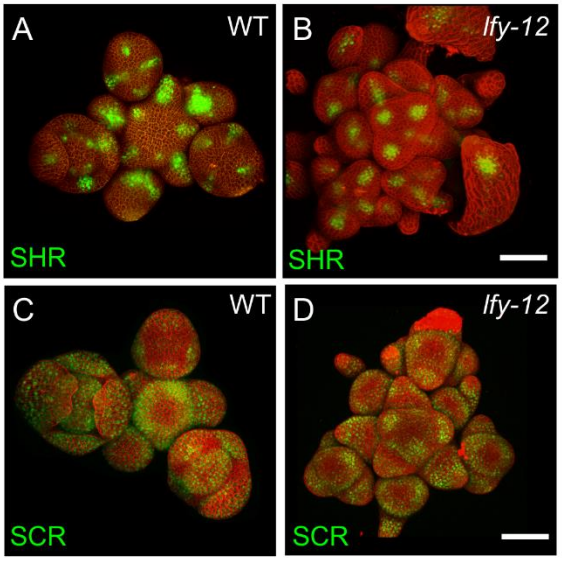

Suppl Fig. 10: The expression pattern of SHR and SCR in *lfy* mutant shoot apical meristem.

(A and B) Representative 3D projection of shoot apical meristems at 5 weeks after germination expressing *pSHR:SHR-YFP* reporter (green) in WT (n≥2) **(A)** and *lfy-12* mutant (n≥4) **(B)**. Cell walls were stained with PI (red). Scale bar represents 50 µm. **(C and D)** Representative 3D projection of shoot apical meristems expressing *pSCR:SCR-YFP* reporter (green) in WT (n≥2) **(C)** and *lfy-12* mutant (n≥3) **(D)**. Cell walls were stained with PI (red). Scale bar represents 50 µm.

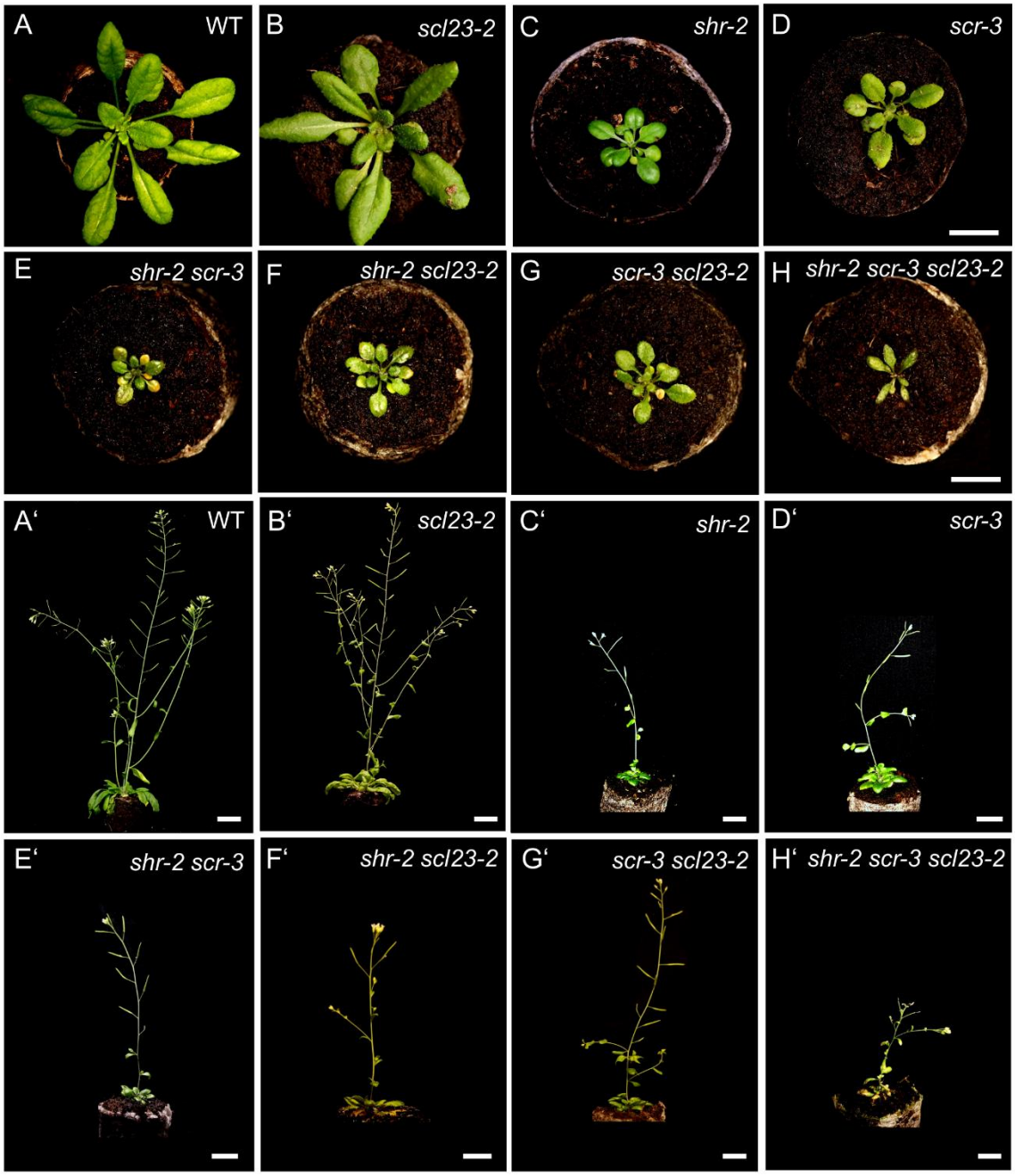

Suppl Fig. 11: Genetic combinations of *shr*, *scr* and *scl23*.

(A-H) Top view of 21-day-old rosettes of WT **(A)**, *scl23-2* mutant **(B)**, *shr-2* mutant **(C)**, *scr-3* mutant **(D)**, *scr-3 shr-2* double mutant **(E)**, *scl23-2 shr-2* double mutant **(F)**, *scl23-2 scr-3* double mutant **(G)**, *scr-3 shr-2 scl23-2* triple mutant **(H)**. Scale bar represents 1 cm. **(A'-H')** Plant phenotypes of 6 weeks old WT **(A')**, *scl23-2* mutant **(B')**, *shr-2* mutant **(C')**, *scr-3* mutant **(D')**, *scr-3 shr-2* double mutant **(E')**, *scl23-2 shr-2* double mutant **(F')**, *scl23-2 scr-3* double mutant **(G')**, *scr-3 shr-2 scl23-2* triple mutant **(H')**. Scale bar represents: 2 cm **(A' and B')**, 1 cm **(C'-H')**.

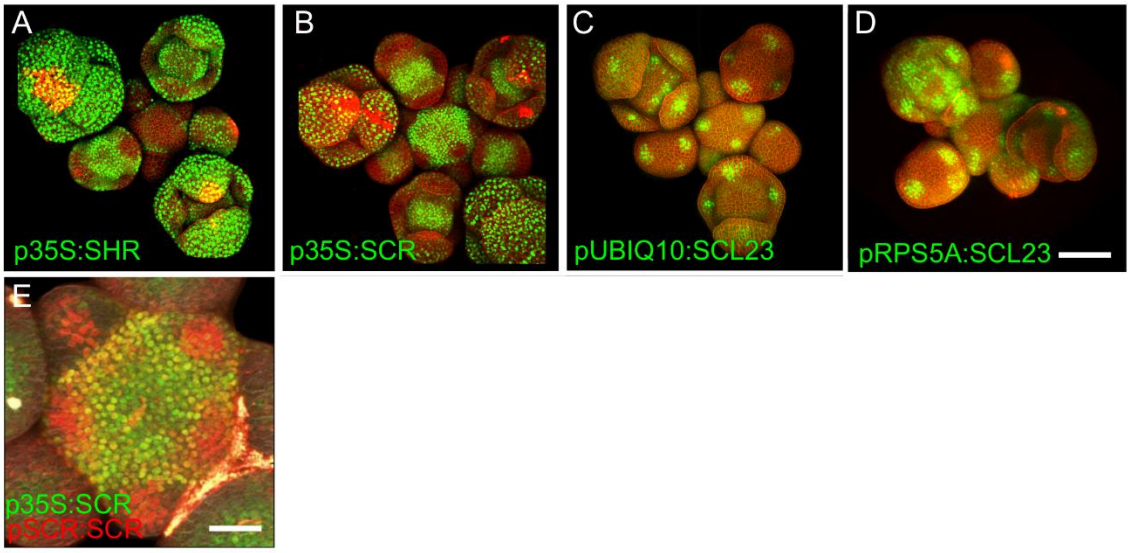

Suppl Fig. 12: The overexpression of SHR, SCR and SCL23 in the SAM.

(A-D) Representative 3D projection of shoot apical meristems at 5 weeks after germination expressing *p35S:SHR-GFP* reporter (green) (n≥6) **(A)**, *p35S:SCR-GFP* reporter (green) (n≥6) **(B)**, *pUBIQ10:SCL23-mVenus* reporter (green) (n≥3) **(C)** and *pRPS5A:SCL23-mVenus* reporter (green) (n≥3) **(D)**. Cell walls were stained with PI (red). Scale bar represents 50 µm. **(E)** Top view of the inflorescence apex coexpressing the *p35S:SCR-GFP* reporter (green) and the *pSCR:SCR-RFP* reporter (red) (n≥2). Cell walls were stained with DAPI (gray). Scale bar represents 50 µm.

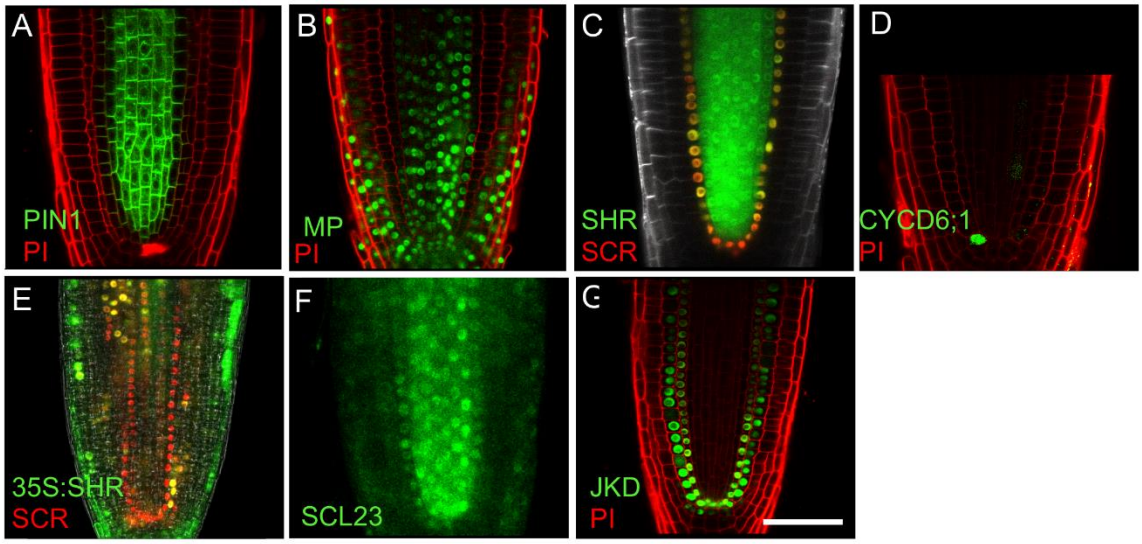

Suppl Fig. 13. The overlapping expression pattern of PIN1, MP, SHR, SCR, *CYCD6;1*, SCL23 and JKD in the RAM.

(A-D) Representative images of root apical meristem at 5 days after germination expressing, *pPIN1:PIN1-GFP* reporter (green) (n≥2) **(A)**, *pMP:MP-GFP* reporter (green) (n≥2) **(B)**, *pSHR:YFP-SHR* reporter (green) and *pSCR:SCR-RFP* reporters (red) (n≥2) **(C)**, *pCYCD6;1:GFP* reporter (green) (n≥2) **(D)**, *p35S:SHR-GFP* reporter (green) and *pSCR:SCR-RFP* reporter (red) (n≥2) **(E)**, *pSCL23:SCL23-YFP* reporter (green) (n≥2) **(F)** and *pJKD:JKD-YFP* reporter (green) (n≥2) **(G)**. Cell walls were stained with PI (red) in **(A) (B) (D) (G)** or DAPI (gray) in **(C)**. Scale bar represents 50 μm.

6.8. References

Aida, M., Vernoux, T., Furutani, M., Traas, J. and Tasaka, M. (2002) Roles of PIN-FORMED1 and MONOPTEROS in pattern formation of the apical region of the Arabidopsis embryo. *Development,* **129,** 3965-3974.

Band, L. R., Wells, D. M., Larrieu, A., Sun, J., Middleton, A. M., French, A. P.*, et al.* (2012) Root gravitropism is regulated by a transient lateral auxin gradient controlled by a tipping-point mechanism. *Proc Natl Acad Sci U S A,* **109,** 4668-4673.

Barbier de Reuille, P., Routier-Kierzkowska, A. L., Kierzkowski, D., Bassel, G. W., Schüpbach, T., Tauriello, G.*, et al.* (2015) MorphoGraphX: A platform for quantifying morphogenesis in 4D. *Elife,* **4,** 05864.

Benfey, P. N., Linstead, P. J., Roberts, K., Schiefelbein, J. W., Hauser, M. T. and Aeschbacher, R. A. (1993) Root development in Arabidopsis: four mutants with dramatically altered root morphogenesis. *Development,* **119,** 57-70.

Benková, E., Michniewicz, M., Sauer, M., Teichmann, T., Seifertová, D., Jürgens, G.*, et al.* (2003) Local, efflux-dependent auxin gradients as a common module for plant organ formation. *Cell,* **115,** 591-602.

Berckmans, B., Kirschner, G., Gerlitz, N., Stadler, R. and Simon, R. (2020) CLE40 Signaling Regulates Root Stem Cell Fate. *Plant Physiol,* **182,** 1776-1792.

Berleth, T. and Jürgens, G. (1993) The role of the monopteros gene in organising the basal body region of the Arabidopsis embryo. *Development,* **118,** 575-587.

Bhatia, N., Bozorg, B., Larsson, A., Ohno, C., Jönsson, H. and Heisler, M. G. (2016) Auxin Acts through MONOPTEROS to Regulate Plant Cell Polarity and Pattern Phyllotaxis. *Curr Biol,* **26,** 3202-3208.

Bleckmann, A. and Simon, R. (2009) Interdomain signaling in stem cell maintenance of plant shoot meristems. *Mol Cells,* **27,** 615-620.

Blilou, I., Xu, J., Wildwater, M., Willemsen, V., Paponov, I., Friml, J.*, et al.* (2005) The PIN auxin efflux facilitator network controls growth and patterning in Arabidopsis roots. *Nature,* **433,** 39-44.

Boer, D. R., Freire-Rios, A., van den Berg, W. A., Saaki, T., Manfield, I. W., Kepinski, S.*, et al.* (2014) Structural basis for DNA binding specificity by the auxin-dependent ARF transcription factors. *Cell,* **156,** 577-589.

Brand, U., Fletcher, J. C., Hobe, M., Meyerowitz, E. M. and Simon, R. (2000) Dependence of stem cell fate in Arabidopsis on a feedback loop regulated by CLV3 activity. *Science,* **289,** 617-619.

Cenci, A. and Rouard, M. (2017) Evolutionary Analyses of GRAS Transcription Factors in Angiosperms. *Front Plant Sci,* **8,** 273.

Clark, N. M., Hinde, E., Winter, C. M., Fisher, A. P., Crosti, G., Blilou, I.*, et al.* (2016) Tracking transcription factor mobility and interaction in Arabidopsis roots with fluorescence correlation spectroscopy. *Elife,* **5**.

Clark, S. E., Williams, R. W. and Meyerowitz, E. M. (1997) The CLAVATA1 gene encodes a putative receptor kinase that controls shoot and floral meristem size in Arabidopsis. *Cell,* **89,** 575-585.

Clough, S. J. and Bent, A. F. (1998) Floral dip: a simplified method for Agrobacterium-mediated transformation of Arabidopsis thaliana. *Plant J,* **16,** 735-743.

Cole, M., Chandler, J., Weijers, D., Jacobs, B., Comelli, P. and Werr, W. (2009) DORNROSCHEN is a direct target of the auxin response factor MONOPTEROS in the Arabidopsis embryo. *Development,* **136,** 1643-1651.

Cruz-Ramírez, A., Díaz-Triviño, S., Blilou, I., Grieneisen, V. A., Sozzani, R., Zamioudis, C*., et al.* (2012) A bistable circuit involving SCARECROW-RETINOBLASTOMA integrates cues to inform asymmetric stem cell division. *Cell,* **150,** 1002-1015.

Cui, H., Kong, D., Liu, X. and Hao, Y. (2014) SCARECROW, SCR-LIKE 23 and SHORT-ROOT control bundle sheath cell fate and function in Arabidopsis thaliana. *Plant J,* **78,** 319-327.

Cui, H., Levesque, M. P., Vernoux, T., Jung, J. W., Paquette, A. J., Gallagher, K. L*., et al.* (2007) An evolutionarily conserved mechanism delimiting SHR movement defines a single layer of endodermis in plants. *Science,* **316,** 421-425.

Czechowski, T., Stitt, M., Altmann, T., Udvardi, M. K. and Scheible, W. R. (2005) Genome-wide identification and testing of superior reference genes for transcript normalization in Arabidopsis. *Plant Physiol,* **139,** 5-17.

Daum, G., Medzihradszky, A., Suzaki, T. and Lohmann, J. U. (2014) A mechanistic framework for noncell autonomous stem cell induction in Arabidopsis. *Proc Natl Acad Sci U S A,* **111,** 14619-14624.

Dellaporta, S. L., Wood, J. and Hicks, J. B. (1983) A plant DNA minipreparation: version II. *Plant molecular biology reporter,* **1,** 19-21.

Desvoyes, B., Arana-Echarri, A., Barea, M. D. and Gutierrez, C. (2020) A comprehensive fluorescent sensor for spatiotemporal cell cycle analysis in Arabidopsis. *Nat Plants,* **6,** 1330-1334.

Dewitte, W., Riou-Khamlichi, C., Scofield, S., Healy, J. M., Jacqmard, A., Kilby, N. J*., et al.* (2003) Altered cell cycle distribution, hyperplasia, and inhibited differentiation in Arabidopsis caused by the D-type cyclin CYCD3. *Plant Cell,* **15,** 79-92.

Dharmasiri, N., Dharmasiri, S. and Estelle, M. (2005a) The F-box protein TIR1 is an auxin receptor. *Nature,* **435,** 441-445.

Dharmasiri, N., Dharmasiri, S., Weijers, D., Lechner, E., Yamada, M., Hobbie, L*., et al.* (2005b) Plant development is regulated by a family of auxin receptor F box proteins. *Dev Cell,* **9,** 109-119.

Dhondt, S., Coppens, F., De Winter, F., Swarup, K., Merks, R. M., Inzé, D*., et al.* (2010) SHORT-ROOT and SCARECROW regulate leaf growth in Arabidopsis by stimulating S-phase progression of the cell cycle. *Plant Physiol,* **154,** 1183-1195.

Di Laurenzio, L., Wysocka-Diller, J., Malamy, J. E., Pysh, L., Helariutta, Y., Freshour, G*., et al.* (1996) The SCARECROW gene regulates an asymmetric cell division that is essential for generating the radial organization of the Arabidopsis root. *Cell,* **86,** 423-433.

Dolan, L., Janmaat, K., Willemsen, V., Linstead, P., Poethig, S., Roberts, K.*, et al.* (1993) Cellular organisation of the Arabidopsis thaliana root. *Development,* **119,** 71-84.

Drisch, R. C. and Stahl, Y. (2015) Function and regulation of transcription factors involved in root apical meristem and stem cell maintenance. *Front Plant Sci,* **6,** 505.

Elliott, R. C., Betzner, A. S., Huttner, E., Oakes, M. P., Tucker, W. Q., Gerentes, D.*, et al.* (1996) AINTEGUMENTA, an APETALA2-like gene of Arabidopsis with pleiotropic roles in ovule development and floral organ growth. *Plant Cell,* **8,** 155-168.

Ellis, C. M., Nagpal, P., Young, J. C., Hagen, G., Guilfoyle, T. J. and Reed, J. W. (2005) AUXIN RESPONSE FACTOR1 and AUXIN RESPONSE FACTOR2 regulate senescence and floral organ abscission in Arabidopsis thaliana. *Development,* **132,** 4563-4574.

Engstrom, E. M., Andersen, C. M., Gumulak-Smith, J., Hu, J., Orlova, E., Sozzani, R.*, et al.* (2011) Arabidopsis homologs of the petunia hairy meristem gene are required for maintenance of shoot and root indeterminacy. *Plant Physiol,* **155,** 735-750.

Fankhauser, C. and Christie, J. M. (2015) Plant phototropic growth. *Curr Biol,* **25,** R384-389.

Fletcher, J. C., Brand, U., Running, M. P., Simon, R. and Meyerowitz, E. M. (1999) Signaling of cell fate decisions by CLAVATA3 in Arabidopsis shoot meristems. *Science,* **283,** 1911-1914.

Friml, J., Yang, X., Michniewicz, M., Weijers, D., Quint, A., Tietz, O.*, et al.* (2004) A PINOID-dependent binary switch in apical-basal PIN polar targeting directs auxin efflux. *Science,* **306,** 862-865.

Fukaki, H., Wysocka-Diller, J., Kato, T., Fujisawa, H., Benfey, P. N. and Tasaka, M. (1998) Genetic evidence that the endodermis is essential for shoot gravitropism in Arabidopsis thaliana. *Plant J,* **14,** 425-430.

Gaillochet, C., Daum, G. and Lohmann, J. U. (2015) O cell, where art thou? The mechanisms of shoot meristem patterning. *Curr Opin Plant Biol,* **23,** 91-97.

Gaillochet, C. and Lohmann, J. U. (2015) The never-ending story: from pluripotency to plant developmental plasticity. *Development,* **142,** 2237-2249.

Gälweiler, L., Guan, C., Müller, A., Wisman, E., Mendgen, K., Yephremov, A.*, et al.* (1998) Regulation of polar auxin transport by AtPIN1 in Arabidopsis vascular tissue. *Science,* **282,** 2226-2230.

Gardiner, J., Donner, T. J. and Scarpella, E. (2011) Simultaneous activation of SHR and ATHB8 expression defines switch to preprocambial cell state in Arabidopsis leaf development. *Dev Dyn,* **240,** 261-270.

Graf, P., Dolzblasz, A., Würschum, T., Lenhard, M., Pfreundt, U. and Laux, T. (2010) MGOUN1 encodes an Arabidopsis type IB DNA topoisomerase required in stem cell regulation and to maintain developmentally regulated gene silencing. *Plant Cell,* **22,** 716-728.

Han, H., Geng, Y., Guo, L., Yan, A., Meyerowitz, E. M., Liu, X.*, et al.* (2020) The Overlapping and Distinct Roles of HAM Family Genes in Arabidopsis Shoot Meristems. *Front Plant Sci,* **11,** 541968.

Hardtke, C. S. and Berleth, T. (1998) The Arabidopsis gene MONOPTEROS encodes a transcription factor mediating embryo axis formation and vascular development. *Embo j,* **17,** 1405-1411.

Hardtke, C. S., Ckurshumova, W., Vidaurre, D. P., Singh, S. A., Stamatiou, G., Tiwari, S. B.*, et al.* (2004) Overlapping and non-redundant functions of the Arabidopsis auxin response factors MONOPTEROS and NONPHOTOTROPIC HYPOCOTYL 4. *Development,* **131,** 1089-1100.

Heidstra, R., Welch, D. and Scheres, B. (2004) Mosaic analyses using marked activation and deletion clones dissect Arabidopsis SCARECROW action in asymmetric cell division. *Genes Dev,* **18,** 1964-1969.

Heisler, M. G., Ohno, C., Das, P., Sieber, P., Reddy, G. V., Long, J. A.*, et al.* (2005) Patterns of auxin transport and gene expression during primordium development revealed by live imaging of the Arabidopsis inflorescence meristem. *Curr Biol,* **15,** 1899-1911.

Helariutta, Y., Fukaki, H., Wysocka-Diller, J., Nakajima, K., Jung, J., Sena, G.*, et al.* (2000) The SHORT-ROOT gene controls radial patterning of the Arabidopsis root through radial signaling. *Cell,* **101,** 555-567.

Höfgen, R. and Willmitzer, L. (1988) Storage of competent cells for Agrobacterium transformation. *Nucleic Acids Res,* **16,** 9877.

Jenik, P. D. and Irish, V. F. (2000) Regulation of cell proliferation patterns by homeotic genes during Arabidopsis floral development. *Development,* **127,** 1267-1276.

Jiang, K. and Feldman, L. J. (2005) Regulation of root apical meristem development. *Annu Rev Cell Dev Biol,* **21,** 485-509.

Kazan, K. and Manners, J. M. (2009) Linking development to defense: auxin in plant-pathogen interactions. *Trends Plant Sci,* **14,** 373-382.

Kepinski, S. and Leyser, O. (2005) The Arabidopsis F-box protein TIR1 is an auxin receptor. *Nature,* **435,** 446-451.

Kim, G., Dhar, S. and Lim, J. (2017) The SHORT-ROOT regulatory network in the endodermis development of Arabidopsis roots and shoots. *Journal of Plant Biology,* **60,** 306-313.

Klucher, K. M., Chow, H., Reiser, L. and Fischer, R. L. (1996) The AINTEGUMENTA gene of Arabidopsis required for ovule and female gametophyte development is related to the floral homeotic gene APETALA2. *Plant Cell,* **8,** 137-153.

Konishi, M., Donner, T. J., Scarpella, E. and Yanagisawa, S. (2015) MONOPTEROS directly activates the auxin-inducible promoter of the Dof5.8 transcription factor gene in Arabidopsis thaliana leaf provascular cells. *J Exp Bot,* **66,** 283-291.

Korasick, D. A., Enders, T. A. and Strader, L. C. (2013) Auxin biosynthesis and storage forms. *J Exp Bot,* **64,** 2541-2555.

Korasick, D. A., Westfall, C. S., Lee, S. G., Nanao, M. H., Dumas, R., Hagen, G.*, et al.* (2014) Molecular basis for AUXIN RESPONSE FACTOR protein interaction and the control of auxin response repression. *Proc Natl Acad Sci U S A,* **111,** 5427-5432.

Lampropoulos, A., Sutikovic, Z., Wenzl, C., Maegele, I., Lohmann, J. U. and Forner, J. (2013) GreenGate---a novel, versatile, and efficient cloning system for plant transgenesis. *PLoS One,* **8,** e83043.

Laux, T., Mayer, K. F., Berger, J. and Jürgens, G. (1996) The WUSCHEL gene is required for shoot and floral meristem integrity in Arabidopsis. *Development,* **122,** 87-96.

Lee, M. H., Kim, B., Song, S. K., Heo, J. O., Yu, N. I., Lee, S. A.*, et al.* (2008) Large-scale analysis of the GRAS gene family in Arabidopsis thaliana. *Plant Mol Biol,* **67,** 659-670.

Liao, C. Y., Smet, W., Brunoud, G., Yoshida, S., Vernoux, T. and Weijers, D. (2015) Reporters for sensitive and quantitative measurement of auxin response. *Nat Methods,* **12,** 207-210, 202 p following 210.

Lieberman-Lazarovich, M., Yahav, C., Israeli, A. and Efroni, I. (2019) Deep Conservation of cis-Element Variants Regulating Plant Hormonal Responses. *Plant Cell,* **31,** 2559-2572.

Lindsey, B. E., 3rd, Rivero, L., Calhoun, C. S., Grotewold, E. and Brkljacic, J. (2017) Standardized Method for High-throughput Sterilization of Arabidopsis Seeds. *J Vis Exp*.

Llave, C., Xie, Z., Kasschau, K. D. and Carrington, J. C. (2002) Cleavage of Scarecrow-like mRNA targets directed by a class of Arabidopsis miRNA. *Science,* **297,** 2053-2056.

Long, Y., Goedhart, J., Schneijderberg, M., Terpstra, I., Shimotohno, A., Bouchet, B. P.*, et al.* (2015a) SCARECROW-LIKE23 and SCARECROW jointly specify endodermal cell fate but distinctly control SHORT-ROOT movement. *Plant J,* **84,** 773-784.

Long, Y., Smet, W., Cruz-Ramírez, A., Castelijns, B., de Jonge, W., Mähönen, A. P.*, et al.* (2015b) Arabidopsis BIRD Zinc Finger Proteins Jointly Stabilize Tissue Boundaries by Confining the Cell Fate Regulator SHORT-ROOT and Contributing to Fate Specification. *Plant Cell,* **27,** 1185-1199.

Long, Y., Stahl, Y., Weidtkamp-Peters, S., Postma, M., Zhou, W., Goedhart, J.*, et al.* (2017) In vivo FRET-FLIM reveals cell-type-specific protein interactions in Arabidopsis roots. *Nature,* **548,** 97-102.

Luo, L., Zeng, J., Wu, H., Tian, Z. and Zhao, Z. (2018) A Molecular Framework for Auxin-Controlled Homeostasis of Shoot Stem Cells in Arabidopsis. *Mol Plant,* **11,** 899-913.

Mayer, K. F., Schoof, H., Haecker, A., Lenhard, M., Jürgens, G. and Laux, T. (1998) Role of WUSCHEL in regulating stem cell fate in the Arabidopsis shoot meristem. *Cell,* **95,** 805-815.

Mockaitis, K. and Estelle, M. (2008) Auxin receptors and plant development: a new signaling paradigm. *Annu Rev Cell Dev Biol,* **24,** 55-80.

Möller, B. K., Ten Hove, C. A., Xiang, D., Williams, N., López, L. G., Yoshida, S.*, et al.* (2017) Auxin response cell-autonomously controls ground tissue initiation in the early Arabidopsis embryo. *Proc Natl Acad Sci U S A,* **114,** E2533-e2539.

Moubayidin, L., Di Mambro, R., Sozzani, R., Pacifici, E., Salvi, E., Terpstra, I.*, et al.* (2013) Spatial coordination between stem cell activity and cell differentiation in the root meristem. *Dev Cell,* **26,** 405-415.

Nakajima, K., Sena, G., Nawy, T. and Benfey, P. N. (2001) Intercellular movement of the putative transcription factor SHR in root patterning. *Nature,* **413,** 307-311.

Nanao, M. H., Vinos-Poyo, T., Brunoud, G., Thévenon, E., Mazzoleni, M., Mast, D.*, et al.* (2014) Structural basis for oligomerization of auxin transcriptional regulators. *Nat Commun,* **5,** 3617.

Nimchuk, Z. L., Zhou, Y., Tarr, P. T., Peterson, B. A. and Meyerowitz, E. M. (2015) Plant stem cell maintenance by transcriptional cross-regulation of related receptor kinases. *Development,* **142,** 1043-1049.

Ogawa, M., Shinohara, H., Sakagami, Y. and Matsubayashi, Y. (2008) Arabidopsis CLV3 peptide directly binds CLV1 ectodomain. *Science,* **319,** 294.

Ohyama, K., Shinohara, H., Ogawa-Ohnishi, M. and Matsubayashi, Y. (2009) A glycopeptide regulating stem cell fate in Arabidopsis thaliana. *Nat Chem Biol,* **5,** 578-580.

Overvoorde, P., Fukaki, H. and Beeckman, T. (2010) Auxin control of root development. *Cold Spring Harb Perspect Biol,* **2,** a001537.

Paque, S. and Weijers, D. (2016) Q&A: Auxin: the plant molecule that influences almost anything. *BMC Biol,* **14,** 67.

Parry, G., Calderon-Villalobos, L. I., Prigge, M., Peret, B., Dharmasiri, S., Itoh, H.*, et al.* (2009) Complex regulation of the TIR1/AFB family of auxin receptors. *Proc Natl Acad Sci U S A,* **106,** 22540-22545.

Perrot-Rechenmann, C. (2010) Cellular responses to auxin: division versus expansion. *Cold Spring Harb Perspect Biol,* **2,** a001446.

Petersson, S. V., Johansson, A. I., Kowalczyk, M., Makoveychuk, A., Wang, J. Y., Moritz, T.*, et al.* (2009) An auxin gradient and maximum in the Arabidopsis root apex shown by high-resolution cell-specific analysis of IAA distribution and synthesis. *Plant Cell,* **21,** 1659-1668.

Pfaffl, M. W. (2001) A new mathematical model for relative quantification in real-time RT-PCR. *Nucleic Acids Res,* **29,** e45.

Pysh, L. D., Wysocka-Diller, J. W., Camilleri, C., Bouchez, D. and Benfey, P. N. (1999) The GRAS gene family in Arabidopsis: sequence characterization and basic expression analysis of the SCARECROW-LIKE genes. *Plant J,* **18,** 111-119.

Rademacher, E. H., Möller, B., Lokerse, A. S., Llavata-Peris, C. I., van den Berg, W. and Weijers, D. (2011) A cellular expression map of the Arabidopsis AUXIN RESPONSE FACTOR gene family. *Plant J,* **68,** 597-606.

Reinhardt, D., Pesce, E. R., Stieger, P., Mandel, T., Baltensperger, K., Bennett, M.*, et al.* (2003) Regulation of phyllotaxis by polar auxin transport. *Nature,* **426,** 255-260.

Remington, D. L., Vision, T. J., Guilfoyle, T. J. and Reed, J. W. (2004) Contrasting modes of diversification in the Aux/IAA and ARF gene families. *Plant Physiol,* **135,** 1738-1752.

Sarkar, A. K., Luijten, M., Miyashima, S., Lenhard, M., Hashimoto, T., Nakajima, K.*, et al.* (2007) Conserved factors regulate signalling in Arabidopsis thaliana shoot and root stem cell organizers. *Nature,* **446,** 811-814.

Scheres, B., Di Laurenzio, L., Willemsen, V., Hauser, M.-T., Janmaat, K., Weisbeek, P.*, et al.* (1995) Mutations affecting the radial organisation of the Arabidopsis root display specific defects throughout the embryonic axis. *Development,* **121,** 53-62.

Scheres, B., Wolkenfelt, H., Willemsen, V., Terlouw, M., Lawson, E., Dean, C.*, et al.* (1994) Embryonic origin of the Arabidopsis primary root and root meristem initials. *Development,* **120,** 2475-2487.

Schlegel, J., Denay, G., Wink, R. H., Pinto, K. G., Stahl, Y., Schmid, J.*, et al.* (2021) Control of Arabidopsis shoot stem cell homeostasis by two antagonistic CLE peptide signalling pathways. *Elife,* **10**.

Schlereth, A., Möller, B., Liu, W., Kientz, M., Flipse, J., Rademacher, E. H.*, et al.* (2010) MONOPTEROS controls embryonic root initiation by regulating a mobile transcription factor. *Nature,* **464,** 913-916.

Schneider, C. A., Rasband, W. S. and Eliceiri, K. W. (2012) NIH Image to ImageJ: 25 years of image analysis. *Nat Methods,* **9,** 671-675.

Schoof, H., Lenhard, M., Haecker, A., Mayer, K. F., Jürgens, G. and Laux, T. (2000) The stem cell population of Arabidopsis shoot meristems in maintained by a regulatory loop between the CLAVATA and WUSCHEL genes. *Cell,* **100,** 635-644.

Schultz, E. A. and Haughn, G. W. (1991) LEAFY, a Homeotic Gene That Regulates Inflorescence Development in Arabidopsis. *Plant Cell,* **3,** 771-781.

Schulze, S., Schäfer, B. N., Parizotto, E. A., Voinnet, O. and Theres, K. (2010) LOST MERISTEMS genes regulate cell differentiation of central zone descendants in Arabidopsis shoot meristems. *Plant J,* **64,** 668-678.

Scott, A. C. (2003) GENSEL, PG & EDWARDS, D.(eds) 2001. Plants Invade the Land. Evolutionary & Environmental Perspectives. Critical Moments & Perspectives in Paleobiology and Earth History Series. xi+ 304 pp. New York: Columbia University Press. Price£ 46.50 (hard covers). ISBN 0 231 11160 6. *Geological Magazine,* **140,** 490-491.

Sidhu, N. S., Pruthi, G., Singh, S., Bishnoi, R. and Singla, D. (2020) Genome-wide identification and analysis of GRAS transcription factors in the bottle gourd genome. *Sci Rep,* **10,** 14338.

Smit, M. E. and Weijers, D. (2015) The role of auxin signaling in early embryo pattern formation. *Curr Opin Plant Biol,* **28,** 99-105.

Somssich, M., Je, B. I., Simon, R. and Jackson, D. (2016) CLAVATA-WUSCHEL signaling in the shoot meristem. *Development,* **143,** 3238-3248.

Sozzani, R., Cui, H., Moreno-Risueno, M. A., Busch, W., Van Norman, J. M., Vernoux, T.*, et al.* (2010) Spatiotemporal regulation of cell-cycle genes by SHORTROOT links patterning and growth. *Nature,* **466,** 128-132.

Stahl, Y., Grabowski, S., Bleckmann, A., Kühnemuth, R., Weidtkamp-Peters, S., Pinto, K. G.*, et al.* (2013) Moderation of Arabidopsis root stemness by CLAVATA1 and ARABIDOPSIS CRINKLY4 receptor kinase complexes. *Curr Biol,* **23,** 362-371.

Stahl, Y. and Simon, R. (2005) Plant stem cell niches. *Int J Dev Biol,* **49,** 479-489.

Stahl, Y., Wink, R. H., Ingram, G. C. and Simon, R. (2009) A signaling module controlling the stem cell niche in Arabidopsis root meristems. *Curr Biol,* **19,** 909-914.

Steeves, T. A. and Sussex, I. M. (1989) *Patterns in plant development*. Cambridge University Press.

Stuurman, J., Jäggi, F. and Kuhlemeier, C. (2002) Shoot meristem maintenance is controlled by a GRAS-gene mediated signal from differentiating cells. *Genes Dev,* **16,** 2213-2218.

Tan, X., Calderon-Villalobos, L. I., Sharon, M., Zheng, C., Robinson, C. V., Estelle, M.*, et al.* (2007) Mechanism of auxin perception by the TIR1 ubiquitin ligase. *Nature,* **446,** 640-645.

Terpstra, I. and Heidstra, R. (2009) Stem cells: The root of all cells. *Semin Cell Dev Biol,* **20,** 1089-1096.

Tian, H., Wabnik, K., Niu, T., Li, H., Yu, Q., Pollmann, S.*, et al.* (2014) WOX5-IAA17 feedback circuit-mediated cellular auxin response is crucial for the patterning of root stem cell niches in Arabidopsis. *Mol Plant,* **7,** 277-289.

Tiwari, S. B., Hagen, G. and Guilfoyle, T. (2003) The roles of auxin response factor domains in auxin-responsive transcription. *Plant Cell,* **15,** 533-543.

Traas, J. (2013) Phyllotaxis. *Development,* **140,** 249-253.

Ulmasov, T., Hagen, G. and Guilfoyle, T. J. (1997a) ARF1, a transcription factor that binds to auxin response elements. *Science,* **276,** 1865-1868.

Ulmasov, T., Hagen, G. and Guilfoyle, T. J. (1999) Dimerization and DNA binding of auxin response factors. *Plant J,* **19,** 309-319.

Ulmasov, T., Liu, Z. B., Hagen, G. and Guilfoyle, T. J. (1995) Composite structure of auxin response elements. *Plant Cell,* **7,** 1611-1623.

Ulmasov, T., Murfett, J., Hagen, G. and Guilfoyle, T. J. (1997b) Aux/IAA proteins repress expression of reporter genes containing natural and highly active synthetic auxin response elements. *Plant Cell,* **9,** 1963-1971.

van den Berg, C., Willemsen, V., Hage, W., Weisbeek, P. and Scheres, B. (1995) Cell fate in the Arabidopsis root meristem determined by directional signalling. *Nature,* **378,** 62-65.

Vernoux, T., Besnard, F. and Traas, J. (2010) Auxin at the shoot apical meristem. *Cold Spring Harb Perspect Biol,* **2,** a001487.

Vernoux, T., Brunoud, G., Farcot, E., Morin, V., Van den Daele, H., Legrand, J.*, et al.* (2011a) The auxin signalling network translates dynamic input into robust patterning at the shoot apex. *Molecular systems biology,* **7,** 508.

Vernoux, T., Brunoud, G., Farcot, E., Morin, V., Van den Daele, H., Legrand, J.*, et al.* (2011b) The auxin signalling network translates dynamic input into robust patterning at the shoot apex. *Mol Syst Biol,* **7,** 508.

Wang, J., Andersson-Gunnerås, S., Gaboreanu, I., Hertzberg, M., Tucker, M. R., Zheng, B.*, et al.* (2011) Reduced expression of the SHORT-ROOT gene increases the rates of growth and development in hybrid poplar and Arabidopsis. *PLoS One,* **6,** e28878.

Weigel, D., Alvarez, J., Smyth, D. R., Yanofsky, M. F. and Meyerowitz, E. M. (1992) LEAFY controls floral meristem identity in Arabidopsis. *Cell,* **69,** 843-859.

Weijers, D., Schlereth, A., Ehrismann, J. S., Schwank, G., Kientz, M. and Jürgens, G. (2006) Auxin triggers transient local signaling for cell specification in Arabidopsis embryogenesis. *Dev Cell,* **10,** 265-270.

Welch, D., Hassan, H., Blilou, I., Immink, R., Heidstra, R. and Scheres, B. (2007) Arabidopsis JACKDAW and MAGPIE zinc finger proteins delimit asymmetric cell division and stabilize tissue boundaries by restricting SHORT-ROOT action. *Genes Dev,* **21,** 2196-2204.

Wenzel, C. L., Marrison, J., Mattsson, J., Haseloff, J. and Bougourd, S. M. (2012) Ectopic divisions in vascular and ground tissues of Arabidopsis thaliana result in distinct leaf venation defects. *J Exp Bot,* **63,** 5351-5364.

Wu, M. F., Yamaguchi, N., Xiao, J., Bargmann, B., Estelle, M., Sang, Y.*, et al.* (2015) Auxin-regulated chromatin switch directs acquisition of flower primordium founder fate. *Elife,* **4,** e09269.

Wu, X., Dinneny, J. R., Crawford, K. M., Rhee, Y., Citovsky, V., Zambryski, P. C.*, et al.* (2003) Modes of intercellular transcription factor movement in the Arabidopsis apex. *Development,* **130,** 3735-3745.

Wysocka-Diller, J. W., Helariutta, Y., Fukaki, H., Malamy, J. E. and Benfey, P. N. (2000) Molecular analysis of SCARECROW function reveals a radial patterning mechanism common to root and shoot. *Development,* **127,** 595-603.

Yadav, R. K., Perales, M., Gruel, J., Girke, T., Jönsson, H. and Reddy, G. V. (2011) WUSCHEL protein movement mediates stem cell homeostasis in the Arabidopsis shoot apex. *Genes Dev,* **25,** 2025-2030.

Yamaguchi, N., Wu, M. F., Winter, C. M., Berns, M. C., Nole-Wilson, S., Yamaguchi, A.*, et al.* (2013) A molecular framework for auxin-mediated initiation of flower primordia. *Dev Cell,* **24,** 271-282.

Yoon, E. K., Dhar, S., Lee, M. H., Song, J. H., Lee, S. A., Kim, G.*, et al.* (2016) Conservation and Diversification of the SHR-SCR-SCL23 Regulatory Network in the Development of the Functional Endodermis in Arabidopsis Shoots. *Mol Plant,* **9,** 1197-1209.

Zhang, Z., Tucker, E., Hermann, M. and Laux, T. (2017) A Molecular Framework for the Embryonic Initiation of Shoot Meristem Stem Cells. *Dev Cell,* **40,** 264-277.e264.

Zhao, Z., Andersen, S. U., Ljung, K., Dolezal, K., Miotk, A., Schultheiss, S. J.*, et al.* (2010) Hormonal control of the shoot stem-cell niche. *Nature,* **465,** 1089-1092.

Zhou, Y., Liu, X., Engstrom, E. M., Nimchuk, Z. L., Pruneda-Paz, J. L., Tarr, P. T.*, et al.* (2015) Control of plant stem cell function by conserved interacting transcriptional regulators. *Nature,* **517,** 377-380.

Zhou, Y., Yan, A., Han, H., Li, T., Geng, Y., Liu, X.*, et al.* (2018) HAIRY MERISTEM with WUSCHEL confines CLAVATA3 expression to the outer apical meristem layers. *Science,* **361,** 502-506.